UC Irvine
UC Irvine Electronic Theses and Dissertations

Title
Seismic and Post-Seismic Behavior of Embankments atop Peat

Permalink
https://escholarship.org/uc/item/7h1189q8

Author
Cappa, Riccardo

Publication Date
2016

License
https://creativecommons.org/licenses/by/4.0/ 4.0

Peer reviewed|Thesis/dissertation

eScholarship.org Powered by the California Digital Library
University of California

UNIVERSITY OF CALIFORNIA,
IRVINE

Seismic and Post-seismic Behavior of Embankments atop Peat

DISSERTATION

submitted in partial satisfaction of the requirements
for the degree of

DOCTOR OF PHILOSOPHY

in Civil Engineering

by

Riccardo Cappa

Dissertation Committee:
Assistant Professor Anne Lemnitzer, Chair
Associate Professor Scott J. Brandenberg
Professor Lizhi Sun

2016

Portion of Chapter 2, 3, 4 & 5 © 2014 NEESHub
Portion of Chapter 2, 3, 4, 5, & 10, © 2015 EERI
Chapter 8 © 2014 ASDSO
All other materials © 2016 Riccardo Cappa

DEDICATION

I dedicate this manuscript to my fiancée, Alessandra, without whose encouragement, happiness and help, I would not have reached this degree. Her strength and faith in our love even when we were thousands miles apart for quite some time fueled my determination to become a better and more responsible man. She has a heart of gold; she is an amazing and divine manifestation of love. I found my half apple. I see this every day. Thank you.

TABLE OF CONTENTS

LIST OF FIGURES v
LIST OF TABLES vii
LIST OF EQUATIONS viii
ACKNOWLEDGMENTS ix
CURRICULUM VITAE xi
ABSTRACT OF THE DISSERTATION xv
1. INTRODUCTION 1
1.1 Project Motivation 1
1.2 Project Objectives 2
1.3 Problem characterization, Literature Review and Previous Studies 2
1.3.1 Seismic Risk in the Delta 3
1.3.2 Flood Risk and Water Discharge in the Delta 5
1.3.3 Subsidence in the Delta and Levee Construction 6
1.3.4 Peat Characteristic and Literature Review 10
1.3.5 Conclusive Thoughts and Facts of the Risk in the Delta 17
1.4 Thesis Structure 20
2. EXPERIMENTAL INVESTIGATIONS 22
2.1 Centrifuge Principles 24
2.2 Experiment Configuration 25
2.3 Materials 30
2.3.1 Peat Layer 30
2.3.2 Modeling Clay 32
2.3.3 Liquefiable Levee Fill 33
2.3.4 Coarse Dense Sand Layer 34
2.3.5 Loam Layer Atop Sandy Levee Fill 35
2.3.6 Viscous Pore Fluid 36
2.4 Pumping System 36
2.5 Construction and Testing Procedures of Clayey Levee Experiments 37
2.6 Construction and Testing Procedures of Sandy Levee Experiments 39
3. INSTRUMENTATION 42
3.1 Sensor Types and Preparation 42
3.2 Sensor Layout and Global Coordinates 43
3.3 Videos and Photos 45
4. LOADINGS AND DATA ARCHIVING 47
4.1 Data Archiving 47
4.2 Applied Loading 50
5. SAMPLE DATA 51
5.1 Slow Data Sample – Experiment 14, RCK02 51

5.2 Fast Data Sample - Experiment 14, RCK02 54
5.3 Shear Wave Velocity Measurements 55
5.4 Compression Wave Velocity of the Peat 58
5.5 CPT Records for Experiments 14 and 15 59
6. CYCLIC STRAIN AND EXCESS PORE PRESSURE GENERATION 62
6.1 Introduction 62
6.2 Centrifuge Experiments 65
6.3 Experimental Results & Data Analysis 66
6.3.1 Computed Shear Strains 68
6.3.2 Direct-Simple-Shear-Equivalent Deviatoric Strain Invariant 72
6.3.3 Relationship between Excess Pore Pressure Generation and Shear Strain Amplitudes 74
6.4 Chapter Summary and Conclusions 80
7. POST-SEISMIC SETTLEMENTS 83
7.1 Introduction 83
7.2 Results of the 9m Radius Centrifuge Test 84
7.3 Results of the 1m Radius Centrifuge Test 87
7.4 Chapter Summary and Conclusions 95
8. INERTIAL ASPECTS OF THE SSI 97
8.1 Seismic Response of Embankments on Peaty Soils 97
8.2 Centrifuge Experiments 98
8.3 Sine Sweep Characterization 100
8.4 Frequency Analysis and Transfer Functions 102
8.5 Chapter Summary and Conclusions 107
9. SANDY LEVEE PERFORMANCE 108
9.1 Introduction 108
9.2 Centrifuge Experiments 109
9.3 Chapter Summary and Conclusions 113
10. THESIS SUMMARY, CONCLUSIONS AND FUTURE WORK 114
10.1 Thesis Summary 114
10.2 Thesis Conclusions and Future Work 116
REFERENCES 118
APPENDIX A: DEVELOPMENT OF SATURATION PROCEDURES 127
A.1 Challenges in Saturation of Sands in Centrifuge Models with Organic Soils 127
A.2 A new pluviation technique 128

LIST OF FIGURES

Figure 1 – Schematic section from Pacific Ocean to Great Valley (Modified from Fuis and Mooney, 1990) 4
Figure 2 – Potentially active faults near and within the Delta (FUGRO, 2009) 4
Figure 3 – Sea level fluctuation in last 18,000 years (Rogers, 2011) 6
Figure 4 – Peat thickness in the Delta (Modified from DWR, 2015) 7
Figure 5 – Anthropogenic accommodation (modified from Mount and Twiss, 2005, after Ingebritsen et al., 2000) 8
Figure 6 – Subsidence in the Delta (Modified from DWR, 1995) 9
Figure 7 – Measures & estimates of elevations on Bacon Island (Deverel and Leighton, 2010) 10
Figure 8 – Peatlands in the world (modified from Joosten, 2010) 11
Figure 9 – Dynamic properties of peat (Wehling et al., 2003) 15
Figure 10 – Salinity intrusion in the Delta (Ingebritsen et al., 2000) 19
Figure 11 – Number of inundation events from levee failures since 1900 (DWR, 2007) 20
Figure 12 – Transparent walls rigid container employed 26
Figure 13 – General configurations (a) Experiment 12 & 14, and (b) Experiment 13 & 15 27
Figure 14 – Best estimate of layout of Experiment 12 at 57g after primary consolidation 28
Figure 15 – Best estimate of layout of Experiment 13 at 57g after primary consolidation 28
Figure 16 – Best estimate of layout of Experiment 14 at 57g after primary consolidation 29
Figure 17 – Best estimate of layout of Experiment 15 at 57g after primary consolidation 29
Figure 18 – Long fibers and large particles we removed 31
Figure 19 – Mold for melted clay and formed clay levee 33
Figure 20 – Model layout for Experiment 14 before moving the model on the centrifuge arm 38
Figure 21 – Side view of Experiment 14 before moving the model on the centrifuge arm 38
Figure 22 – Model layout for Experiment 15 before start spinning 40
Figure 23 – Side view of Experiment 15 before start spinning 40
Figure 24 – (a) Local and (b) global coordinate systems in the centrifuge 44
Figure 25 – Definition of FF and CL vertical arrays of sensors 52
Figure 26 – Slow data for (a) acceleration field, (b) pore pressures and (c) settlements during Experiment 14, RCK02 53
Figure 27 – Fast data for (a) acceleration at CL levee crest, (b) acceleration at FF peat top, (c) acceleration at CL peat bottom, (d) pore pressure beneath the levee and (e) settlement of the levee during Trial 4 (Strong Kobe) for Experiment 14, RCK02 55
Figure 28 – Sample data for the BE set in the peat layer CL array at 57g during Experiment 15 57
Figure 29 – Regression of *Vs1* and *n* parameters for the soil layers 58
Figure 30 – Records from ICPs in the peat at 1g, RCK01 59
Figure 31 – Location of CPT during Experiment 14 60
Figure 32 – Location of CPT during Experiment 15 60
Figure 33 – Example of CPT record for Experiment 15 61
Figure 34 – Vertical effective stress and shear wave velocities profile of the peat stratum at 57g 66
Figure 35 – Fast data time histories of accelerations at (a) levee crest, (b) free field peat top and (c) base of the container, and (d) excess pore pressures ratios at peat mid-elevation in the CL array during Trial 4 (Strong Kobe) of RCK02 67

Figure 36 – Section of RCK02 model at 57g showing the quadrilateral elements and the isoparametric element 69
Figure 37 – Horizontal (a), vertical (b) and shear (c) strains at various mid-elevation locations beneath the levee during Strong Kobe motion, RCK02 72
Figure 38 – Strain components during Strong Kobe motion (Trial 4) at mid-height of peat layer beneath (a) the levee crest and (b) the levee toe 74
Figure 39 – Equivalent shear strain vs excess pore pressure ratio histories at P7 elevation during the Strong Kobe motion (Trial 4) for RCK02 75
Figure 40 – Residual excess pore pressure $r_{u,r}$ vs (a) PBA and (b) $\gamma_{DSS,eq}$ 76
Figure 41 – Example of conversion from $\gamma_{DSS,eq}$ to $(\gamma_{c,ref})_{N=15}$ for strain time history at P7 for Strong Kobe (Trial 4) during Experiment 14, RCK02 78
Figure 42 – Comparison of $(\gamma_{c,ref})_{N=15}$ for centrifuge data and regression line according to Shafiee (2016) 80
Figure 43 – Slow data records of (a) acceleration, (b) pore pressures and (c) vertical settlements during Experiment 14, RCK02 85
Figure 44 – Illustration of secondary compression rates after cyclic loading 86
Figure 45 – Side view of Experiment 16 at 1g before start the first day of spinning 88
Figure 46 – Model before start second spinning day of Experiment 16 89
Figure 47 – Slow data of second spinning day of Experiment 16 showing (a) centrifugal accelerations, (b) pore pressure, and (c) settlements in model scale 90
Figure 48 – Slow data of CL array in log scale of time after $t_{0,consolidation}$ showing (a) accelerations, (b) pore pressure and (c) settlements in model scale 93
Figure 49 – Side view and plan of Experiment 16 at 1g before starting the spin on the second day 94
Figure 50 – FF and CL arrays for Experiment 14, and notation of important ICPs used in the analyses hereafter 99
Figure 51 – FF and CL prototype soil profiles for RCK01 (a) and RCK02 (b) 100
Figure 52 – Variation of peat unit weight with effective stress 100
Figure 53 – Accelerations at peat bottom, free field peat top and levee crest for RCK01 (a) and RCK02 (b) during application of the Sine Sweep 101
Figure 54 – Records of horizontal accelerometers for RCK02 for FF and CL arrays 102
Figure 55 – Fourier amplitude spectra for (a) RCK01 and (b) RCK02. FFT algorithm is indicated as inset 103
Figure 56 – Amplification factors for the FF (a) and CL (b) profiles for RCK01 104
Figure 57 – Fourier spectra for vertical and horizontal pairs of accelerometers (a) and transfer function for the horizontal pair of accelerometers (b) for RCK01 105
Figure 58 – Amplification factors for the FF (a) and CL (b) profiles for RCK02 106
Figure 59 – Fourier spectra for vertical and horizontal pairs of accelerometers (a) and transfer function for the horizontal pair of accelerometer (b) for RCK02 107
Figure 60 – Slow data Experiment 15 110
Figure 61 – Side view of Experiment 15 (a) before start spinning and (b) after application of the target Kobe motion (Trial 3) 112
Figure 62 – Fast data for Experiment 15 during target Kobe motion (Trial 3) 112
Figure 63 – Water pluviation saturation device (Yniesta et al., 2015a) 129
Figure 64 – Electric mixing chamber available at the facility 130

LIST OF TABLES

Table 1 – Major faults potentially affecting the Delta (modified from SJC, 2014) 5
Table 2 – Summary of Experiments performed as part of this project 23
Table 3 – Scale factors that apply to centrifuge modeling 24
Table 4 – Properties of Sherman Island peat according to Reinert et al. (2014) 30
Table 5 – Initial properties of processed peat 32
Table 6 – Records of slow and fast data for RCK01 and RCK02 available on the project warehouse 48
Table 7 – Bender element positions and direction before and after testing – Experiment 14 and 15 56
Table 8 – Bender element positions and direction before and after testing – Experiment 14 and 15 56
Table 9 – Settlement rates calculated for various stages of Experiment 16 95

LIST OF EQUATIONS

Equation 1 – $V_s = f(V_{s1}, \sigma_v', p_A, n)$ 57
Equation 2 – $e = f(C_c, \sigma_p', \sigma_{v,ref}', C_r, \sigma_v')$ 65
Equation 3 – $\gamma_{sat} = f(\gamma_w, G_s, e)$ 66
Equation 4 – $V_s = f(V_{s1}, \sigma_v', p_A, n)$ 66
Equation 5 – {ε} 69
Equation 6 – {u} 69
Equation 7 – [B] 69
Equation 8 – (J11) 70
Equation 9 – (J12) 70
Equation 10 – (J21) 70
Equation 11 – (J22) 70
Equation 12 – {N1,ξ} 70
Equation 13 – {N1,η} 70
Equation 14 – $\gamma_{OCT} = f(\varepsilon_{xx}, \varepsilon_{zz}, \gamma_{xz})$ 73
Equation 15 – $\gamma_{DSS,eq} = f(\gamma_{OCT})$ 73
Equation 16 – $r_{ur} = f(\gamma_c, \gamma_{tp}, N, OCR, OC)$ 77
Equation 17 – Equivalent Number of Cycles 77
Equation 18 – $N_{ref} = f(\gamma_c, \gamma_{c,ref}, \gamma_{tp})$ 78
Equation 19 – $\Delta e = f(C_c, C_r, OCR)$ 79
Equation 20 – $OCR = f(\Delta e, C_c, C_r)$ 79

ACKNOWLEDGMENTS

I would like to first express my sincere gratitude to my adviser Prof. Anne Lemnitzer, who blindly believed in my potential and gave me the chance to be part of a wonderful project. Her continuous support of my Ph.D. program was above and beyond any expectation from an adviser. Her guidance helped me in conducting research, writing this thesis, submitting papers to well respected journals and writing and receiving multiple prestigious scholarships, in bright days as well as gray moments. I found a mentor, a motivator, a true friend.

I am also grateful to Prof. Scott J. Brandenberg, PI of the project, for sharing his invaluable expertise and enthusiasm during every aspect of the research. Every meeting we had fostered my knowledge and longing for improvement. His positive approach to teaching is extraordinary; I will treasure this wonderful experience during my future career.

A special thanks to Samuel Yniesta, a wonderful teammate, an awesome roommate, a smart researcher and a genuine friend that I wish I could have close forever. I hope our lives will meet again in the future.

I would like to thank my defense-, qualifying-, and preliminary-exam committee members: Prof. Farzin Zareian, Prof. Lizhi Sun, Prof. Jasper Vrugt and Prof. Lorenzo Valdevit of UCI. Thank for giving me the opportunity to arrive where I am today. I was fortunate to be your master student and learn different approaches to study, and to achieve goals – academically and in life. I truly believe in diversity, and it is astonishing that my 6 committee members come from 6 different nations.

My Ph.D. research and support was made possible with the financial assistance of NSF - NEES, *under the award # NEES R 1208170 (July 2012)* and UC Irvine which are both gratefully acknowledged.

I also thank the NEES@UCDavis personnel, including Dan Wilson, Ross Boulanger, Bruce Kutter, Chad Justice, Peter Rojas, Lars Pedersen, Tom Kohnke, Anatoliy Ganchenko, and Jenny Chen for their assistance during this challenging project. I received an incredible amount of wisdom and knowledge not teachable in coursework, and I loved the family-like atmosphere I breathed there.

Special thanks are also expressed to all other graduate and undergraduate students that shared with me their knowledge, time and ideas: Mohammed Kohsravi, Ben Turner, Ali Shafiee, Mike Gomez, and Bahareh Heidarzadeh. Thanks for stimulating discussions, for the sleepless nights filled with work and research, and for the fun we had during the last four years.

The most special, deep, touching, endless thank you goes to my family: my mom, dad, and brother. The real reason I am here today is because they took on their shoulders the burden of giving me the chance to study abroad during my bachelor program. They pushed me and helped me every day. They never asked me to change my life-goals, even when I know my presence at home would have helped a lot. Their unconditional love and happiness in seeing me achieving my dreams is an indescribable fortune, a boundless luck beyond words. I will always feel indebted for what you have done for me. I truly love you.

CURRICULUM VITAE

ACADEMIC CAREER

2011	B.S. in Architecture and Building Engineering, University of Bologna, Italy
2012	M.S. in Structural Engineering, University of California, Irvine
2012-15	Teaching Assistant, Civil and Environmental Engineering department, University of California, Irvine
2016	Ph.D. in Civil Engineering, University of California, Irvine

FIELD OF STUDY

Civil Engineering

PUBLICATIONS

1. Cappa, R., Yniesta, S., Brandenberg, S., Stewart, J.P. and Lemnitzer, A. (2014a) "NEESR: Levees and Earthquakes: Averting and Impending Disaster- Data Report for Centrifuge Experiments 12L and 13L", *NEESHub*, Final Project Report, https://nees.org/warehouse/project/1161

2. Cappa, R., Yniesta, S., Brandenberg, S., Stewart, J.P. and Lemnitzer, A. (2014b) "NEESR: Levees and Earthquakes: Averting and Impending Disaster- Data Report for Centrifuge Experiments 14L and 15L", *NEESHub*, Final Project Report, https://nees.org/warehouse/project/1161
3. Cappa, R., Yniesta, S., Lemnitzer, A., Brandenberg, S.J. and Stewart, J.P. (2014c) "Centrifuge Experiments to Evaluate the Seismic Performance of Levees on Peaty Soils in the Sacramento-San Joaquin Delta", *ASDSO Dam Safety National Conference 2014*, San Diego, USA, September 2014
4. Cappa, R., Yniesta, S., Lemnitzer, A. and Brandenberg, S.J. (2015a) "Experimental and Analytical Modeling of Settlements of Levees Resting atop Organic Soils", *IFCEE & Geo-Congress 2015*, San Antonio, USA, March 2015
5. Cappa, R., Yniesta, S., Brandenberg, S.J. and Lemnitzer, A. (2015b) "Settlements and excess pore pressure generation in peaty soils under embankments during cyclic loading", *6ICEGE*, Christhchurch, New Zealand, November 2015
6. Lemnitzer, A., Cappa, R., Yniesta, S. and Brandenberg, S.J. (2015) "Centrifuge Testing of Model Levees atop Peat: Experimental Data", *EERI Earthquake Spectra*, Manuscript ID #032715EQS048
7. Yniesta, S., Lemnitzer, A., Cappa, R. and Brandenberg, S.J. (2015a) "Vacuum pluviation device for achieving saturated sand without backpressure", *Geotechnical Testing Journal*, Manuscript ID GTJ-2014-0173
8. Yniesta, S., Cappa, R., Lemnitzer, A. and Brandenberg, S.J. (2015b) "Centrifuge Testing of Levees: Saturation Techniques during Model Construction", *IFCEE & Geo-Congress 2015*, San Antonio, USA, March 2015

9. Cappa, R., Yniesta, S., Brandenberg, S.J. and Lemnitzer, A. (2016) "Strains and Pore Pressures Generated during Cyclic Loading of Embankments on Organic Soil", paper currently under peer review

PRESENTATIONS

1. Cappa, R., Yniesta, S., Brandenberg, S., Lemnitzer, A. and Stewart, J.P. – "NEESR: Levees and Earthquakes: Averting an Impending Disaster", (Poster Presentation), *PEER – Northridge 20th Anniversary Symposium (Pacific Earthquake Engineering Research Center)*, January 16th-17th, 2014, UCLA, Los Angeles

2. Lemnitzer, A. and Cappa, R., Brandenberg, S.J. and Schmutte, C. – "Centrifuge Experiments to investigate levee deformation potential in the Sacramento – San Joaquin Delta", *ASCE Geotechnical Seminar (American Society of Civil Engineering)*, May 18th, 2014, San Diego

3. Cappa, R., Yniesta, S., Brandenberg, S.J., Lemnitzer, A. – "Centrifuge Experiments to Investigate Levee Deformation Potential in the Sacramento-San Joaquin Delta", *CalGeo Seminar (California Geotechnical Engineering Association)*, May 28th, 2014, Los Angeles

4. Cappa, R., Lemnitzer, A., Brandenberg, S.J. and Stewart, J.P. – "Centrifuge Experiments to Evaluate the Seismic Performance of Levees on Peaty Soils in the Sacramento-San

Joaquin Delta", *ASDSO Dam Safety National Conference 2014 (Association of State Dam Safety Officials)*, September 22nd, 2014, San Diego

5. Cappa, R. – "Centrifuge Experiments to Evaluate the Seismic Performance of Levees on Peaty Soils in the Sacramento-San Joaquin Delta", *SGH Professional Development Seminars at (Simpson Gumpertz and Heger)*, January 30th, 2015, Newport Beach, California

6. Cappa, R., Brandenberg, S.J. and Lemnitzer, A. – "Experimental and Analytical Modeling of Settlements of Levees Resting atop Organic Soils", (Interactive Poster Presentation), *IFCEE 2015 (International Foundations Congress and Equipment Expo 2015)*, San Antonio, March 17th-21st, 2015

7. Cappa, R. – "NEESR: Levees and Earthquakes: Averting an Impending Disaster", *A.A.A.S. Make our C.A.S.E. program (American Association for the Advancement of Science – Catalyzing Advocacy for Science and Engineering), Advocacy for Science at the United States Congress*, April 12-15th, 2015, Capitol Hill, Washington

8. Cappa, R. – "NEESR: Levees and Earthquakes: Averting an Impending Disaster", *University of California G.R.A.D. program (Graduate Research Advocacy Day), Advocacy for Graduate Research at the California State Congress*, April 28th, 2015, California State Capitol, Sacramento

9. Cappa, R., Yniesta, S., Brandenberg, S.J., Lemnitzer, A. – "Settlements and excess pore pressure generation in peaty soils under embankments during cyclic loading", *6ICEGE Conference (6th International Conference on Earthquake Geotechnical Engineering)*, November 1st–4th, 2015, Christchurch, New Zealand

ABSTRACT OF THE DISSERTATION

Seismic and Post-seismic Behavior of Embankments atop Peat

By

Riccardo Cappa

Doctor of Philosophy in Civil Engineering

University of California, Irvine, 2016

Project Team:

Assistant Professor Anne Lemnitzer, UC Irvine

Associate Professor Scott J. Brandenberg, UC Los Angeles

Professor Jonathan P. Stewart, UC Los Angeles

Ph.D. Candidate Samuel Yniesta, UC Los Angeles

The vast 2,800 km^2 Sacramento-San Joaquin Delta, California, lies in a seismically active region and was originally marshland, whose reclamation started 150 years ago by building un-engineered levees on top of the organic soil. Today, after more than a century of intensive agricultural activities, the majority of the Delta inlands subsided below mean sea level, reducing the stability of the fragile embankment structures. With the chance of experiencing moderate earthquake activity in the Delta of up to 0.4g in the next 500 years, the potential of a massive levee system failure due to simultaneous breaching of levees poses a significant hazard. Consequences could include flooding of thousands of acres of agricultural farm land, draw-in of

saline water from the Pacific Ocean causing a breakdown of Southern California's water supply system, destruction of the Delta's ecological environment and an estimated economic loss of up to $ 40 billion to the state of California. Seismic risk assessments, mitigation techniques and safety plans proposed so far lack of solid scientific bases. Estimations of free board loss in practice neglect (a) the performance of the organic foundation and (b) its interaction with the relatively stiffer embankment structure atop, both of which are insufficiently understood. In addition, the liquefaction potential of Delta levee fills subjected to the 500 year earthquake scenario is unclear. Four large scale 9m radius and twelve 1m radius centrifuge tests were performed at the NEES@UCDavis equipment site to study the seismic and post-seismic behavior of model levee structures resting atop soft organic peat. Findings of the project include (1) definition of a 1% cyclic strain threshold for pore pressure generation in peat, (2) documentation of augmented post-seismic volume change rates in the organic foundation with an increase in secondary compression settlement rates of up to 30%, (3) identification of substantial inertial SSI effects and stress concentrations beneath the embankment toes, and (4) verification of free board loss of model Delta levees cyclically loaded with ground motions comparable to the 500 year earthquake scenario. Data from the project will serve as a tool to guide legislators in their important decisions, and as unique benchmarks for validation of improved constitutive models and risk assessments.

1. INTRODUCTION

1.1 Project Motivation

The Sacramento-San Joaquin Delta, California, lies in a seismically active region and was originally marshland, whose reclamation started 150 years ago by building un-engineered levees on top of the organic soil. The Delta covers 2,800 km^2 and comprises nearly 70 islands, encompassed by 1800 km of levees. This vast region is the hub of California's water distribution system and provides agricultural and urban water to approximately 25 million residents. Simultaneously it is the home of a highly unique ecosystem. Today, after more than a century of intensive agricultural activities, the majority of the Delta inlands subsided below mean sea level, hereby reducing the stability of the fragile embankment structures. With the chance of experiencing moderate earthquake activity in the Delta of up to 0.4g in the next 500 years (CDWR, 2009-6) from nearby faults, as well as predictions of 7+ magnitude earthquakes on the San Andreas and Hayward faults (Greensfelder, 1974), the potential of a massive levee system failure due simultaneous breaching of levees poses a significant hazard. Consequences could include flooding of thousands of acres of agricultural farm land, draw-in of saline water from the Pacific Ocean causing a breakdown of Southern California's water supply system, destruction of the Delta's ecological environment and an estimated economic loss of up to $ 40 billion to the State of California.

Currently, the seismic and post-seismic behavior of peaty soils underlying Delta levees is insufficiently understood and poses significant challenges in predicting the levee deformations

and settlements during and after cyclic loading. Typical estimations of free board loss in practice neglect the performance of the organic foundation soil and its interaction with the relatively stiffer embankment structure atop (i.e., soil-structure interaction between the peat foundation and the levee structure). This project aims to investigate the response of earthen embankments atop peats as found in the San Joaquin – Sacramento Delta and in other regions worldwide.

1.2 Project Objectives

Project objectives include (1) understanding the complex seismic and post-seismic behavior of organic soils and documenting the magnitudes of excess pore water pressures developed during and after cyclic straining therein, (2) studying the interaction between the soft peaty soil and the sandy levee material, and (3) investigating the potential of levee deformation/breaching under various ground motion intensities (settlement and liquefaction).

While the liquefaction of sandy fills is a relatively well understood mechanism, limited experimental results are currently available to estimate the cyclic and post-cyclic consolidation behavior of organic soils. Through sets of 1m and 9m radius centrifuge tests, a better understanding of pore pressure development and peat-levee interaction is offered.

1.3 Problem characterization, Literature Review and Previous Studies

The risk in the Delta is characterized by (1) the complex, dense and active fault system in the region, (2) the abundant amount of water discharged daily through the Delta (3) the subsidence

of the inlands initiated by human activities, and (4) the unique characteristics of peats and its uncertain seismic and post-seismic behavior.

1.3.1 Seismic Risk in the Delta

The moderate seismic hazard in the region poses a serious danger to the fragile Delta levees. The complex fault system along the coasts of Northern California is characterized by decreasing crust shallowness from the Central Valley towards the ocean (Figure 1). A series of minor faults align in the same direction as the San Andreas Fault (Figure 1, Figure 2 & Table 1). Fault activity is highest in close vicinity of the shallow ocean crust, and decreases towards the Central Valley, as the increasing crust thickness allows for higher strain energy storage (Rogers, 2011). According to the Uniform Building Code the Delta lies in a Seismic Zone 3 and 4, with design peak ground accelerations of 0.3g and 0.4g, respectively, for a 500 year return period scenario. The seismic risk in the Delta is controlled by local faults such as the Antioch, Greenville, Midland, and Concord faults located within its boundaries (Figure 2). These faults are expected to produce 6.6+ magnitude maximum credible earthquakes (Table 1), resulting in a "moderate" seismic risk in the region with relatively short recurrence intervals, e.g. 264-319 years. Maximum probable earthquakes indicated in Table 1 are defined as maximum earthquake magnitudes that appear to be reasonably expected within a100-year period, while the maximum credible earthquake is defined as the maximum earthquake that might occur under the currently known conditions according to SJC (2014).

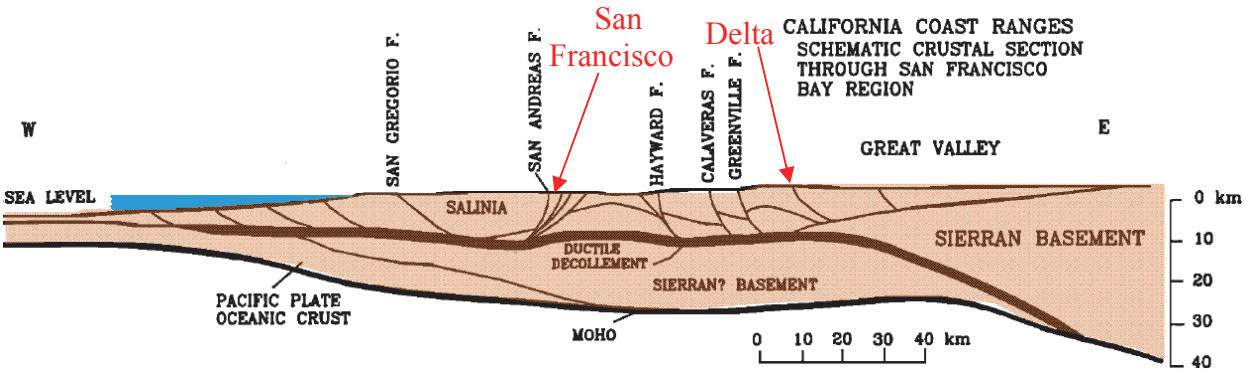

Figure 1 – Schematic section from Pacific Ocean to Great Valley (Modified from Fuis and Mooney, 1990)

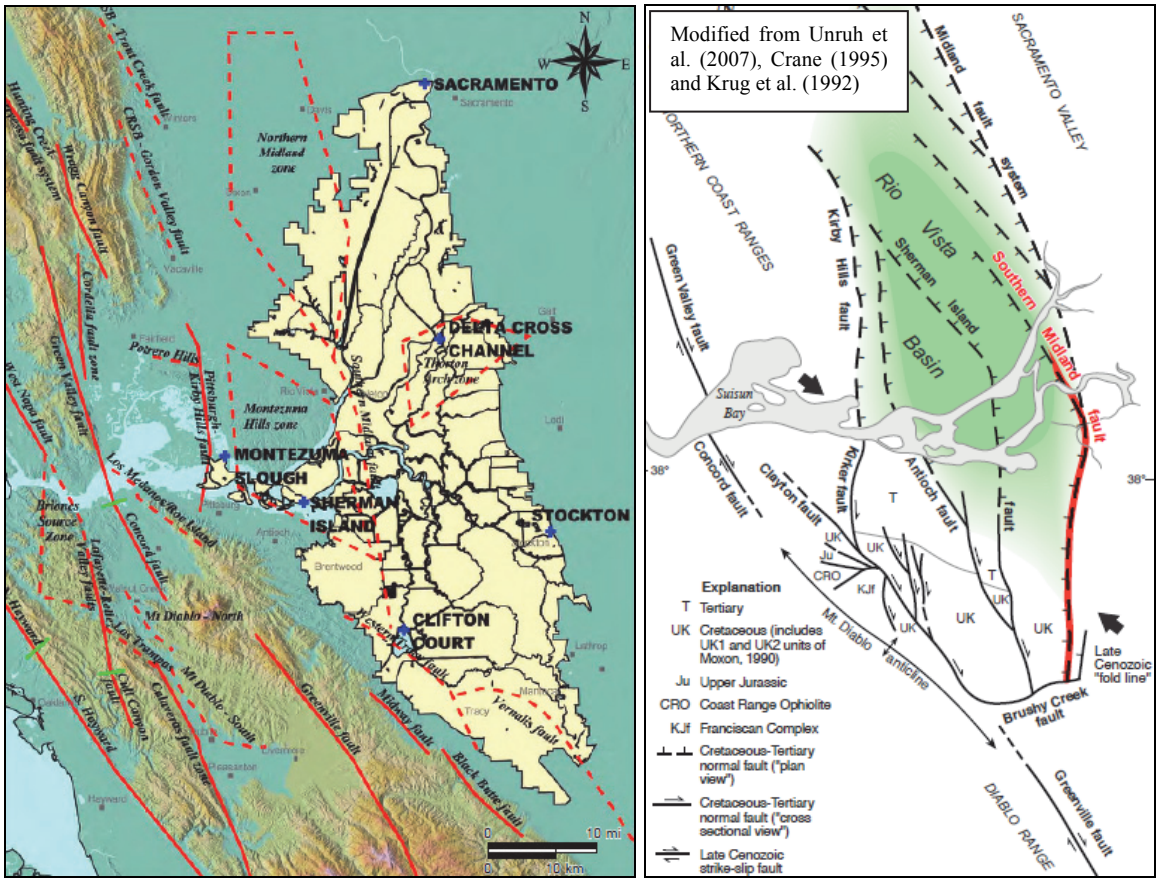

Figure 2 – Potentially active faults near and within the Delta (FUGRO, 2009)

Table 1 – Major faults potentially affecting the Delta (modified from SJC, 2014)

Fault	Distance from Stockton (km)	Maximum Probable Earthquake [1]	Maximum Credible Earthquake [2]	Recurrence Interval (years)	Maximum Intensity of M.C.E. (S.J. County)	Years of Historic Damaging Earthquakes
Foothills	20.9	6.9	6.0	> 10,000	VIII-X	1975
Midland	30.6	6.6 *	7.2 *	Unknown	VIII-X	1889 ?
Midway	38.6	6.3	6.3	2,651	VII-VIII	None known
Antioch	48.3	6.6	5.75-6.6	319	VII-VIII	1889 ?, 1965
Greenville	48.3	6.8	6.9	> 10,000	VII-VIII	1980
Ortigalita	51.5	6.7	6.7	10,000	VII-VIII	None known
San Joaquin	51.5	6.6	Unknown	1,083	Unknown	None known
Calaveras	67.6	6.5	6.75-7.3	140	VIII-X	1861
Green Valley / Concord	70.8	6.7	6.5-7.25	264	VII-VIII	1955
Hayward	77.2	7.25	7.0-7.5	150	VIII-X	1836, 1868
San Andreas	106.2	7.8-8.25	8.25-8.5	300	VIII-X	1838, 1906

**** Values added from a report by FUGRO (2009)***

[1] M.P.E. is the maximum earthquake that appears to be reasonably expected within 100-year period

[2] M.C.E. is the maximum earthquake that might reasonably occur under presently known conditions

1.3.2 Flood Risk and Water Discharge in the Delta

The 150,000 km^2 Sacramento and San Joaquin basins collect almost 50% of total state runoffs, providing an estimated water volume of 8.5 km^3 per year. The Sacramento and SJ rivers merge near Lodi, CA, and create an "inverse" Delta, whose corner faces the San Francisco Bay. As a result of sea level rise and tectonic movements, the location of the merging point of the two

rivers has changed over the millennia (Figure 3). The current location stabilized after the last glacial period (approx. 12,000 years ago).

The large amount of daily water discharged through the Delta poses a continuous flood risk to the region. With the construction of water diverting structures such as dams and sluices, civil engineers have tried to mitigate flood damage for over 150 year. Today, flood stages could be forecasted up to a week ahead of time, rendering loadings predictable. However, because of the important volume of water flowing in the region, any failure along the levee system often results in a catastrophic and at least partial inundation of nearby lands, such as the Jones Tract in 2004.

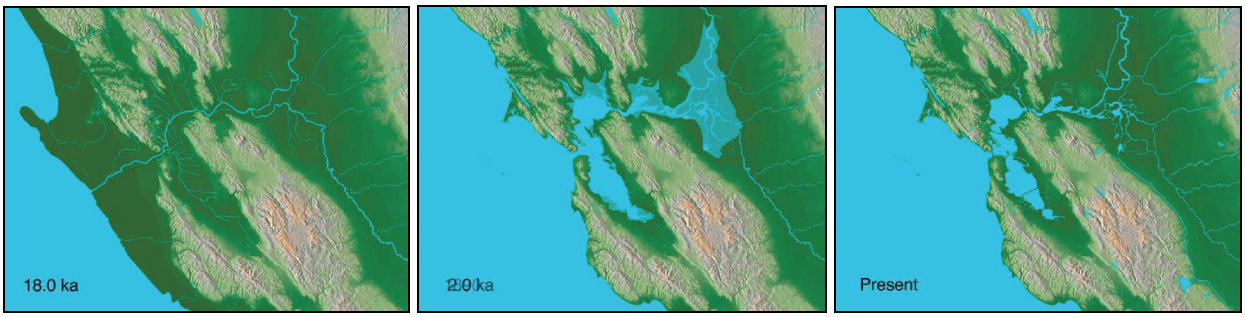

Figure 3 – Sea level fluctuation in last 18,000 years (Rogers, 2011)

1.3.3 Subsidence in the Delta and Levee Construction

As part of the historical inundations and frequent tides over the course of several millennia, a thick layer of organic depositional stratum (peat) formed in the region. Figure 4 shows the current peat layer across the Delta. The peat layers often exceed a thickness of 3-6 m (10-20 feet), with some locations exceeding 13 m of peat stratum, e.g. Sherman Island.

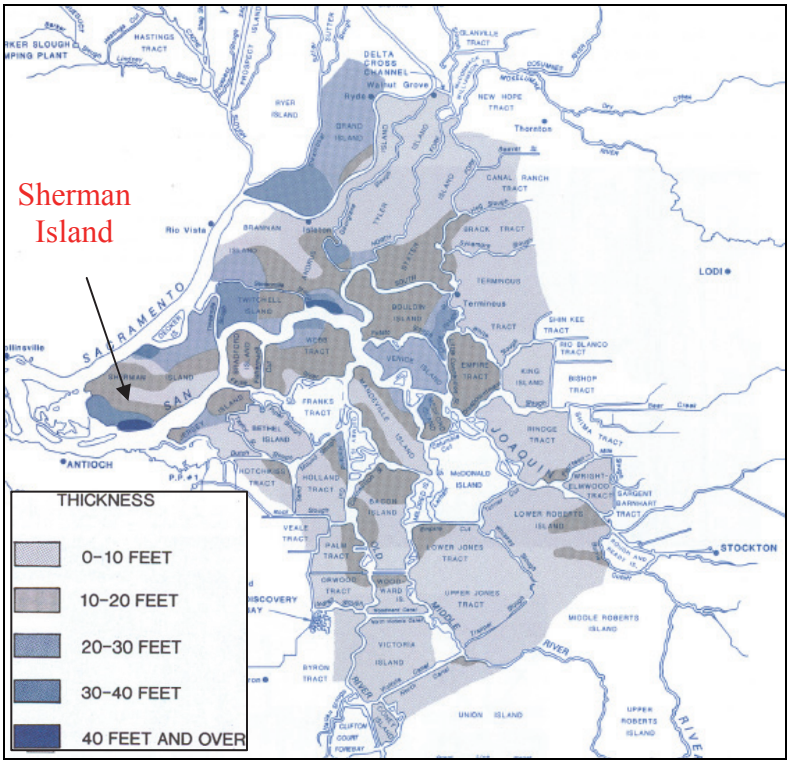

Figure 4 – Peat thickness in the Delta (Modified from DWR, 2015)

Due to it exceptional fertility and its location near the San Francisco market, the Delta and its islands were reclaimed for agricultural purposes starting in the1860's. Initially, blocks of peat were shaped from a ditch and piled on top of each other to form levees on top of the natural low dikes. Construction of peaty levees was cheap, but the organic embankments were prone to leakage and high shrinkage. The continuous settlements and failures of the peat levees was costly later resolved by scooping loose sands dredged from river beds atop the levee crests, therefore creating very liquefaction-prone structures. In addition, burning the virgin ground was a common technique employed for reclamation of many islands, but it started a process of subsidence that eventually lowered the inlands and impeded gravity drainage after tides. Furthermore, after an

initial primary settlement due to mechanical loads, a secondary subsidence was caused by erosion, oxidation and decomposition of the organic material, ultimately worsening the ongoing subsidence. Figure 5 shows the difference in typical inland elevations from pre-1880 to 1900's in the Delta. Mount and Twiss (2005) defined these "gaps" as "anthropogenic accommodations" and estimated their volumes to total 2.5 km^3.

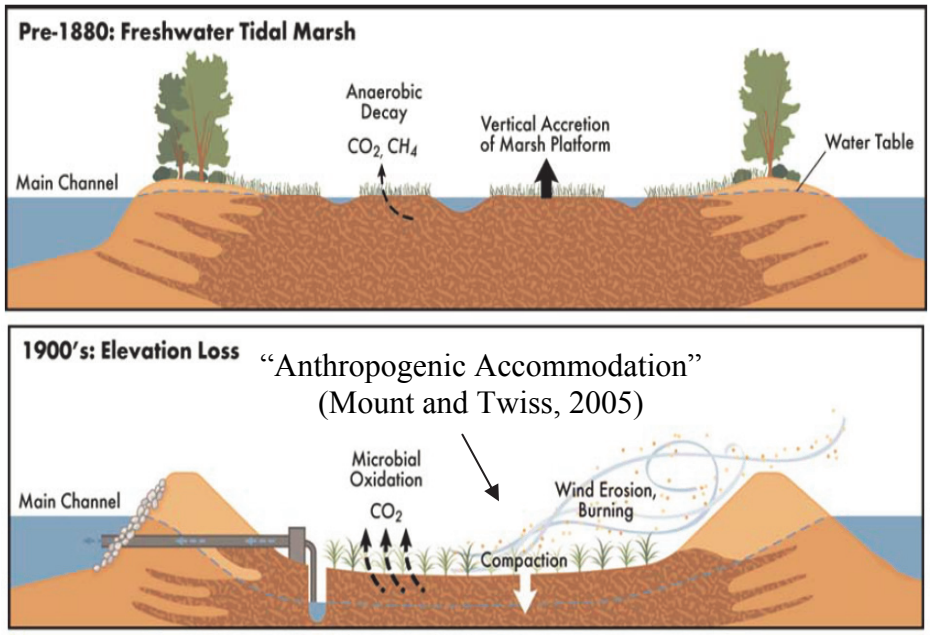

Figure 5 – Anthropogenic accommodation (modified from Mount and Twiss, 2005, after Ingebritsen et al., 2000)

Semi-continuous pumps (Figure 5) drain the fields and keeps the inland water table low, altering the normal decaying process of organic material. As plants are exposed to air they tend to decompose faster, i.e. in aerobic condition, without accumulating matter and therefore creating more subsidence. Figure 6 shows the average subsidence in the region in 1995, after a century of subsidence, and suggests the amount of water that would be needed to fill each gap.

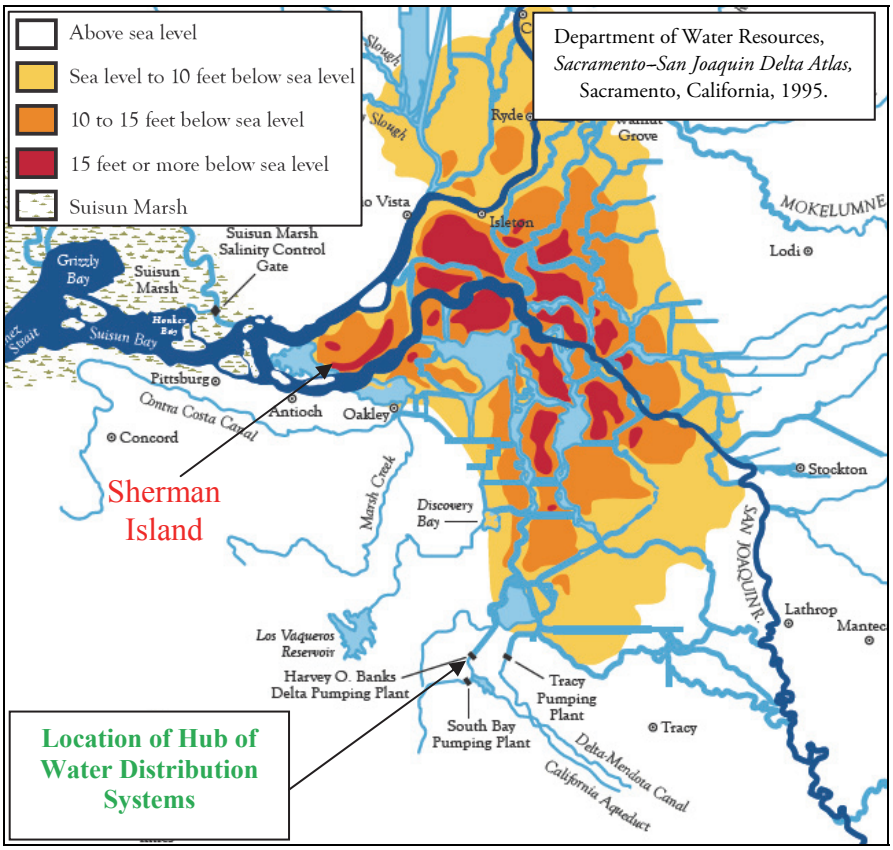

Figure 6 – Subsidence in the Delta (Modified from DWR, 1995)

The reclamation of these lands and their draining will continue to lower the surface of the ground, although burning and other techniques are prohibited today. Deverel and Leighton (2010) studied the subsidence rate at Sherman Island in the last century and observed a substantial rate decrease (66% reduction) in the last 25 years, but also indicated the process is still severe, with estimated average rates of 1.2 cm per year between 1988 and 2006. According to their study, a collection of recorded inland elevation data since 1920 at Bacon Island was found to be in good agreement with their model predictions and suggested an additional 1 m of subsidence of the island in the next 40 years (Figure 7). As the inlands subside the hydrostatic pressures on the levees increase, endangering their limited stability. In addition, since Delta

levees continuously impound water throughout the year, these earthen embankments really behave more like dams, without being designed for dam-like loading conditions.

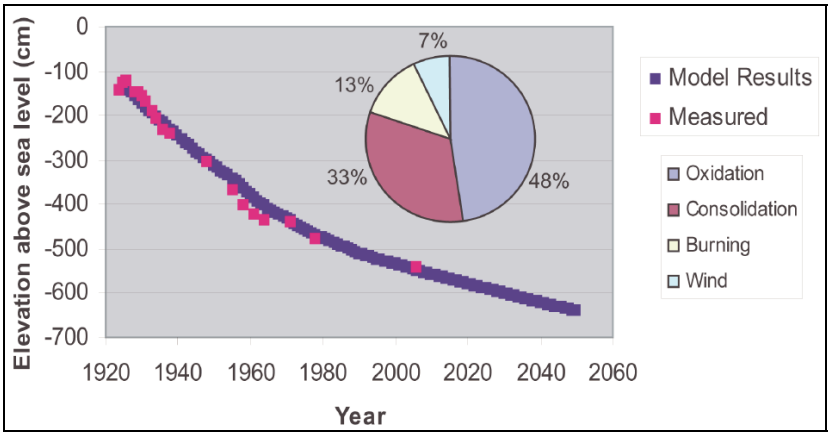

Figure 7 – Measures & estimates of elevations on Bacon Island (Deverel and Leighton, 2010)

1.3.4 Peat Characteristic and Literature Review

The behavior of organic materials has been recognized as a primary source of uncertainty in seismic risk evaluation (Boulanger et al., 2008, CDWR 2009-6). Geotechnical investigations on peat have been limited in the past by the fact that (1) this material is very compressible and therefore usually avoided as foundation of large civil infrastructures, and (2) it is mistakenly assumed an infrequently encountered material. Despite common thoughts, peatlands have been found in 175 nations worldwide (Bain et al., 2011). According to Kaat and Joosten (2008), over 4 million of squared kilometers (i.e. 3% of the world's land area) are globally covered by peatlands (Figure 8). In Europe peatlands extend to ca. 450,000 km², while the U.S.A. has the 3rd largest peatlands area (625,000 km^2) in the world after Russia and Canada (WEC, 2013).

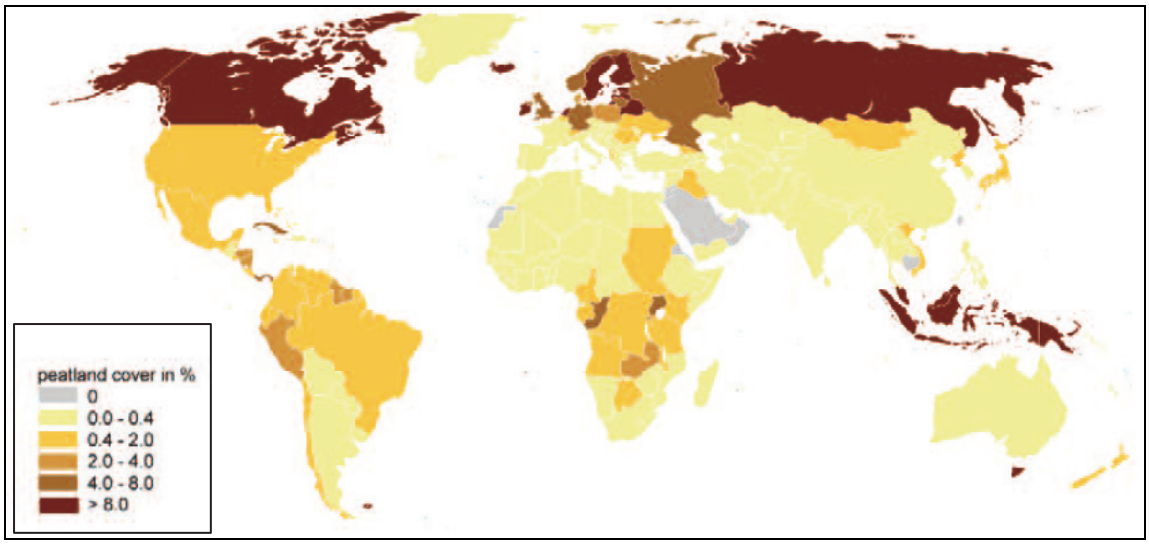

Figure 8 – Peatlands in the world (modified from Joosten, 2010)

Peat characteristics are greatly influenced by the plant debris (mosses, reeds, grasses, shrubs, trees) that originated the stratum, but its general behavior is mainly due to the slow decomposition process of the vegetation under water, which results in unique properties such as high water content (w), high void ratio (e), low unit weight (γ), small shear wave velocity (V_s), etc., and a particular fiber structure that differs significantly from that of inorganic materials.

Early literature studies on this unique geo-material investigated first its (1) consolidation behavior (Hanrahan, 1954, Adams, 1963, Berry and Vickers, 1975, Mesri and Godleski, 1977) and later the (2) dynamic response (Landva and LaRochelle, 1983, Kramer, 1996, Stokoe et al., 1996). Following an increased public interest in the performance of earthen embankments atop peat, especially in economically relevant regions such as California, Japan and Canada, further attention on both static and dynamic peat responses has been devoted in the last 20 years. This rejuvenated interest fostered a series of research efforts that greatly contributed to improve our still limited understanding of peat, and opened the doors for future work on new construction and

mitigation techniques. However, a conclusive definition of a comprehensive constitutive model for peat is still missing and seems the focus of the next decade of research projects.

Lab data suggest that general consolidation principles developed for granular materials do not apply as well to organic and fiber soils. In addition, it is often difficult to separate the stages of primary consolidation to secondary compression. Adams (1963) was one of the first researchers to discuss the micro and macro types of pores in fibrous peat and divide their contribution in the consolidation process. Kogure and Ohira (1979) proposed a volume change model for highly organic soils that captures movement of water through the pore space and within the fibers at the same time. Similar mechanism was also suggested by the rheological model of Barry and Poskitt (1972). Fox et al. (1992) observed that it is more reliable to divide the effects of primary consolidation and secondary compression by studying the variation of excess pore water pressure, and proposed a model (Fox and Edil, 1994) to consider them as concurrent phenomenon. Other researchers followed this approach (Lan, 1992, Kogure, 1993, Den Haan, 1996, Meyer, 1997), while earlier studies proposed to treat the two phases separately (Mesri and Godleski, 1977, Mesri and Castro, 1987).

Few studies in literature have proposed models to estimate consolidation settlements in peat (Kogure, 1993, Den Haan, 1996, Meyer, 1997) by relating strains to various parameters such void ratio (e), water content (w), unit weight (γ), organic content (OC), compression index (C_c), coefficient of permeability (k), elastic modulus (E), load increment ratio (LIR) and vertical effective stress (σ_v'). However, the heterogeneity of peat deposits often poses great uncertainty on such predictions. Many research teams (Kazemian et al., 2011, Huat et al., 2011, Mesri et al., 1997, Mesri and Ajlouni, 2007) have investigated the range of values of various states properties of peats and highlighted their great variability. For example, Mesri and Ajlouni (2007) conducted

an extensive study on various peats and reported characteristics such as high water contents w = 500-800%, low unit weight γ = 10-12 kN/m^3, high compression indices C_c = 2-12, and low shear wave velocities V_s = 25-100 m/s. They also found initial permeability k in the 10^{-5} to 10^{-7} range, some 100-1,000 times higher than for soft clay and silt deposits. In addition, Shafiee (2016) and Mesri and Ajlouni (2007) have shown that peat permeability dramatically drops by orders of magnitudes when subject to substantial increase in void ratio. Holtz et al. (2011) reported a correlation between the amount of settlement and the surcharge imposed on specimens, while the secondary compression index (C_α) remained essentially the same. Walker and Raymond (1968) found that the secondary consolidation rate appeared to be linearly dependent on the compression index (C_c) of the primary consolidation over the entire pressure range. While Jain and Nanda (2010) have found that smaller load increment ratio (*LIR*) leads to smaller secondary compression, previous studies from Mesri and Godlewski (1977) showed that C_α is not a function of the load increment ratio but is dependent on the applied effective stress (σ_v') and its relation to the preconsolidation pressure (σ_p).

Mesri et al. (1997) investigated the high secondary compression index (C_α) of various peats and found that the average ratio of C_α/C_c ~ 0.05-0.06 for peats to be approximately 3 times higher than that of granular soils. Dhowian and Edil (1980) observed that the secondary compression curve for peat does not follow the well-known path described for clays, presenting instead what they called "tertiary compression stage", which normally takes place after a long period of time and still under constant effective stress. This tertiary stage of course weakens the usual assumption that C_α/C_c can be considered constant. It has been recognized by many researches that the degradation which peats are subject to in lab tests can have a big influence on this

phenomenon, but Chandler and Chartres (1988) have reported a similar behavior studying field settlements of peat embankments on fibrous peat.

Estimation of pre-construction-induced settlements of soft foundations has always been a challenge for professionals, particularly since peats tend to rebound (heave) when surcharge loads are removed. Pichan and Kelly (2012) investigated techniques to accelerate the consolidation of peat soils without imposing massive fills, i.e. without employing high vertical surcharges. Their studies focused on the effect of decomposition on the compressibility of peats, and started by assuming that "the more" decomposed the peat material is, "the lower" is its compressibility. Pichan and Kelly showed that (1) fibrous peat has the potential to be decomposed further and (2) its decomposition rate could be accelerated by controlling the influencing factors (namely oxygen supply, C/N ratio, pH, temperature). Since the decomposition of organic material has a significant effect on the compression behavior of a peat deposit, the ability to pre-decompose this material may mitigate against the possibility of an increase in the compression rate observed during the tertiary compression stage. This field of research has recently become of great interest, especially for grouting techniques employing binders (Karol, 2003, Ahnberg, 2006, Kazemian et al., 2010, Kazemian and Moayedi, 2014).

Dynamic properties of peats have been investigated by various research teams using lab testing, but data in literature are still limited and only applicable to the specific materials. Boulanger et al. (1998) tested high quality samples of Delta peats in staged cyclic triaxial loading to characterize the stress-strain relationship and investigate the effects of loading frequency, structural anisotropy and consolidation stress history. Wehling et al. (2003) extended the work of Boulanger et al. (1998) and proposed modulus reduction (*G/Gmax*) and damping (ξ) curves for two sets of confining stresses. Figure 9 plots his results against the previous work of Kramer

(1996) on cyclic TXT tests on peat from Mercer Slough in Washington, and data from Stokoe et al. (1996) obtained via resonant column tests on peat from Queensborough Bridge in New York. These studies showed unusual limited shear modulus degradation up to high strain amplitudes. High damping ratios (ξ > 5%) were instead generated after 0.1% shear strain, suggesting that peats maintain an essentially linear behavior at higher shear strain thresholds than inorganic materials.

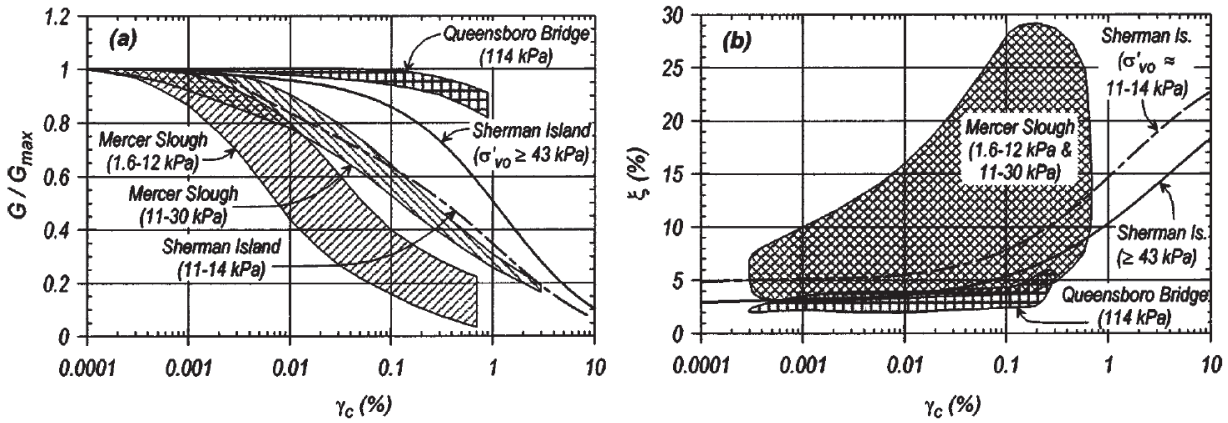

Figure 9 – Dynamic properties of peat (Wehling et al., 2003)

The effect of shear strain on pore pressure generation is a critical geotechnical aspect that has been extensively investigated for inorganic soils but not for peats. Dissipation of excess pore pressure involves significant volumetric strain because the peat is highly compressible. In case of levees atop peats this deformation could result in sufficient settlement to induce cracks or loss of freeboard. The cyclic shear strain amplitude vs. residual excess pore pressure relationship has not been investigated through experimental testing yet, and it was one of the main objectives of our centrifuge experiments. Shafiee (2016) conducted cyclic DSS constant volume tests on peat samples from Sherman Island and observed pore pressure build-up after 0.5-1.0 % shear strain

with largest residual excess pressures of $r_{u,residual}$ = 0.2-0.4 at 10-15% strain amplitudes, and proposed a regression for $r_{u,residual}$ as a function of organic content (*OC*), over-consolidation-ratio (*OCR*), number of cycles (*N*) and cyclic shear strain amplitude (γ_c). Shafiee also investigated the pre- and post-cyclic volume change properties of peat and observed a novel behavior by which the material resets the consolidation clock following cyclic straining higher than a ~1% threshold (Shafiee et al. 2015). The magnitude of post-cyclic secondary compression increases with the residual pore pressure ratio, which would result in augmented free board loss for Delta levees. Excess pore pressures in peat specimens were also observed beyond 5-10% axial strain under consolidated-undrained (CU) and drained (CD) triaxial compressions tests by Yamaguchi et al. (1985), Cola and Cortellazzo (2005) and O'Kelly and Zhang (2013) among many others. Zainorabidin and Wijeyesekera (2008) tested peat samples in cyclic TXT tests and found a relationship between pore pressure generation and frequency of loading, showing that liquefaction could be reached in the peat at critical conditions, as also testified by peat boils observed at railroads by Wong et al. (2006).

Hendry et al. (2013) collected data of pore-water pressures and settlements at three railway embankments founded on peat and observed excess pore pressures up to 9.8 kPa developing during cyclic axle loads producing cyclic vertical strains of 0.25-0.67% and horizontal at peat base of about 0.09-0.35%. The vertical strains were almost fully recoverable after train-loading, and no residual excess pore pressure ratios ($r_{u,r}$) was recorded, suggesting again an essentially elastic behavior at such strain amplitudes. Reinert et al. (2014) built a real scale model levee on Sherman Island to investigate the cyclic behavior of the underlying beneath using an eccentric shaker on the crest. Deformation of the levee could not mobilize high strain amplitudes in the foundation material, which in fact did not generate excess pore pressures, also because of the

presence of an unsaturated stratum of peat. This field experiment was among the first to investigate the embankment-soft foundation interaction. Stresses and rotations (especially at the interface) were collected to characterize the transmission of energy along the structure. Subsequent numerical analyses highlighted the substantial rocking of the embankment and critical stress concentrations at the toes. Similar conclusions were addressed by the work of Athanasopoulos-Zekkos and Seed (2013), and Lobbestael and Athanasopoulos-Zekkos (2013) through numerical simulations of model levees. Despite the scientific knowledge of the interaction problem, this feature has not been investigated through experimental testing yet. The NIST report (2012) introduced a simplified analysis for professionals to include the effects of SSI on the structure response, but the focus is on the analysis of structures atop mat or group pile foundations rather than a relatively stiffer embankment atop soft material. Kinematic and inertial interactions can play an important role in the response of the structure by lengthening the structure period and increasing the damping. These aspects can be remarkable for Delta levees, given that the wave energy propagation through the peat stratum has been shown to be substantial in either centrifuge tests (Arulnathan, 2000, Egawa et al., 2004), field data (Tokimatsu and Sekiguchi, 2006) and analytical simulations (Kishida et al., 2009b).

1.3.5 Conclusive Thoughts and Facts of the Risk in the Delta

In conclusion, all the aspects presented contribute to the risk in the Delta, with the geo-technical understanding of the peat behavior probably being the least understood. Although very little is known on the cyclic and post-cyclic behavior of peat and its interaction with superstructures, we might intuitively predict it would cause an increase in demands and a poorer response of levee

systems. This intuition seems to be confirmed by the limited field observations. Rogers (2011) reported that Delta levees dredged directly on a peat stratum performed worse than those build accreting the natural dikes, therefore suggesting that the underlying peat layer had a great influence on the levee response. Similar observations were also documented in other reconnaissance reports on the seismic performance of earthen embankments atop soft organic soils following earthquakes in Japan (Sasaki, 2009, Okamura and Tamamura, 2011). In spite of these facts, current seismic levee analysis methods do not account for potentially increased demands and reduced capacities, nor do they account for the seismic and post-seismic vertical contraction of the peat that may contribute to earthquake-induced levee deformations. In addition, regardless of the increasing head pressures and the fact that Delta levees are dated and un-engineered, California economy heavily and almost blindly relies on their safety, given that the hub of its water distribution system lies within Delta boundaries. A multiple simultaneous failures in the levee system due to exceptional events (storms or earthquakes) would potentially lead to a catastrophic scenario: saline water could start to draw back in from the Bay to fill these anthropogenic accommodations, forcing salt to intrude in the region and resulting in shutting the water delivery system down for months and destroying the local ecosystem. The salinity intrusion (Figure 10) from the bay area into the Delta varied in time and today is regulated by an upstream dam (Ingebritsen et al., 2000) which pushes it outland. A decrease in freshwater flow such in the last 5 dry years would cause salt water to migrate even more into the region in case of this catastrophic scenario. Repair operations would be costly and could take up to several years to restore the original conditions, with many cases in which the lands could be impossible to drain, resulting in a permanent change of the environment.

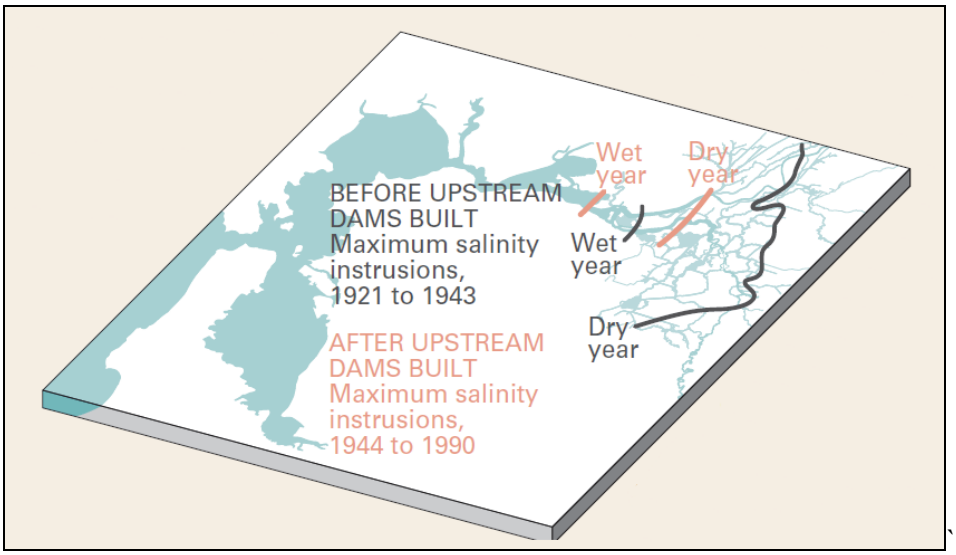

Figure 10 – Salinity intrusion in the Delta (Ingebritsen et al., 2000)

Contrary to common belief, Delta levees have failed many times. Figure 11 shows that almost all Delta islands have been inundated at least once in the last 115 years. A moderate seismic event in the region could worsen these statistics in a matter of seconds. Torres et al. (2000) investigated the probability of number of levee failures in the Delta for a 100-year seismic event and indicated an alarming 50% chance of experiencing 5 to 20 simultaneous section failures. Fortunately up to date the closest major seismic events (6.9 M Loma Prieta in 1989, 6.0 M Napa in 2014) were too far away to cause any damage. In addition, when the San Francisco earthquake (7.8 Mw) hit the Bay in 1906 most of the lands already reclaimed in the Delta were known to be under sea level, but the subsidence, and so the head pressure, was still contained (Finch, 1985). However, some seismic effects along the levee system in the Delta were described by Finch (1985), who reported a number of failures in the early 1980's directly caused by seismic events (such as 5.9 M Livermore 1980 and 6.7 M Coalinga 1983). Moreover, besides no damage was reported in the relatively "young" levee system during the 1906 San Francisco quake, some railroads, bridges and river bed sank. Today many Delta island host power or gas lines, and the

ability to operate water delivery infrastructures is also interrelated to their safety during seismic events. A thorough understanding of the seismic response of Delta levee would help averting such impending disasters.

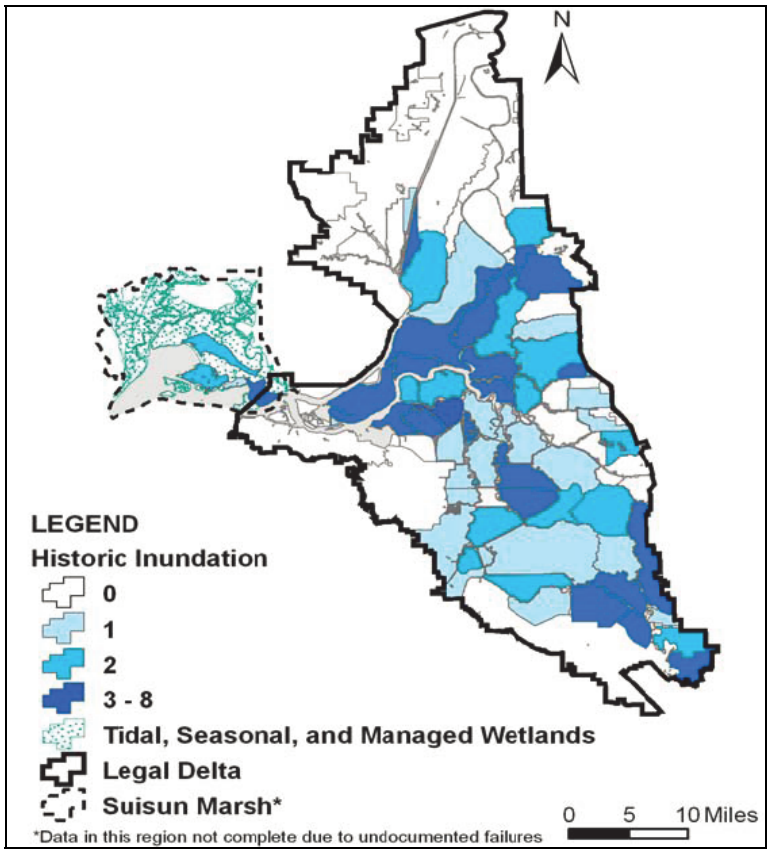

Figure 11 – Number of inundation events from levee failures since 1900 (DWR, 2007)

1.4 Thesis Structure

In the following chapters, the model construction and setup for each of the large scale centrifuge experiment is introduced (Chapter 2), followed by a description of the specimen instrumentation (Chapter 3), and the model loading and data archiving (Chapter 4). Examples of model scale

slow and fast data collected during each experiment are then presented, along with shear and pressure waves records from the bender element sensors and CPT data (Chapter 5). Project findings and related implications are then discussed in four separate chapters. Chapter 6 presents the findings on the relationship between cyclic shear loadings and excess pore pressure generation in the peat, and reviews the FEM analyses investigating strains and rocking features in the models. Chapter 7 discusses experimental data that support the proposed increase in settlement rate when peat is strained over a specific threshold. This mechanism was observed in previous lab tests (Shafiee, 2016) but was never documented experimentally before. Inertial interaction mechanisms between the stiff levee and soft foundation are the focus of Chapter 8. Chapter 9 discusses the deformation potential of model sandy levees mimicking Delta dykes when subjected to target ground motions representative of the seismic hazard of the region (~0.4g for a 500 year return period scenario). The document concludes summarizing the findings and presenting potential research that could extend this work in the future (Chapter 10), followed by References and Appendix A, which discusses challenges and solutions for achieving high degree of saturation of sands in viscous fluids.

2. EXPERIMENTAL INVESTIGATIONS

A set of small and large scale centrifuge tests at the NEES facilities at UC Davis were conducted to gain insight into the complex behavior of organic soils and shed light on the development of cyclic strains, excess pore water pressures, the interaction between the soft peaty soil and the sandy levee material as well as the potential of levee deformation/breaching under various ground motion intensities. This project consisted of eleven preliminary experiments conducted on the 1m radius Schaevitz centrifuge prior to conducting four experiments on the 9m radius large geotechnical centrifuge. An additional 1m radius test was conducted following the large experiments in order to validate part of the findings.

Table 1 lists the 16 centrifuge experiments in chronological order. This thesis specifically focuses on the large scale experiments conducted on the 9m radius centrifuge (Experiments 12 to 15). Additional information, data and reports of the small scale experiments can be found at the NEES project warehouse (nees.org/warehouse/project/1161). Experiments 12 and 13 are two phases of the same investigation, named RCK01 in compliance with the NEES@UCDavis standard to label separate centrifuge investigation with the lead student researcher's initials. Experiments 14 and 15 represent the second investigation, named RCK02. Each investigation was performed during the span of approximately 8 weeks. RCK01 was conducted in the Fall of 2013, RCK02 in the Winter of 2014.

Experiments 12 and 14 tested a non-liquefiable clay levee composed of oil-based modeling clay. After spinning up to a target acceleration of 57g the model was allowed adequate time to

consolidate and exhibit a small amount of secondary compression before being shaken by several ground motions. The objective of this stage was to investigate the seismic behavior of the peat underlying the non-liquefiable levee and the interaction between the stiffer levee and the softer foundation soil. In the following Experiments 13 and 15, keeping the same model container and peat soil, the clay levee was replaced by a saturated sandy levee without removing the container from the centrifuge arm. A target ground motion consistent with the seismic hazard analysis for the western Delta was imposed at 57g on the model resulting in liquefaction and significant settlement of the levee. For Experiment 15 only, additional weaker waves investigated the system response to possible aftershocks.

Table 2 – Summary of Experiments performed as part of this project

Exp.	Centrif. Radius	Brief Description	Investigation Phase
1	1m	Normally consolidated peat slurry under surcharge	Preliminary Schaevitz Test
2	1m	Normally consolidated peat passed through #4 sieve, under surcharge	
3	1m	Peat processed through blender, under surcharge	
4	1m	Peat passed through #4 sieve, no surcharge	
5	1m	Peat passed through #4 sieve, no surcharge	
6	1m	Sandy levee on peat shaken by strong ground motion	
7	1m	Sandy levee shaken by strong ground motion	
8	1m	Consolidation of peat under a sand layer	
9	1m	Sandy levee on peat shaken by strong ground motion	
10	1m	Saturated sandy levee constructed on arm by water pluviation	
11	1m	Clay levee on peat shaken by strong ground motion sequence	
12	9m	Clay levee on peat shaken by strong ground motion sequence	**RCK01**
13	9m	Saturated sandy levee on peat shaken by strong ground motion	
14	9m	Clay levee on peat shaken by strong ground motion sequence	**RCK02**
15	9m	Saturated sandy levee on peat shaken by strong motion & aftershocks	
16	1m	Clay levee on peat shaken by strong ground motion sequence	Confirming Investigation

2.1 Centrifuge Principles

Centrifuge modeling techniques have emerged as a very effective routine to investigate the behavior of various engineered structures such as retaining walls, bridges, foundations, embankments, etc. The main reason behind this success is the advantage of allowing collection of reliable, repeatable, and relatively inexpensive data that could be used as benchmarks of numerical modeling or real-scale simulations. Regardless of the structure, geo-materials are always involved in engineering design as foundations. Unlike other engineering materials such as wood, concrete, and steel; geo-materials are usually highly heterogeneous and nonlinear, with properties greatly depending on the stress history and current effective stresses condition. The basic idea behind centrifuge experiments is to increase the gravitational field of physical models to recreate the same stresses the model would have experienced in real-scale (in-situ conditions). Model properties at equivalent prototype scale can be calculated as a function of the centrifuge gravitational field, where the factor *N* represents the ratio between the centripetal acceleration and the earth gravitational field (1 g = 9.81 m/s^2). Following the suggestions from Kutter (1992) the scaling factors that apply to centrifuge modeling can be summarized as follow in Table 3:

Table 3 – Scale factors that apply to centrifuge modeling

Quantity	Prototype Dimension / Model Dimension
Time (dynamic)	N/1
Time (diffusion)	$N^2/1$ [a]
Displacement, Length	N/1
Volume	$N^3/1$

Mass	$N^3/1$
Acceleration, Gravity	1/N
Force	$N^2/1$
Pressure, Stress	1
Moduli	1
Permeability	*

[a] ***If the diffusion coefficient is constant (i.e. soil used in the model is the same in prototype)***

In order to collect meaningful data, it is crucial to correctly model the soil properties such that they would correspond to those at prototype scale. A useful additional reference is available at: http://nees.ucdavis.edu/principles.php

2.2 Experiment Configuration

Correct centrifuge testing can greatly depend on the boundary conditions of the geotechnical model, as suggested by the work of Whitman and Lambe (1986). The various available centrifuge containers (shear beam, hinged-plate, rigid, etc.) provide different boundary effects and should be selected accordingly. An important aspect of our investigation was the need to monitor the model and record media files during spinning. In order to achieve this goal, the transparent wall rigid container was utilized (Figure 12). The container measures 175.8 cm in length, 90.9 cm in width and 53.7 cm in height. The rigid walls of the container pose undesired boundary conditions for earthquake loading by introducing p-waves at the rigid walls oriented perpendicular to the direction of shaking (end walls). However, the rigid container was used because the value of recording video of the levee response during shaking outweighed the value of providing better boundary conditions that could be achieved, for example, using a flexible

shear beam or hinged plate container. After completion of construction, the container lid was mounted on the top in order to avoid deformations of the walls when spinning at high g-levels.

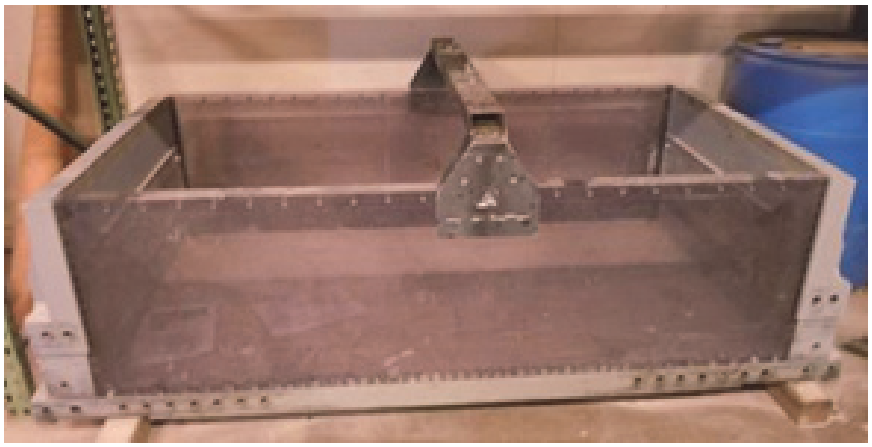

Figure 12 – Transparent walls rigid container employed

The general configuration of the four large scale centrifuge experiments considers a levee resting atop a peat layer which in turn is standing on a dense coarse sand layer. Each configuration consisted of a drainage layer of coarse sand with thickness *D* at the bottom of the model, followed by a peat layer with varying thicknesses (*H*) and a model levee consisting of (a) modeling clay (Experiments 12 and 14) or (b) saturated sand (Experiments 13 and 15), with model scale (cm) geometries as indicated in Figure 13. The model system consist of a 9 cm tall levee resting atop of a 16.5 cm and 10.5 cm thick layer of soft peat for RCK01 and RCK02, respectively. The models were spun to a centrifugal acceleration of 57g, therefore the prototype scale dimensions were a 5 m tall levee resting atop 9.5 m and 6 m of peat for RCK01 and RCK02, respectively. The peat thickness during RCK01 was selected to match conditions at a site on Sherman Island where a previous field testing program was conducted on a non-liquefiable model levee using the UCLA eccentric shaker (Reinert et al. 2014). Both cross-

sections however are typical representations of levee peat geometries in the Delta. A drainage chimney composed of coarse sand was placed against one end wall of the container to provide the dense coarse sand layer a drainage path to the surface of the model. The dense coarse sand and peat layers are common to both experiments of each investigation. Observed model configurations at 57g before applying the ground motion series for these four experiments are shown in Figure 14 to Figure 17.

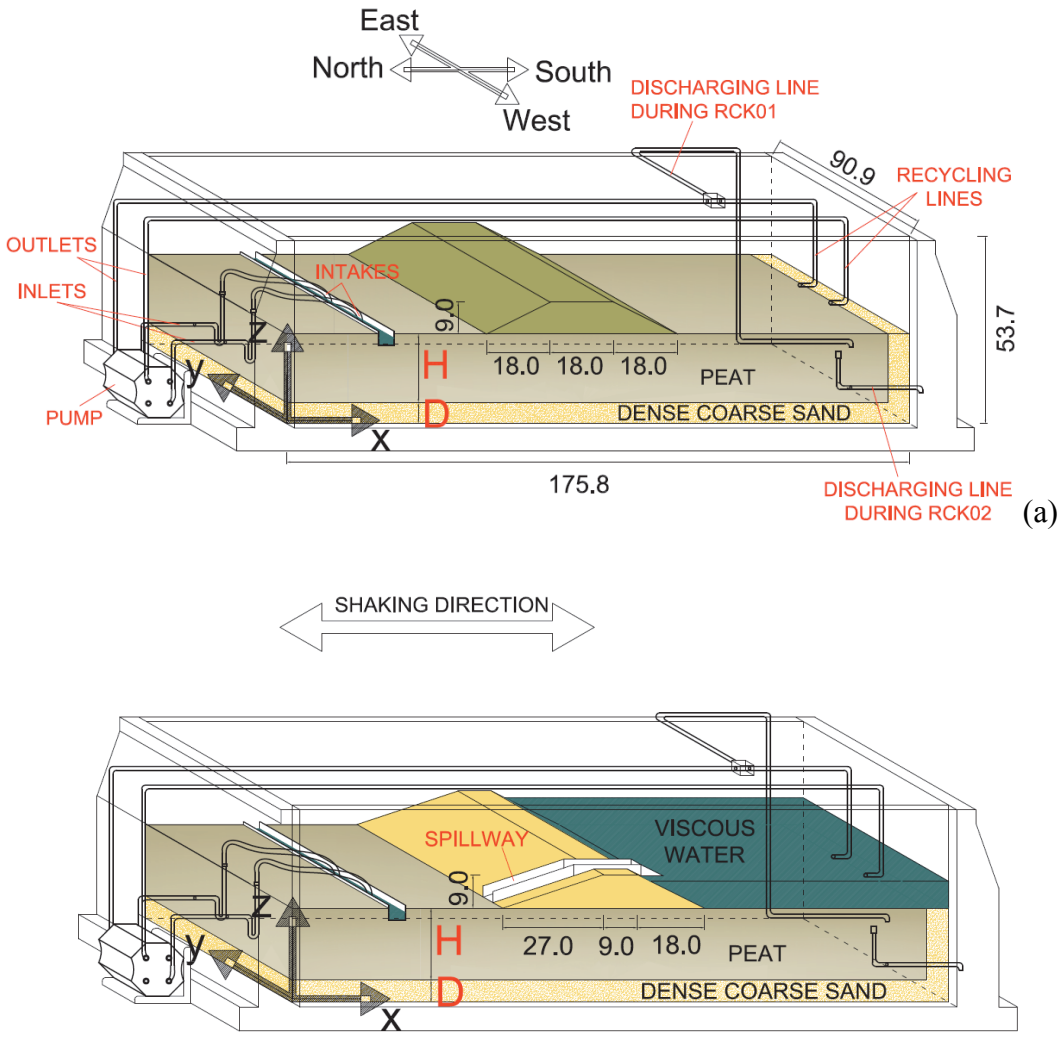

Figure 13 – General configurations (a) Experiment 12 & 14, and (b) Experiment 13 & 15

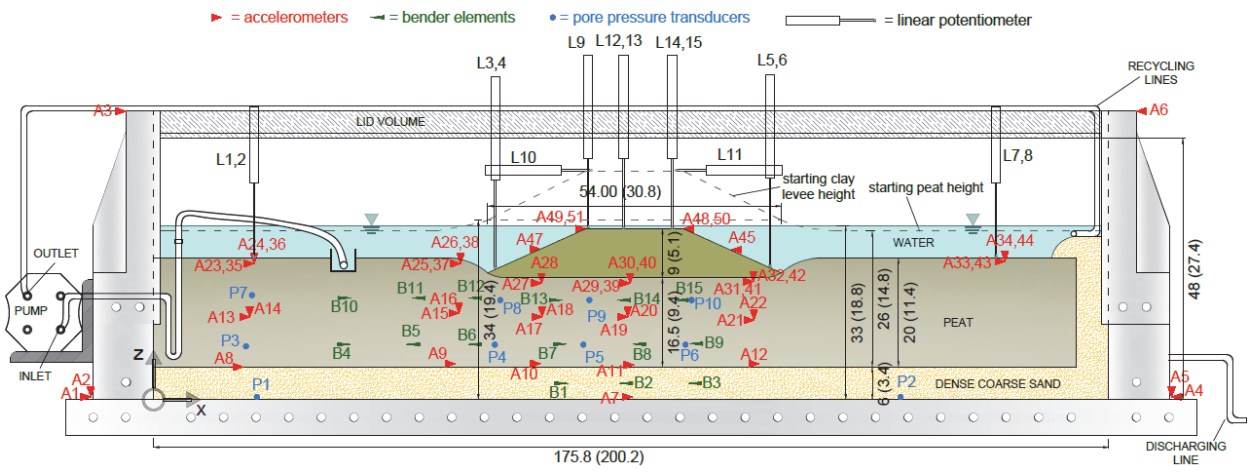

Figure 14 – Best estimate of layout of Experiment 12 at 57g after primary consolidation

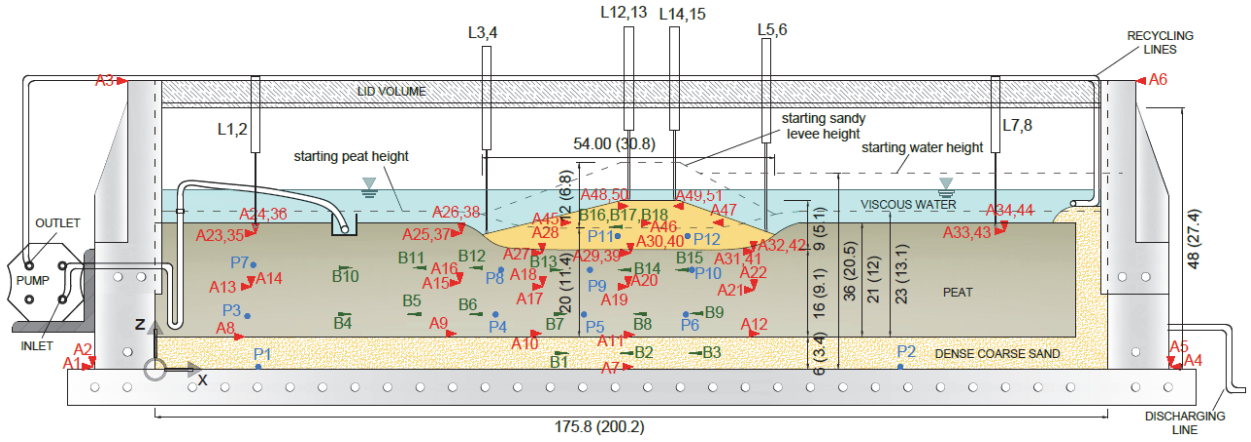

Figure 15 – Best estimate of layout of Experiment 13 at 57g after primary consolidation

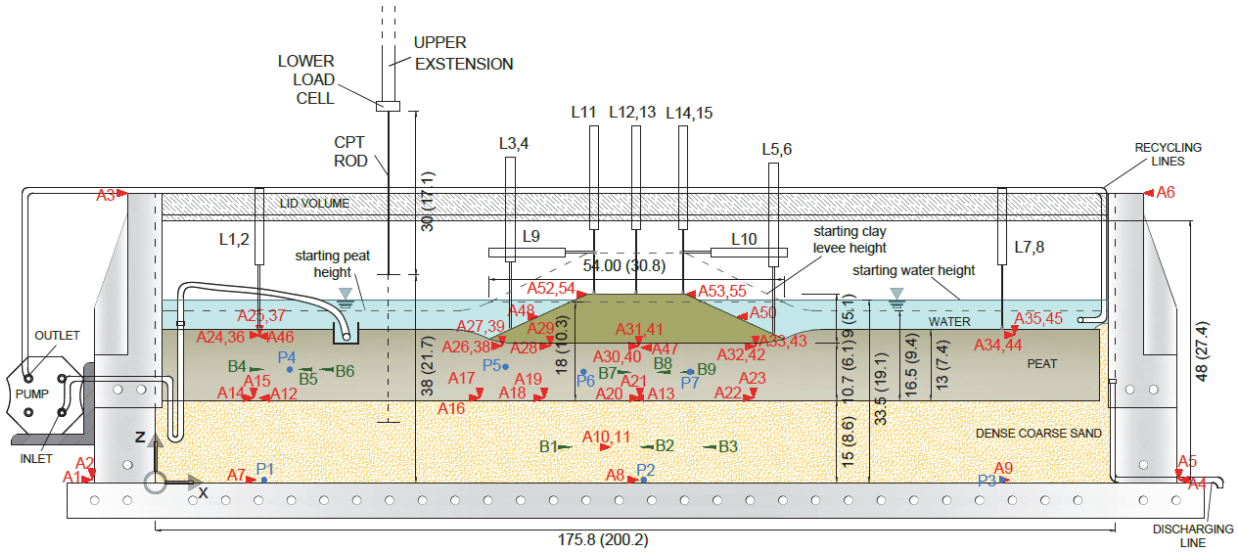

Figure 16 – Best estimate of layout of Experiment 14 at 57g after primary consolidation

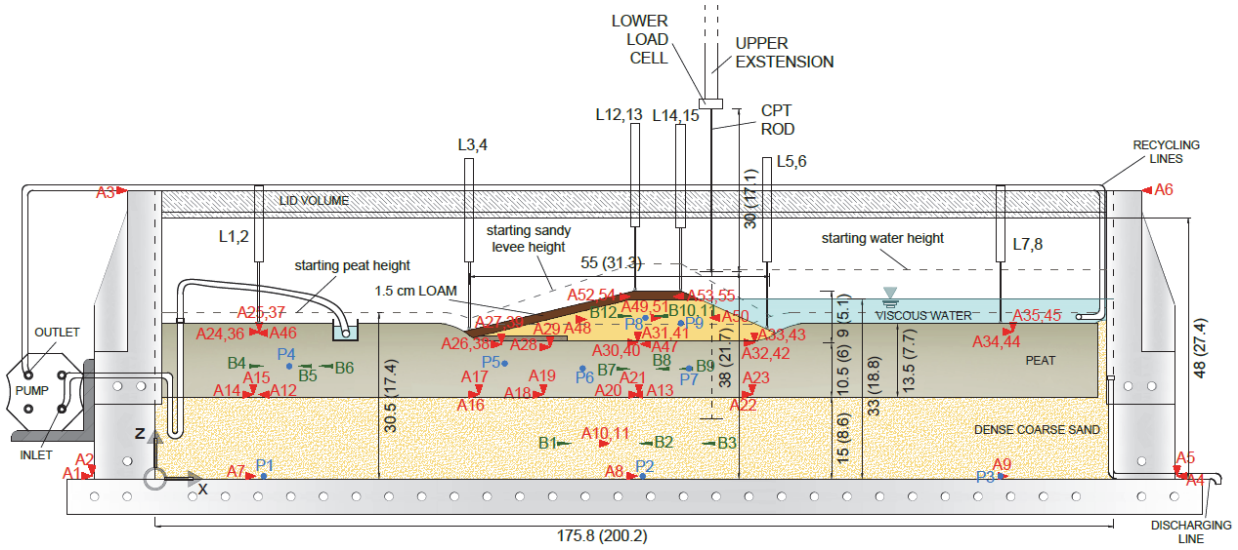

Figure 17 – Best estimate of layout of Experiment 15 at 57g after primary consolidation

2.3 Materials

The selection of the materials was a crucial step in order to properly simulate realistic field conditions. Drainage behavior, stiffness, particle size, relative density, unit weight and saturation degree are all important characteristics to replicate the response of prototype structures in centrifuge experiments. Six basic materials were used: coarse dense sand, peat, modeling clay, liquefiable levee fill, viscous pore fluid and loam (RCK02 only). Each material was selected to meet particular objectives.

2.3.1 Peat Layer

The peat was collected from Sherman Island in the Sacramento-San Joaquin Delta at the site of the study by Reinert et al. (2014), and was excavated with a backhoe from approximately 2 to 3 m below ground surface. The peat was stored in 4 plastic-lined steel 55 gallon drums. The drums were topped off with water to prevent the peat from becoming desiccated during storage. A total of four drums were collected from the site. In-situ properties of the excavated peat as summarized by Reinert et al. (2014) are presented in Table 4:

Table 4 – Properties of Sherman Island peat according to Reinert et al. (2014)

Property	Value
Average Water Content, w	450%
Average Organic Content, OC	64%
Average Total Unit Weight, γ	10.7 kN/m^3

Specific Gravity of Solids, G_s	1.85
[a] Shear Wave Velocity, V_s	25 to 30 m/s
Virgin Compression Index, C_c	3.9
Recompression Index, C_r	0.4
Initial Void Ratio, e_o	8.3

[a] Shear wave velocity measured using spectral analysis of surface waves

The excavated peat consisted primarily of a matrix of organic material with short fibers, but also had some long fibers (Figure 18) and large clumps of hard organic and inorganic material. These large fibers and hard particles were gently removed by hand so that the peat in the model container is homogeneous and representative of the soft matrix. This process was conducted extremely carefully to not squeeze water out of the fibers, and water was added to prevent evaporation. The processed material was stored inside closed barrels and kept under water. The water content of the peat ranged from 670-870% when it was removed from the barrels, and it behaved as a slurry that could be poured into the model container from a bucket.

Figure 18 – Long fibers and large particles we removed

Table 5 reports some important characteristics of the processed peat after conducting preliminary laboratory tests. The peat had a specific gravity G_s of 1.79 and an average organic content, OC, of 69%. Across an overburden pressure range of 5-150 kPa, the virgin compression index C_c and the recompression index C_r were determined to be 3.8 and 0.4, respectively. Shear wave velocity regression parameters were back calculated from bender element records collected during centrifuge testing and found to be V_{s1}= 33 m/s and n = 0.31. Initial void ratio of the peat slurry was in the e_0 = 12-15.5 range, with correspondent initial unit weight of γ= 10.28-10.41 kN/m^3.

Table 5 – Initial properties of processed peat

Property	Value
Initial Water Content, w	670-870%
Average Organic Content, OC	69%
Initial Total Unit Weight, γ	10.28-10.41 kN/m^3
Specific Gravity of Solids, G_s	1.79
Virgin Compression Index, C_c	3.8
Recompression Index, C_r	0.4
Initial Void Ratio, e_o	12-15.5
[a] Shear Wave Velocity, $V_s = V_{s1}(\sigma_v')^n$	V_{s1} = 33 m/s and n = 0.31

[a] Shear wave velocity measured using spectral analysis of surface waves

2.3.2 Modeling Clay

The clayey levee (utilized in Experiment 12 and 14 only) was built by melting modeling clay into a mold (Figure 19). The material has a unit weight of 18 kN/m^3 and its voids are full of oil,

making it essentially impermeable. The modeling clayey has a limited deformability, allowing for small differential settlements of the levee in flight. The modeling clay used is the product "Plastalina" by "Van Aken", ivory color, ID number 10110. For the modeling clay, shear wave velocity at 1g was calculated as 400 m/s. No data were recorded for the shear wave of the clayey levee at 57g, but due to the stiffness of the material and lack of consolidation during spinning, in the in-flight stiffness is anticipated to be the same as at 1-g.

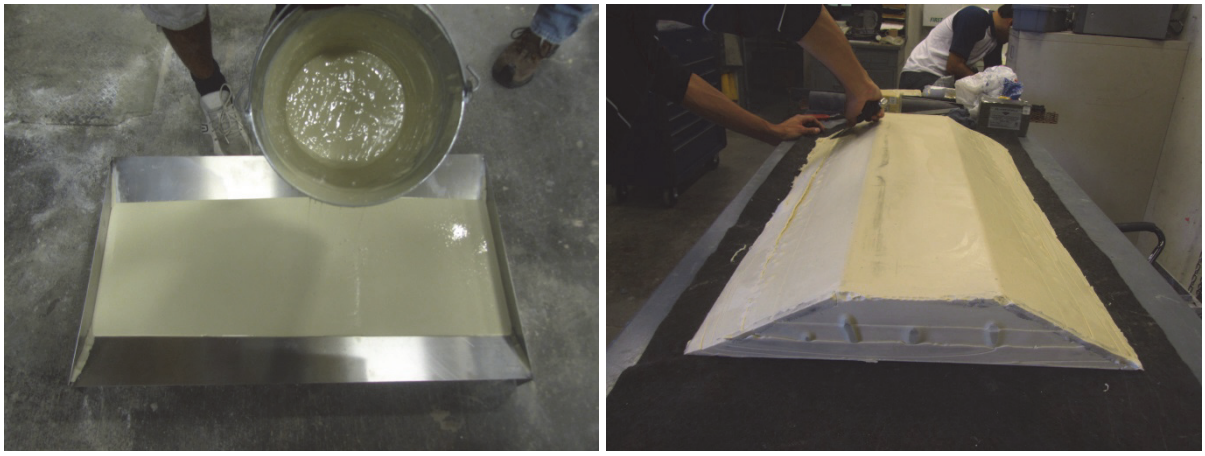

Figure 19 – Mold for melted clay and formed clay levee

2.3.3 Liquefiable Levee Fill

The liquefiable levee fill (Experiments 13 and 15) consisted of saturated Nevada sand with a mean grain size D_{50} of 0.14 mm, a specific gravity G_s of 2.66, a maximum and minimum void ratio $e_{max/min}$ of 0.78 and 0.51 respectively, a coefficient of uniformity C_u of 2, and a hydraulic conductivity (k) of approximately 10^{-3} cm/s in non-viscous water (Dashti 2009). Correct

saturation procedures for such sand were identified as an important part of testing, and are discussed in Appendix A of this thesis. The fines content passing # 200 sieve was removed from the sand during saturation procedures with a viscous pore fluid. The material was then pluviated under viscous water inside the container without air contact. The relative density, D_R, of the sand placed by this method was 27 – 58%, with an average density of 42% and a standard deviation of 8.3%. This density range matches well with D_R values of 30 – 50% observed in non-engineered hydraulic fill in the field. Water pluviation has the benefit of matching the manner in which many liquefiable sand deposits are placed. Fabric is known to exert a significant influence on liquefaction potential of sand (Abdoun et al., 2013). Shear wave velocity measurements of the material obtained during the second investigation (RCK02) suggested shear wave velocity parameters V_{s1} and n of 151 m/s and 0.228, respectively.

2.3.4 Coarse Dense Sand Layer

A coarse sand layer consisting of #0/30 Monterey Sand was placed at the bottom of the container to represent the natural geologic strata typical for the Delta, and to provide drainage at the bottom of the peat layer during consolidation. The granular material was dry pluviated to a relative density of 90%, thereby preventing liquefaction during shaking. A chimney drain constructed of the same coarse sand material was placed along the south wall of the container. Dashti (2009) determined this particular material to have a mean grain size D_{50} = 0.40 mm, a coefficient of uniformity C_u = 1.3, a specific gravity G_s of 2.64, and a maximum/minimum void

ratio $e_{max/min}$ of 0.843 and 0.536, respectively. The hydraulic conductivity (k) is approximately 10^{-2} cm/s. Shear wave velocity parameters $V_{s,1}$ and n were 195 m/s and 0.26, respectively.

2.3.5 Loam Layer Atop Sandy Levee Fill

In order to highlight the deformation of the sandy levee during consolidation and shaking stages the liquefiable levee fill was covered with about 1.5 cm of a loam-sand mix. Being darker in color compared to the Nevada sand used for the levee fill it proved to be a very effective solution to observe cracks, erosion and differential settlements during videotaping. The loam was excavated in the facility backyard and it is a typical loam frequently found in the Sacramento region near the ground surface.

Several 1m radius Schaevitz tests were conducted to test the performance of different loam-sand mixes and pluviation techniques. The selected procedure considered mixing 1/4 (in mass) of Monterey sand with 3/4 of loam, dry pluviating the mix atop the sandy levee, and then adding an additional thin layer of Monterey sand atop the loam to prevent the material from washing away during lowering of the water table on the "inland" side of the model. The material was not characterized through any test, and it was only meant to highlight the levee deformation. On the other hand it also mimic the in-situ conditions were a thin crust of vegetation and fine material covers the levee fill, lowering the hydraulic conductivity and increasing the surface roughness.

2.3.6 Viscous Pore Fluid

The body of water impounded by the sandy levee in Experiment 13 and 15 (Figure 15 and Figure 17) was made of viscous fluid obtained by adding methylcellulose to water following the recommendations of Stewart et al. (1998). The kinematic viscosity of the fluid was tested right before spinning and was found to be 18 times the viscosity of water ν = 14 cSt (1 centistokes = 1 mm^2/s) at a room temperature of 20 °C. The viscous fluid results in more realistic conditions because shaking-induced pore pressures within the levee fill would dissipate too quickly if water were used instead. The viscous fluid also reduces the-seepage, thereby reducing the volume of water that must be pumped to maintain a steady-state seepage condition. Water expelled through consolidation inevitably reduced the viscosity, which was found to be about ν = 4 cSt and 2 cSt at the end of the Experiment 13 and 15 respectively, during excavation.

2.4 Pumping System

During spinning, viscous water that seeped through the levee was collected in a U-shaped ditch installed in the downstream peat, and collected fluid was pumped back to the channel to maintain a steady-state seepage condition. Furthermore, a spillway was installed in the levee to regulate the elevation of the channel relative to the levee crest and prevent over-topping during spin up as the levee settled. For RCK01, the spillway was formed of a stiff metal U-channel that settled less than the levee during consolidation, resulting in erosion of the sand from beneath the channel. As a result, the water table was hydrostatic. A more flexible spillway was implemented in RCK02,

enabling a channel to be maintained on one side of the levee. Details and pictures of the pumping system setups of both investigations are discusses in Cappa et al. (2014 a,b).

2.5 Construction and Testing Procedures of Clayey Levee Experiments

The centrifuge model was constructed in layers with thickness determined by either the elevation at which the sensors were placed, or the elevation of the corresponding soil layers. The coarse dense sand stratum at the bottom of the model was dry pluviated in two lifts to accommodate placement of sensors after the first lift. The coarse sand was water saturated by pouring water on a sponge resting on the sand surface. Peat slurry was then poured from buckets onto the sand and smoothed with trowels at elevations where sensors would be placed. The amount of peat slurry required to achieve the target peat thickness after consolidation in-flight was based on laboratory consolidation studies (Shafiee, 2016), settlement predictions using Settle^{3D} software (version 3.0, Rocscience©) and preliminary findings from the Schaevitz centrifuge test program (Cappa et al., 2015a).

The peat slurry was too weak to support the clay levee, so a layer of Nevada sand (γ_{dry} = 17 kN/m3) was placed on top of the peat to pre-consolidate the material over the course of three days. The thickness of the Nevada sand was 3.5 cm for RCK01 and 9 cm for RCK02. Following the pre-consolidation at 1g, the Nevada sand layer along with the expelled water was removed and the clayey levee was placed on a thin (1 mm needle-punched non-woven) geotextile atop the peat to help water expelled during consolidation to escape the base of the non-permeable levee. Based on anticipated settlement of the peat beneath the levee, peat was removed from the free-field at this stage to achieve an approximately horizontal peat surface during spinning after

consolidation at 57g (Cappa et al. 2014 a,b). Final construction steps included the installation of lights, attachment of racks for sensor instrumentation, placement of all external sensors and CPT (RCK02 only), and installation of video cameras and connection of all instrumentation to the data acquisition system. Figure 20 and Figure 21 show the model for Experiment 14 before start spinning.

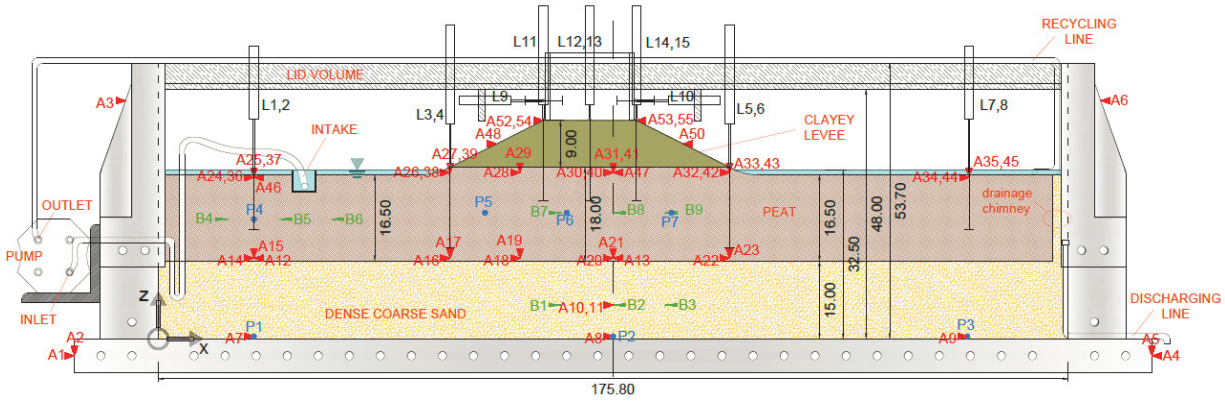

Figure 20 – Model layout for Experiment 14 before moving the model on the centrifuge arm

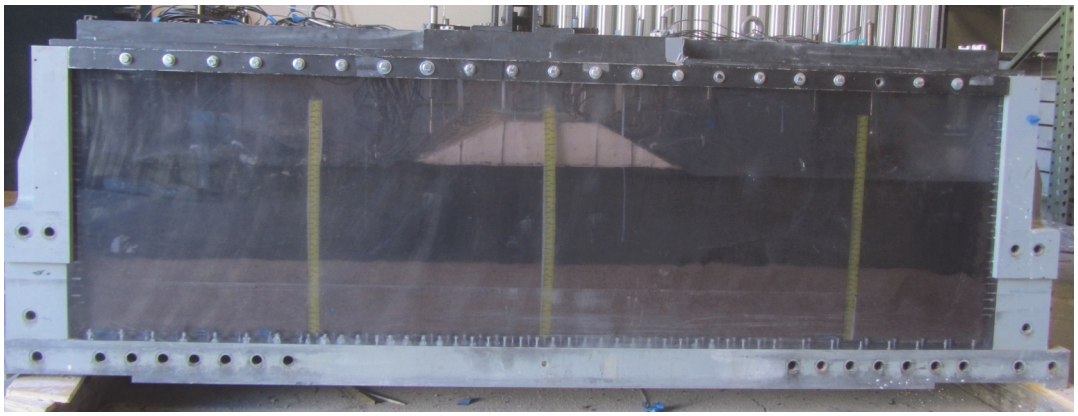

Figure 21 – Side view of Experiment 14 before moving the model on the centrifuge arm

Centrifuge spin-up proceeded incrementally to avoid undrained bearing failure of the peat, as suggested by Cappa et al. (2015a). After reaching target 57g acceleration the model was allowed to consolidate before applying the desired ground motion series.

The clayey levee was tested for two consecutive days in RCK01, the first dedicated to consolidating the peat for several hours at various g-levels (day 1), and the second to cyclic testing (day 2). During investigation RCK02 the clayey levee test required only one day because the peat thickness was less and consolidation therefore required less time, and also because we preferred a single long day of spinning rather than two separate days.

During spin-up, the levees settled significantly and became submerged in water expelled from the peat. We originally intended to pump the expelled water out of the models to bring the water table near the surface of the peat. However, the pumping system failed during RCK01, and we elected to test RCK02 with the free water in place to facilitate comparison with RCK01. Furthermore, during spin-down the peat swelled back to near its initial position, re-absorbing part of the expelled water. If this water were pumped out, the peat could have become desiccated during spin-down and we wished to maintain saturation of the peat for the sandy levee experiments.

2.6 Construction and Testing Procedures of Sandy Levee Experiments

Upon test completion, the clayey levee was removed and replaced with a sandy levee. A 10 cm wide drainage blanket consisting of coarse sand wrapped with filter paper was placed beneath the downstream toe of the levee to prevent piping erosion and maintain the phreatic surface within the levee prism. The container was filled with viscous fluid and the sandy levee was pluviated into the model. Vertical sheet metal barriers constrained the pluviated sand within the desired footprint area, and the levee was then manually re-shaped with caution to the desired geometry. The sandy levee was constructed with a 3:1 slope on the dry side to reduce the amount of erosion

due to seepage during flight and to represent typical levee conditions in the field. The upstream slope was constructed with a 2:1 angle. After water pluviation, the viscous fluid was slowly siphoned out from the dry-side of the levee only before spinning. Figure 22 and Figure 23 show the model for Experiment 15 before start spinning.

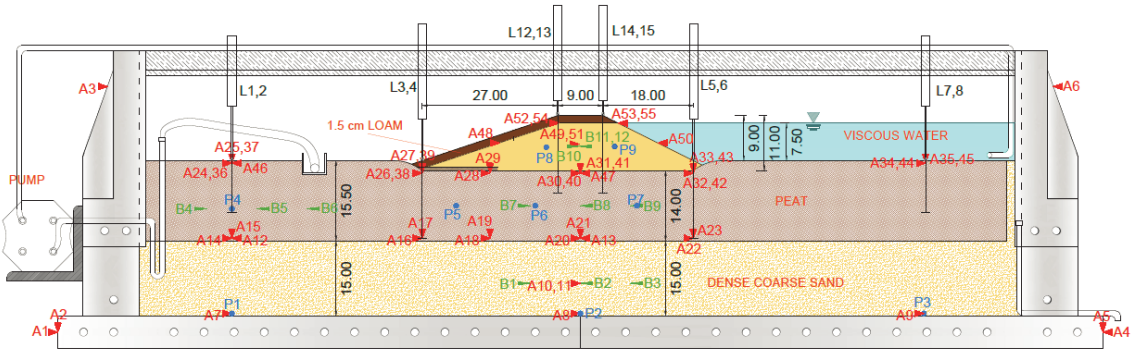

Figure 22 – Model layout for Experiment 15 before start spinning

Figure 23 – Side view of Experiment 15 before start spinning

We started to spin the model slowly increasing the g-level and monitoring the deformation of the levee. Some overtopping was observed at the very early stages of increasing velocities. Overtopping partially eroded the levee surface, but didn't prevent testing. A ground motion with

a target peak peat base acceleration of about 0.35-0.4g was applied to the model after primary consolidation was over. Video tapes and records of sensors embedded in the levee verified liquefaction mechanisms and free board loss. For Experiment 15 only, additional weaker ground motions investigated the system performance to simulate possible aftershocks. The model was finally spun down and excavated to collect additional information on the material performance.

3. INSTRUMENTATION

3.1 Sensor Types and Preparation

Sensor selection and preparation was an important task of the large scale experiments. Each experiment included more than 100 sensors. Sensors used to characterize model response include accelerometers (A) [PCB Piezotronics, models 352B68, 352C68, 352M54, 355M69, 353B18 & 353B31; range: 50g, 100g and 500g], pore pressure transducers (P) [Keller, model 2Mi-100-81840 range: 0 - 689.5kPa], linear potentiometers (L) [BEI Duncan, models: 606R6KL.12 & 604R4KL.15, stroke: 10cm and 15cm], and bender elements (BE) [Piezo Systems Inc., 2 layer transducer with PSI-5A4E piezoceramic (nickel electrodes) and brass center reinforcement]. Additional data were collected through a miniature CPT [Full axial bride HC42965, HITEC Corporation, 500 lb max load].

Accelerometers and bender elements were coated with a waterproofing layer prior to being placed into the model. Linear potentiometers were attached to racks mounted to the top of the container. Vertical linear potentiometer rods rested on small footing plates to prevent penetration into the soft soil. Horizontal linear potentiometer rods were attached to a metal frame cantilevered from the soil. These horizontal linear potentiometers provide accurate low frequency response for measuring permanent ground deformations, but the metal frame alters the high frequency response. The high frequency response is typically obtained from an accelerometer embedded in the soil near the anchor frame. Some of the accelerometers were

fastened to a right-angle connector to maintain a 90° angle between sensors, which sometimes tend to shift during model construction and/or testing on the centrifuge. Additional sensor preparation and installment solutions and details are discussed in Cappa et al. (2014 a,b).

3.2 Sensor Layout and Global Coordinates

The general instrumentation layout for each experiment is shown in Figure 15 - Figure 18. The position of each sensor was measured during installation and again during excavation following testing. The sign conventions were set to the global coordinate system; horizontal motion (X direction) is positive from north to south (Figure 24a and Figure 24b) vertical motion (Z direction) is positive upward and lateral motion (Y direction) is positive from west to east.

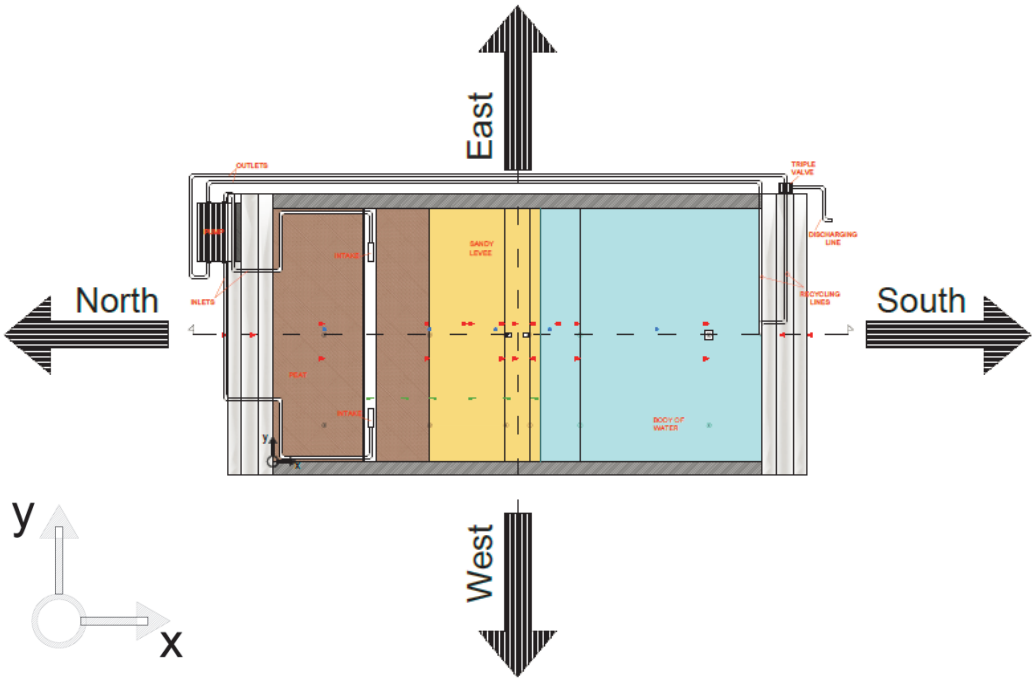

(a)

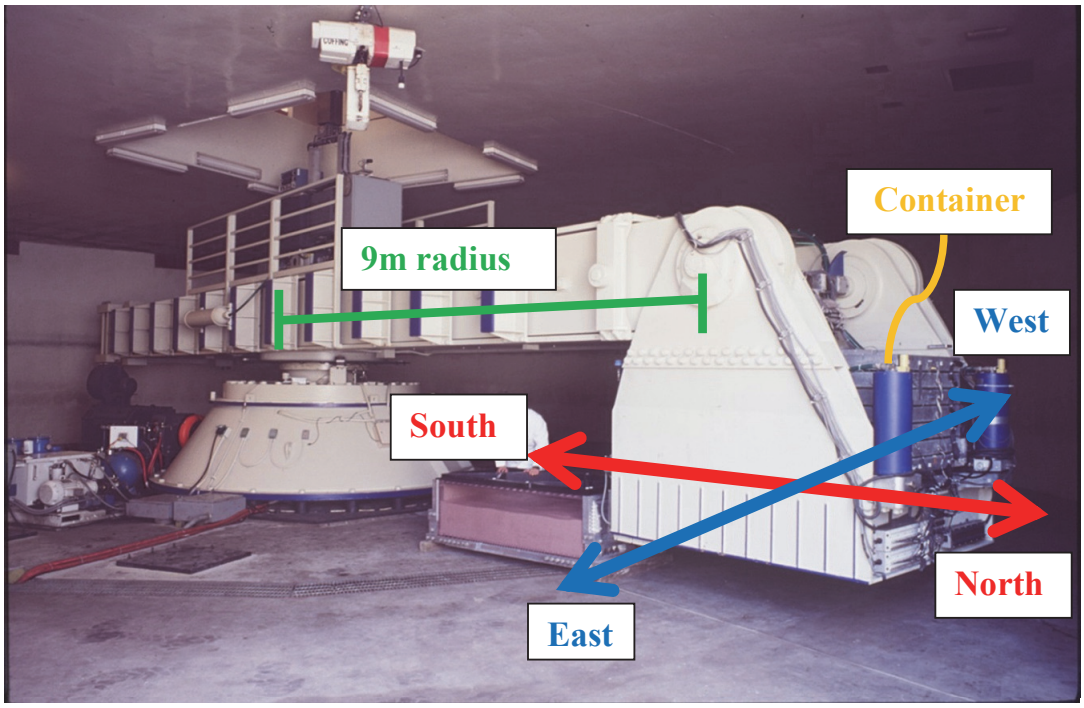

(b)

Figure 24 – (a) Local and (b) global coordinate systems in the centrifuge

Sensor lists containing sensor positions, orientations, serial numbers, calibrations and measurements are available at the NEES project warehouse. The sensor positions reported in the sensor lists represent the best estimate of the sensor positions during the stage to which the sensor lists correspond. Estimating model settlement, and by extension, the position of each sensor during spinning is a significant challenge due to the unusual high vertical strains observed during spinning in the model, dictated by the deformation of the soft organic material under increased stresses. A significant rebound during spin-down also contributed to uncertainty in estimation of the position estimates at 57g before applying the ground motion series.

Calibration factors were obtained either by applying a known load and measuring the voltage response (Ps and Ls), or by using manufacturer specifications (As). The response of the PPTs

varies with respect to the porous stones used. For our test we employed a plastic filter with pore diameter of 1000 μm. Instruments were calibrated before and after the test to verify the consistency of the calibration factors.

Some of the sensors ceased to function properly during experimental activities, and they are indicated in red in the sensor lists (see Cappa et al., 2014 a,b). Loss of sensor functionality is a natural part of experimental testing, and only a small fraction of the sensors failed to function properly. Loss of functionality was observed in 10 sensors out of 99 for the second stage of RCK01 (2 As, 2 Ls and 5 Ps), and in 3 sensors out of 96 total for RCK02 (2 As and 1 CPT load cell). Main problems regarded unusual wire stretching due to the remarkable peat vertical strains.

3.3 Videos and Photos

A total of 8 cameras (6 high-definition and 2 high-speed) were employed to record the levee behavior during cyclic loading. Two high speed cameras were mounted on the west and east side of the container and recorded through the transparent walls. These high speed cameras are "Go-pro Black Editions" that were set at a resolution of 848x480, which is the max resolution achievable with the highest possible frame rate (240 fps). Records from these two cameras are useful to analyze the behavior of the system in the instant of time when the ground motion is applied. As discussed earlier in Section 2.1, the dynamic time should be scaled by a factor equal to the g-field, therefore 1 second in model scale correspond to 57 second in prototype scale in our case, which means 1/(57/240) = 4.21 Hz in prototype = 4 frames per seconds. Due to the high quality setting, the file size is on the order of 6 MB/sec. The high definition cameras

collected photos at a 30 fps with a resolution of 2704x1524. These cameras were useful to observe the model in flight and check for possible issues.

Photos were taken throughout the experiment, from the beginning of construction until the model was taken apart. A Go-pro camera was used while work was performed on the container before and after the experiment. Photos were collected at a low frame (either 1 or 2 frames per minute) from a fixed point of view. These photos were then merged to form a fast motion clip uploaded in NEESHub (time lapse). Another camera (Canon sx210 IS, 14x zoom, 14.1 MP) was used to collect pictures from a closer distances during important construction steps. A selection of the most useful pictures is uploaded on NEESHub.

4. LOADINGS AND DATA ARCHIVING

4.1 Data Archiving

The data recorded for each experiment archived in the NEES repository (http://nees.org/warehouse/project/1161) consists of:

I. Data sampled at 1Hz for the duration of the centrifuge spin up from 1g (zero RPM centrifugal rotation rate) to 57g, during all testing activities at 57g, and during spin down of the centrifuge. The sampling rate of 1Hz is too low to capture the high frequency ground motions, and the intended purpose is to capture the low frequency model response, including consolidation behavior during spin-up and testing, dissipation of any excess pore pressures developed during shaking and the associated settlement, and heave during spin-down of the centrifuge. For this reason, this data is denoted "slow data".

II. Data sampled at 4166 Hz for about 13-18 seconds during each shake event, denoted "fast data". The purpose of fast data is to record the response of the model during centrifuge shaking. The sampling frequency is significantly higher than for typical earthquake ground motion records (i.e., 4166 Hz compared to only 200 Hz) because of the time scaling associated with centrifuge modeling and the associated high model-scale frequencies required to replicate the desired prototype ground motion.

III. Visual materials such as videos and photos taken during model construction and testing via high speed and high definition cameras.

IV. Additional records from bender elements embedded in the model.

V. Additional records from CPT pushes (Experiment 14 and 15 only).

For each Experiment, Slow and Fast Data on NEESHub are organized in Trials and Repetitions in a manner consistent with NEES data archiving standards, as shown in Table 6 for Experiment 12 to 16. An Experiment is defined as a particular configuration of the model specimen. A Trial corresponds to a single slow data record or to particular loading condition imposed on the model (i.e. an earthquake ground motions imposed on the base). Within each Trial, a Repetition is an iteration of a particular Trial. In most cases, a single Repetition was performed for each Trial because the base motions varied among the Trials. An exception is the slow data files, which are archived as Repetitions within a single Trial to avoid complicating the metadata structure. In addition to the Experiment, Trial, and Repetitions numbers, Table 6 also summarizes the date of the recordings, the observed peak base acceleration (PBA) for fast data, and the sensor list that corresponds to each Trial.

Table 6 – Records of slow and fast data for RCK01 and RCK02 available on the project warehouse

Experiment	Trial	Repetition	Date	Description	PBA at Container base (g)	Sensor List Name
12	1	1	11/4/2013	Slow data file for first spin	-	1-a
12	1	2	11/4/2013	Slow data file for first spin	-	1-b
12	1	3	11/4/2013	Rpm record	-	-
12	2	1	11/4/2013	Step wave 1	0.006	1-c
12	3	1	11/5/2013	Slow data file for second spin	-	1-d

12	4	1	11/5/2013	Step wave 2	0.006	1-d
12	5	1	11/5/2013	Sine sweep 1	0.021	1-d
12	6	1	11/5/2013	Small Loma Prieta	0.036	1-d
12	7	1	11/5/2013	Small Kobe	0.034	1-d
12	8	1	11/5/2013	Medium Loma Prieta	0.174	1-d
12	9	1	11/5/2013	Medium Kobe	0.194	1-d
12	10	1	11/5/2013	Large Kobe	0.491	1-d
12	11	1	11/5/2013	Large Loma Prieta	0.476	1-d
12	12	1	11/5/2013	Sine sweep 2	0.021	1-d
13	1	1	11/21/2013	Slow data file for second spin	-	2-a
13	2	1	11/21/2013	Step wave 3	0.005	2-b
13	3	1	11/21/2013	Moderate Kobe	0.375	2-b
14	1	1	2/27/2014	Slow data file for first spin	-	3-a
14	2	1	2/27/2014	Step wave 1	0.006	3-b
14	3	1	2/27/2014	Sine sweep 1	0.018	3-b
14	4	1	2/27/2014	Large Kobe	0.526	3-b
14	5	1	2/27/2014	Large Loma Prieta	0.439	3-b
14	6	1	2/27/2014	Sine sweep 2	0.020	3-b
14	7	1	2/27/2014	Step wave 2	0.007	3-b
14	8	1	2/27/2014	Medium Kobe	0.270	3-b
14	9	1	2/27/2014	Small Kobe	0.131	3-b
15	1	1	3/12/2014	Slow data file for second spin	-	4-a
15	2	1	3/12/2014	Step wave 3	0.006	4-b
15	3	1	3/12/2014	Moderate Kobe	0.336	4-b
15	4	1	3/12/2014	Small Kobe	0.101	4-b
15	5	1	3/12/2014	Very small Kobe	0.057	4-b
16*	1	1	9/22/2015	Slow data file for first spinning day	-	5-a
16*	2	1	9/22/2015	Slow data file for second spinning day	-	5-a
16*	3	1	9/22/2015	Strong Chile	0.85	5-b
16*	4	1	9/22/2015	Sine Sweep	0.95	5-b

**** Data files for Experiments 16 have not currently been uploaded yet online, and are expected to be available for public after Spring 2016***

For each repetition, an Unprocessed binary data file, an ASCII format Converted text file, and an ASCII format Corrected text file are uploaded to the project warehouse. The Unprocessed data is uploaded precisely as it was saved by the data acquisition system, whereas the Converted data is simply a conversion of the file from binary to ASCII format. The Corrected data (still in model

scale) are multiplied by a constant to convert data quantities to global-coordinates, and then data are truncated, offset, sorted, and merged (as described later) to ease the post-processing phase. We suggest that users of the data to download the Corrected data files rather than the Unprocessed or Converted data. Additional details on data conversion and correction are included in Cappa et al. (2014 a,b).

4.2 Applied Loading

Applied ground motions during the 9m radius experiments include: (1) scaled versions of ground motions recorded during the 1989 Loma Prieta Earthquake at the USCS/Lick Lab, Ch. 1 – 90°, and the 1995 Kobe Earthquake recorded at a depth of 83 m at the Port Island downhole array, (2) low-amplitude step waves imposed primarily to verify sensor function, and (3) sine sweeps intended to characterize the dynamic response of the model. The magnitudes of the Loma Prieta and Kobe earthquakes are in the range that contributes the most to seismic hazard in the Delta (DRMS 2009). Scaled versions of these motions with amplitudes ranging from 0.006g to 0.52g in prototype scale were imposed on the base of the model container.

For each Trial corresponding to a Fast Data, Table 6 reports the observed peak base acceleration (PBA). Additional information for each Trial is listed in Lemnitzer et al. (2015) and Cappa et al. (2014 a, b), including time stamps, duration, filename of the base motion imposed on the centrifuge model container (ASCII file format with displacement history), input parameters used (frequency and amplification factor), and applied ground motion .txt file name as saved in the DAQ system of the centrifuge.

5. SAMPLE DATA

This section presents sample data to illustrate interesting features of the test and demonstrate data quality. More complete presentation of the experimental data to support conclusions from the experimental study is reserved for future publications. Additional sample plots and details are included in Cappa et al. (2014 a,b). Figure 14 to Figure 17 and sensor lists in Cappa et al. (2014 a,b) should be consulted for locating the sensor records presented hereafter.

5.1 Slow Data Sample – Experiment 14, RCK02

Slow data were recorded at 1Hz during spin-up, for the duration of the shaking events, and during spin down to investigate the low frequency response of the model including such as consolidation settlement and pore pressure dissipation throughout the experiment. Thus, the most important slow data are collected by LPs and PPTs. Figure 25 indicates two important arrays of sensors, name hereafter FF (Free-Field) and CL (Center Levee). Given that soil behavior is highly dependent on stress history, the two arrays are expected to produce different responses.

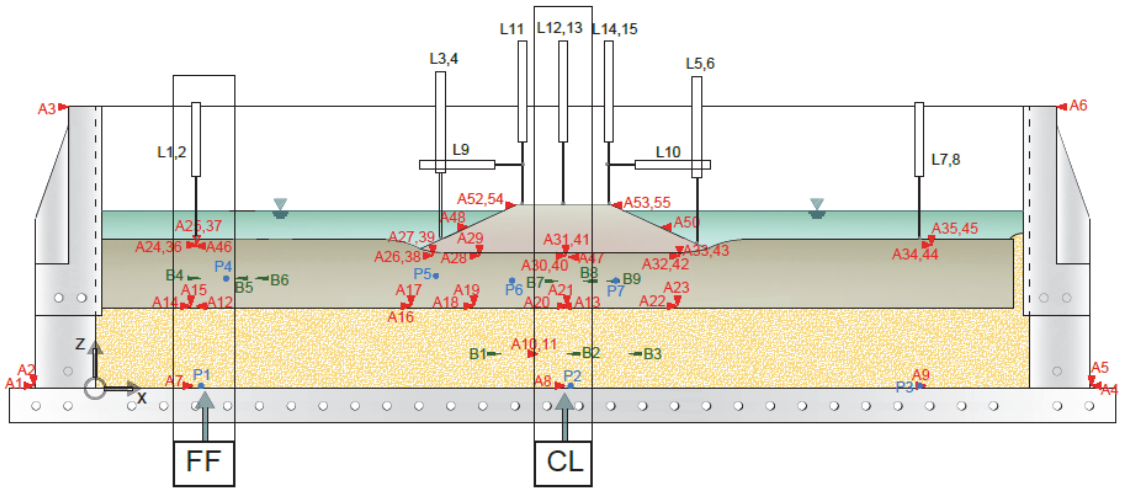

Figure 25 – Definition of FF and CL vertical arrays of sensors

Figure 26 plots the slow data recorded for two PPTS and LPs in the FF and CL arrays during Experiment 14, and shows their dependency to increased g-field, which translate in increased stresses on the soils. The model was spun for about 10 hours (model scale of time), 2.5 of which were required to spin up incrementally from 0 to 57g. After primary consolidation a series of ground motions was applied to investigate the response of the model under different scenarios. The moment of application of ground motions is highlighted with dashed vertical lines reporting the corresponding Trial. A small step wave motion (Trial 2) was first imposed to verify proper function of the sensors, followed by another small amplitude wave (Sine Sweep, Trial 3) that investigated the dynamic response of the system. Trial 4 (Strong Kobe) was the first strong motion that generated pore pressure and co-seismic settlements. The model was then let entering secondary compression phase to allow characterization of peat to post-cyclic volumetric deformation. Same approach was followed for the subsequent weaker motions, which generated a lower system response. The moment at which the model reached 57g represents the zero of the consolidation time, and it's indicated in Figure 26 by $t_{0,consolidation}$.

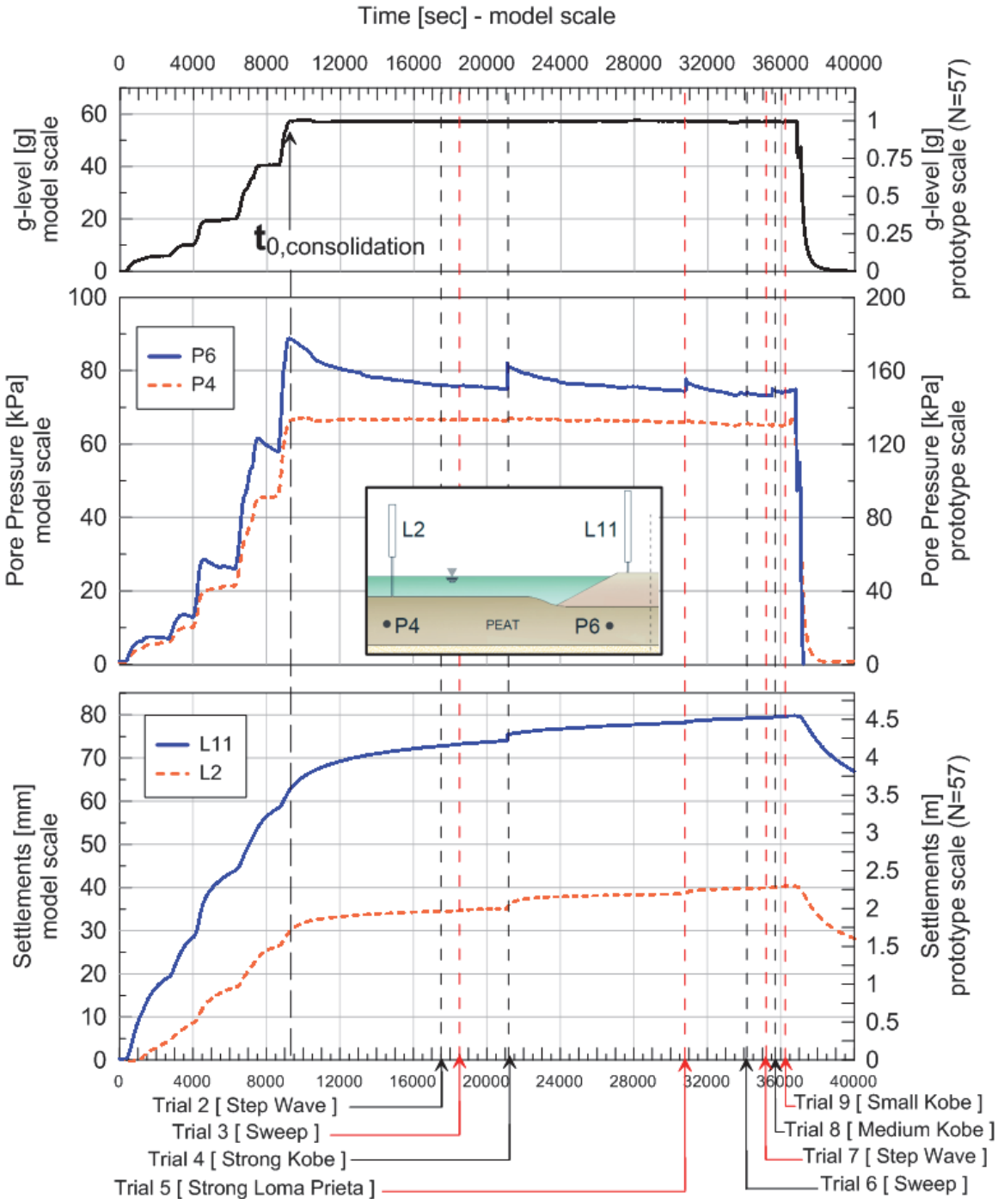

Figure 26 – Slow data for (a) acceleration field, (b) pore pressures and (c) settlements during Experiment 14, RCK02

5.2 Fast Data Sample - Experiment 14, RCK02

Fast data are sampled at 4166.6 Hz during the application of ground motions to adequately capture the dynamic response of the model. Most valuable fast data are therefore collected by accelerometers and pore pressure transducers. LP records are usually poor at such high frequency of loading, but they can still provide some insight on the system response.

Figure 27 shows sample data for selected sensors collected during the application of the large Kobe ground motion (Trial 4 in Table 6) during Experiment 14, RCK02. The ICPs records show that seismic waves propagating vertically are de-amplified and amplified differently in the FF and CL arrays. The PPT record shows pore pressure built up during shaking, while the LP indicates a co-seismic settlement of the levee.

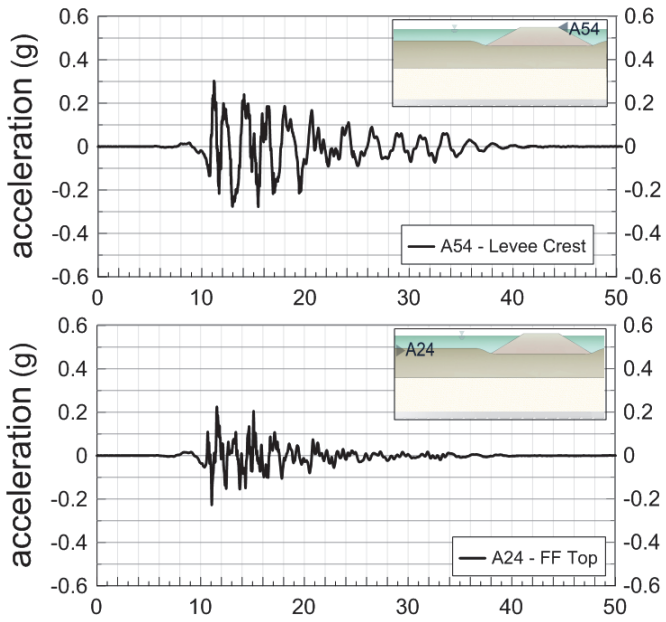

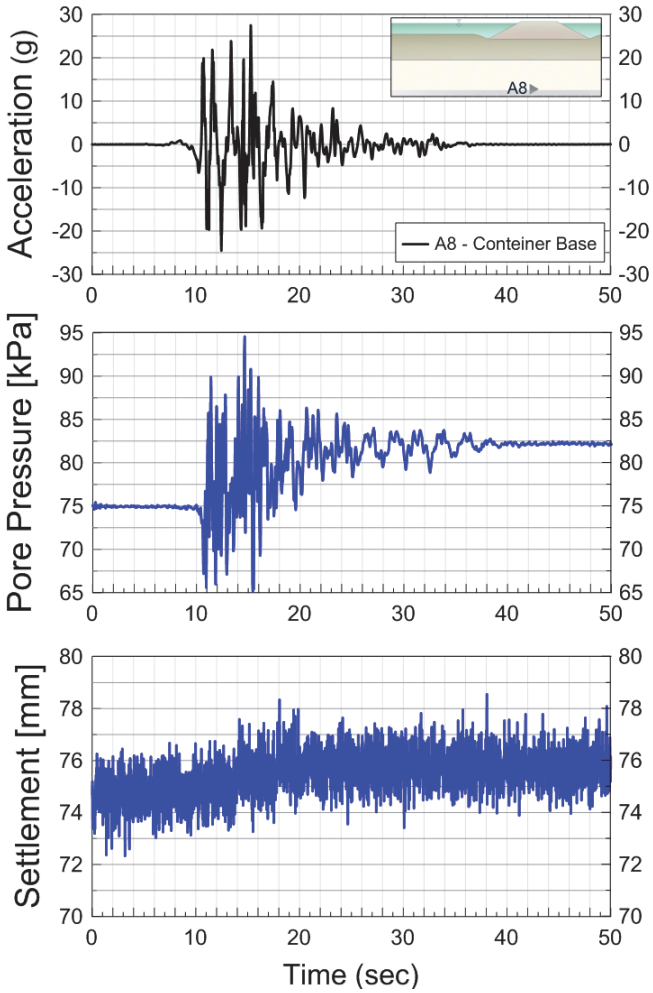

Figure 27 – Fast data for (a) acceleration at CL levee crest, (b) acceleration at FF peat top, (c) acceleration at CL peat bottom, (d) pore pressure beneath the levee and (e) settlement of the levee during Trial 4 (Strong Kobe) for Experiment 14, RCK02

5.3 Shear Wave Velocity Measurements

Experiment 12 to 15 were instrumented with multiple sets of bender elements (BE), which recorded shear wave velocities at accelerations of 1, 5, 10, 20, 40, and 57g during spin-up, thereby enabling characterization of the shear wave velocity as a function of confining pressure. Table 7 and Table 8 include BE location and direction for each experiment.

Table 7 – Bender element positions and direction before and after testing – Experiment 14 and 15

Sensor Name	DURING CONTRUCTION OF EXPERIMENT 12L						DURING EXCAVATION AFTER EXPERIMENT 13L						Layer
	DIRECTION			POSITION			DIRECTION			POSITION			
	x	y	z	x	y	z	x	y	z	x	y	z	
B1	1	0	0	76.2	46.1	2.5	1	0	0	73.3	46.2	2.3	dense coarse sand
B2	-1	0	0	85.8	46.1	2.5	-1	0	0	83.7	45.4	2.5	
B3	-1	0	0	98.5	49.4	2.5	-1	0	0	95.4	49.5	2.8	
B4	1	0	0	36.2	18.9	12.9	1	0	0	35.5	18.7	10.9	peat layer
B5	-1	0	0	46.6	20.3	12.9	-1	0	0	43.2	27.5	8.4	
B6	-1	0	0	58	20.2	12.9	-1	0	0	56	19.9	9.1	
B7	1	0	0	76	25.9	16	1	0	0	78.6	22.6	10.8	
B8	-1	0	0	88.2	28.1	15.3	-1	0	0	88.1	27.8	11.5	
B9	-1	0	0	98.7	24.6	16.1	-1	0	0	101	23.2	11.1	
B10	1	0	0	36.3	23.3	27	1	0	0	30.2	24.7	22.7	
B11	-1	0	0	47.6	22.7	27	-1	0	0	40.5	23.6	21.8	
B12	-1	0	0	5.8	21.9	27	-1	0	0	49.5	20.4	23.9	
B13	1	0	0	75.2	23.3	33	1	0	0	71.2	23.4	21.5	
B14	-1	0	0	85.4	22	33	-1	0	0	83.6	22.7	21.5	
B15	-1	0	0	96	22.7	33	-1	0	0	97	22.1	22.2	
B16	-	-	-	-	-	-	0	1	0	84.8	30.7	30.8	liquefiable levee fill
B17	-	-	-	-	-	-	0	-1	0	78.6	43.1	30	
B18	-	-	-	-	-	-	0	-1	0	83.8	39.1	30.3	

Table 8 – Bender element positions and direction before and after testing – Experiment 14 and 15

Sensor Name	DURING CONTRUCTION OF EXPERIMENT 14M						DURING EXCAVATION AFTER EXPERIMENT 15M						Layer
	DIRECTION			POSITION			DIRECTION			POSITION			
	x	y	z	x	y	z	x	y	z	x	y	z	
B1	1	0	0	76.2	28.6	7	1	0	0	75.8	28.6	7	dense coarse sand
B2	-1	0	0	88.8	27.5	7	-1	0	0	88.2	27.4	7.3	
B3	-1	0	0	100.3	29.8	7.3	-1	0	0	99.3	30	7.2	
B4	1	0	0	19.8	28.6	24.7	1	0	0	19.5	27.9	22.5	peat layer
B5	-1	0	0	26.3	28.7	24.7	-1	0	0	23.5	28.2	22.3	
B6	-1	0	0	30.1	26	24.4	-1	0	0	24.6	25.6	22	
B7	1	0	0	87	28.1	27.9	1	0	0	84.5	27.1	20.3	
B8	-1	0	0	91.9	23.9	27.7	-1	0	0	90.9	21.6	21.3	
B9	-1	0	0	96.2	28.2	27.5	-1	0	0	98.7	26.1	22	
B10	1	0	0	91.6	17	36	0	1	0	88	22.1	31.3	liquefiable levee fill
B11	-1	0	0	91.6	21.6	36	0	-1	0	94	22.2	32.5	
B12	-1	0	0	87.4	21.6	35.5	0	-1	0	93.2	18.2	32.7	

Figure 28 presents a sample measurement of shear wave velocities during RCK02 at 57g. The bender elements exhibited capacitive coupling with the conductive peat soil, and the desired elastic wave signal is superposed on an undesired portion of the signal corresponding to capacitive decay. The travel time corresponding to first arrival of the shear wave can nevertheless be measured from the two receivers, enabling calculation of the shear wave velocity.

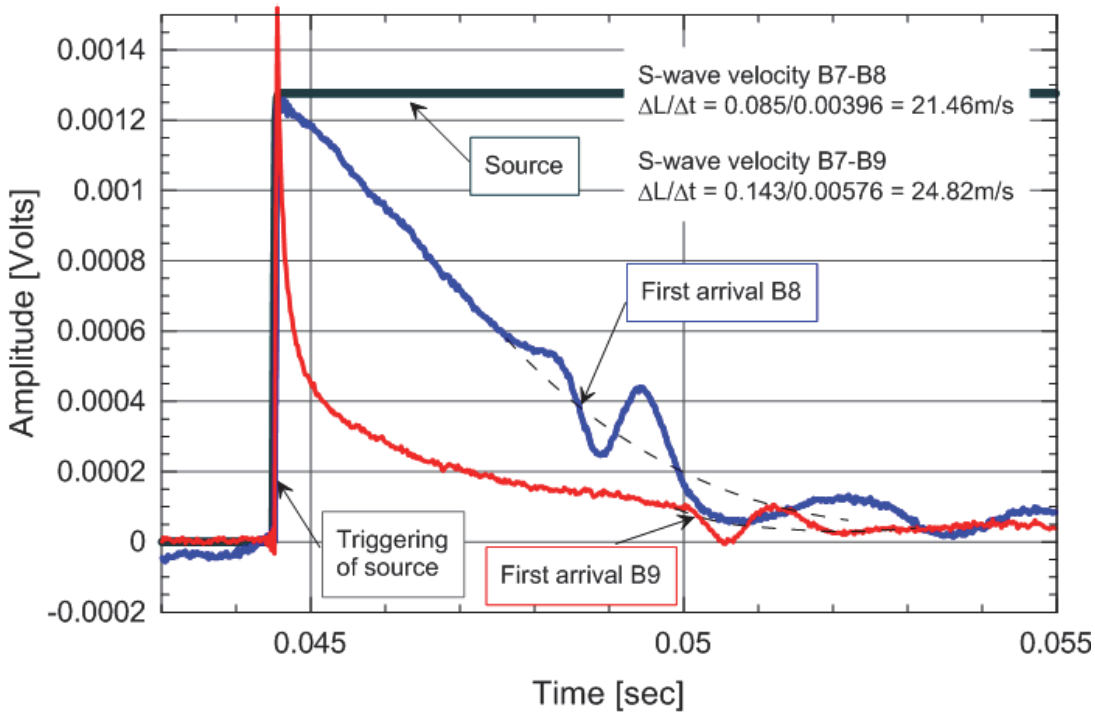

Figure 28 – Sample data for the BE set in the peat layer CL array at 57g during Experiment 15

Equation 1 is a general form for characterizing shear wave velocity as a function of vertical effective stress, σ_v':

Equation 1 – $V_s = f(V_{s1}, \sigma_v', p_A, n)$

$$V_s = V_{s1} \cdot \left(\frac{\sigma_v'}{p_A} \right)^n$$

where *pA* is the atmospheric pressure (1 atm = 101.3 kPa). By plotting shear wave velocities measured across a range of centrifugal accelerations, the parameters *Vs1* and *n* can be determined via least squares regression, as shown in Figure 29.

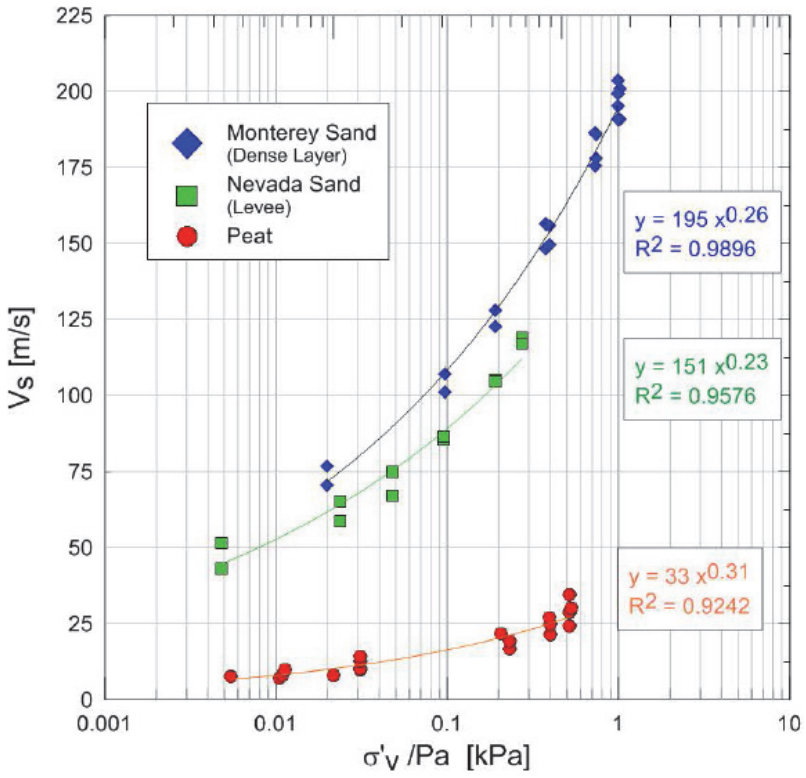

Figure 29 – Regression of *Vs1* and *n* parameters for the soil layers

5.4 Compression Wave Velocity of the Peat

P-wave velocities were measured at 1g by gently striking the top of the modeling clay levee and measuring the downward-propagating compressive wave using vertical accelerometers. P-wave signals were recorded at a sampling rate of 16,666 Hz. The p-wave velocity of the peat was found to be approximately 419 m/s in RCK01 and approximately 172 m/s in RCK02. Both measurements indicate that the peat was unsaturated. This is consistent with field conditions, in which the peat holds a significant amount of entrapped gasses due to its past and ongoing decomposition. Figure 30 shows sample data for P-waves records collected for RCK01 at 1g.

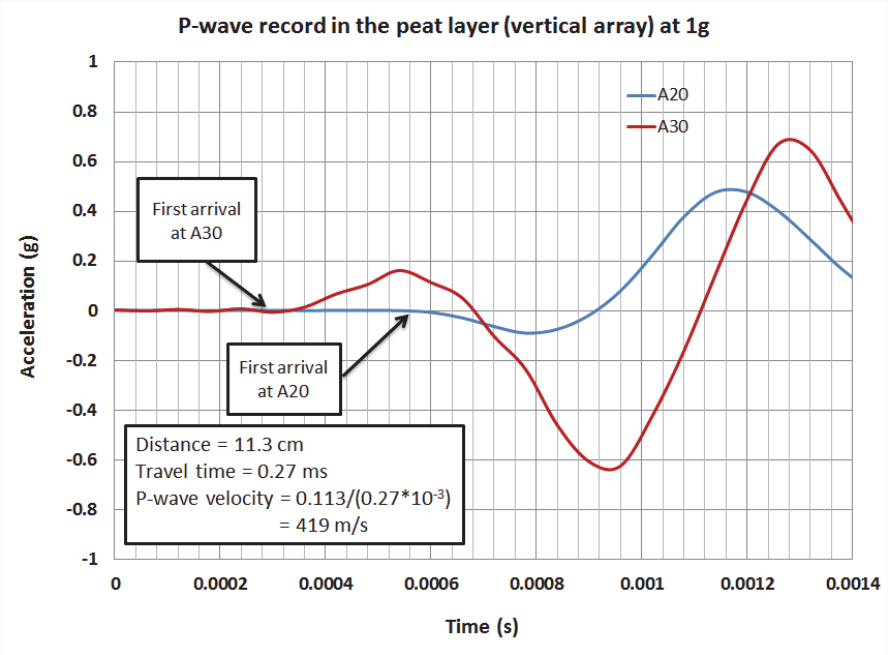

Figure 30 – Records from ICPs in the peat at 1g, RCK01

5.5 CPT Records for Experiments 14 and 15

A miniature CPT test was performed in-flight during RCK02, measuring tip resistance over a depth range of 27 cm. The CPT apparatus [Full axial bride HC42965, HITEC Corporation, 500 lb max load] was placed in the free field region during Experiment 14 (Figure 31) and was pushed through the mid-point of the upstream levee slope during Experiment 15 (Figure 32). CPT testing was performed before and after Trial 4 in Experiment 14, and before Trial 2 as well as 6 after Trial 3 during Experiment 15. The free-field peat exhibited a very low tip resistance that increased slightly with depth (Figure 33), reaching a maximum near 0.24 MPa at the bottom of the peat layer. The relatively low tip resistance is due to low consolidation stresses in the free field. By contrast, the resistance in the peat beneath the sandy levee was significantly higher,

increasing from about 0.5 MPa at the top of the peat to 1.0 MPa at the bottom of the peat. Consolidation stresses from the overlying levee clearly increased the peat strength. Tip resistance increased dramatically below the peat as the CPT probe pushed into the dense coarse sand.

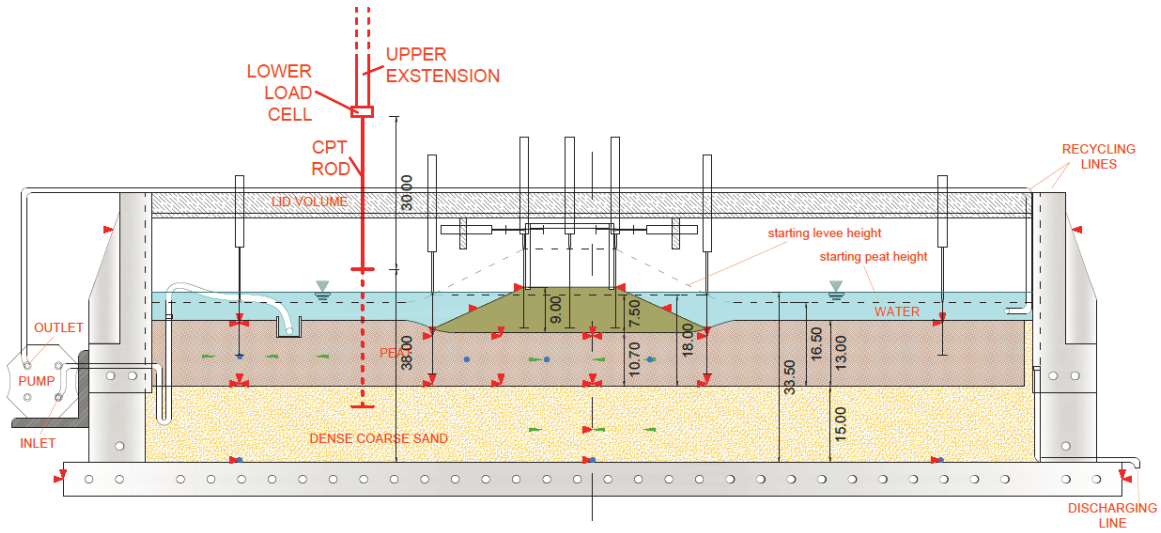

Figure 31 – Location of CPT during Experiment 14

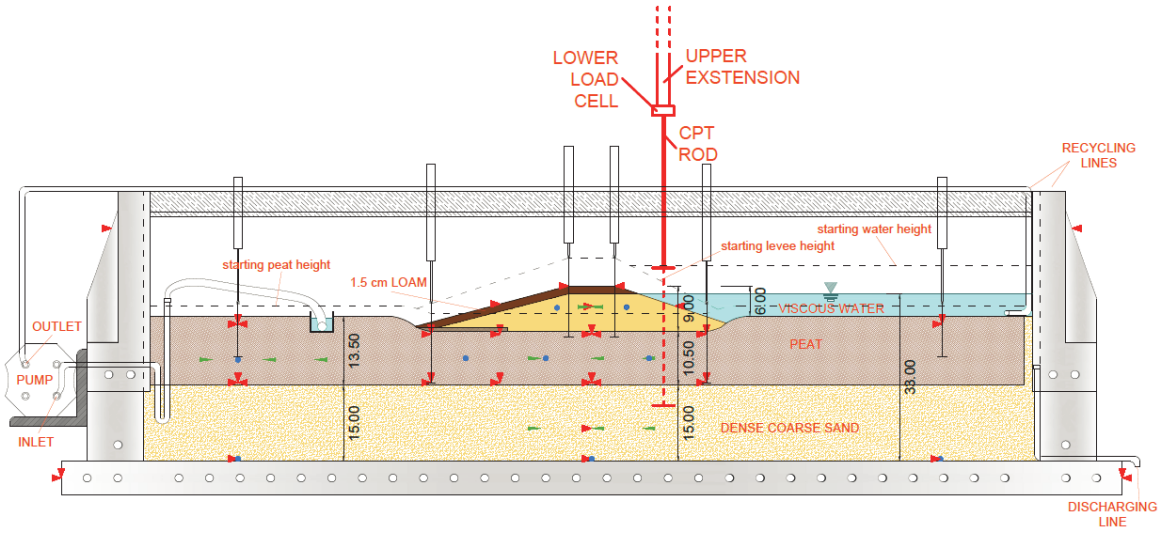

Figure 32 – Location of CPT during Experiment 15

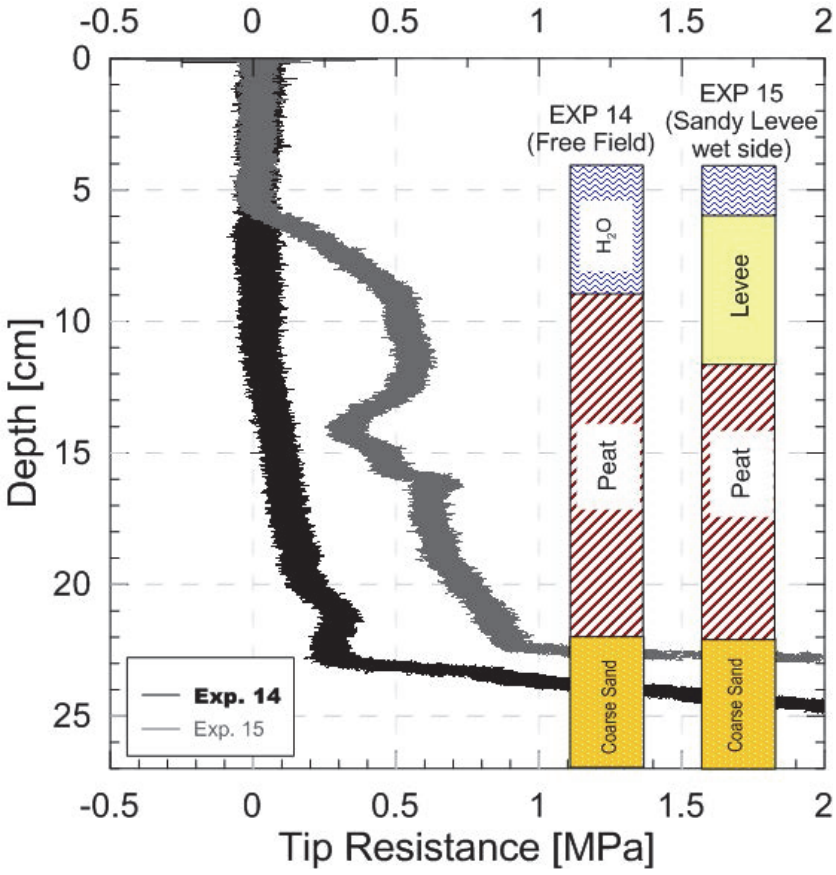

Figure 33 – Example of CPT record for Experiment 15

6. CYCLIC STRAIN AND EXCESS PORE PRESSURE GENERATION

Cyclic and post cyclic behavior of organic foundation soil can increase demands on embankments and likely induce extra settlements because dissipation of excess pore pressures in this soft material involves remarkable volumetric strains. The relationship between cyclic straining and pore pressure generation in peats has not been conclusively understood and is the focus of this chapter.

6.1 Introduction

Correlations between cyclic strain amplitudes and excess pore pressures in peaty soils have previously been documented via field and lab testing. For example, Hendry et al. (2013) collected data of pore-water pressures and settlements of three railway embankments founded on peat. Under heavy axle railway loading, Hendry et al.'s results show maximum excess pore pressures of Δu = 9.8-10.7 kPa generated for cyclic vertical strain magnitudes of γ_c = 0.36 - 0.67%. It was observed that vertical strains of such low amplitudes were fully recoverable after train-loading and no residual excess pore pressure ratios ($r_{u,r}$) were recorded after 3 hours. The data suggest an essentially elastic behavior of peat at low strain amplitudes.

Much higher strain amplitudes and excess pore pressure ratios were reached via triaxial laboratory testing. Moreno and Rodriguez (2004) performed a series of cyclic triaxial tests for Bogota peats and observed an exponential relation in log scale of shear strain vs excess pore

pressure ratio for a peat sample under an effective stress of 55 kPa. Under strain controlled loading, they mobilized cyclic strain amplitudes between 0.13 – 1.46% which generated peak excess pore pressure ratios up to 0.16 after 10 cycles. Impedance ratios of ≤0.7 were observed after 1% cyclic shear strain threshold, which the authors indicated as the validity limit for equivalent linear dynamic analysis. Yamaguchi et al. (1985) tested peats with Loss of Ignition of L_{ig} = 10-70% in monotonic triaxial undrained conditions and observed excess pore pressure ratios of r_u = 0.4-0.8 at axial strain amplitudes of ε_a = 10%, with the lower ratios for L_{ig} < 40%. Using similar testing conditions but different peats, Andersland et al. (1981), Oikawa and Miyakwa (1980), Marachi et al. (1983) and Cola and Cortellazzo (2005) found excess pore pressures can equal confining effective stresses in monotonic tests at axial strain amplitudes of approximately ε_a = 15%, 10%, 10% and 5%, respectively. Excess pore pressure ratios of 1.0 were also observed in cyclic triaxial tests by Zainorabidin & Wijeyesekera (2008), which indicated a relationship between excess pore pressure magnitude and loading frequency.

The potential for liquefaction of organic soils is also suggested by field observations. Peat boils and ejections along rail embankments were documented by Wong et al. (2006), proving that peat could reach liquefaction under certain loading conditions. They indicated the stress redistribution during cyclic axle loading between the stiff levee fill and the soft organic soil as a possible mechanism leading to vertical piping effects through the foundation material.

Samples of Delta peats have been studied to characterize the dynamic parameters (Boulanger et al. 1998, Aulnathan et al., 2001, Wehling et al., 2003) and consolidation properties (Cappa et al. 2015, Shafiee et al. 2013, Marachi et al., 1983), but little is known regarding the relation between excess pore pressure generation and cyclic straining. Boulanger et al. (1998) found excess pore pressure can equal radial confining stress in slow monotonic triaxial tests on high quality

samples of Delta peats. Moss and Hollenbak (2011) investigated the large strain dynamic response of peaty samples manufactured to closely mimic undisturbed Delta specimens, and observed maximum excess pore water pressure ratios of 0.4-0.45 in cyclic stress-controlled ICU TXT tests after 30 cycles at 1 Hz for cyclic-stress-ratios up to CSR = 0.5. Wehling et al. (2003) extended the work of Boulanger et al. (1998) on field samples from Delta islands and observed r_u = 0.05-0.55 after the last loading cycle generated shear strain amplitudes of γ_c = 9% in cyclic ICU TXT tests. According to their assumptions following considerations on quantum mechanics, cyclic TXT shear strain in the nearly saturated peat can be estimated as 1.5 times the axial strain for undrained condition and implied Poisson ratio of r_u = 0.5. Prevost (1977) suggested a correlation of $\gamma_c = 1.73\ \varepsilon_a$ is instead derived if incremental theory of plasticity is used.

Strain thresholds for organic materials are therefore thought to be larger than thresholds for low plasticity clays (0.024-0.06% [Hsu and Vucetic, 2006]), high plasticity clays (0.035-0.08% [Mortezaie, 2005, thesis]) or granular soils (0.01-0.02% [Dobry et al., 1982]). The higher peat threshold could be attributed to the larger amount of energy required to disturb the fiber matrix of the organic soil (Wehling et al., 2003). Wehling's results indicated that shear strains less than 0.1% produce relatively low amounts of fiber breakage or unrecoverable slippage, and essentially result into elastic material response during straining.

This chapter presents strain and pore pressure measurements from Experiment 14 that were used to evaluate the strain threshold for excess pore pressure generation of peat. Centrifuge data were compared to lab DSS test (Shafiee, 2016) and found to confirm an approximated 1% cyclic shear strain threshold for excess pore pressure generation. In addition, calculated vertical strains at different locations beneath the embankment proved a substantial rocking of the super-structure, indicating that SSI effects are non-negligible. Levee-foundation interaction has not yet been

documented experimentally, although increased demands on the embankment systems due to inertial effects were postulated in previous studies via 2D numerical simulations (Athanasopoulos-Zekkos and Seed, 2013, Reinert et al., 2014) estimating cyclic-stress-ratios (CSR) and peak accelerations along the embankments section. Their calculated predictions of high CSRs in the region beneath the toes and increased crest accelerations are in agreement with the rocking-interaction described here.

6.2 Centrifuge Experiments

Experiment 14 forms the basis for the following strain analyses. This experiment in introduced in Section 2.2, Figure 16. Corresponding specimen materials and their properties are discussed in Section 2.3. The unit weight, void ratio, and shear wave velocity of the peat depend significantly on stress history and can be computed for a particular vertical effective stress, σ_v', and maximum past pressure, σ_p' using Eqs. 2-4 where the reference void ratio e_{ref} = 9.6 and the reference vertical effective stress $\sigma_{v\,ref}'$ = 10 kPa. The peat consolidation behavior is highly nonlinear in e-$\log\sigma_v'$ space at low effective stress (Cappa et al. 2015), therefore the void ratio should not exceed 13.8, which is the void ratio for the peat slurry prior to placement in the model. The vertical effective stress profile at 57g after consolidation was computed using the Rocscience software package, Settle3D, and is presented in Figure 34.

Equation 2 – e = f (C_c, σ_p', $\sigma_{v,ref}'$, C_r, σ_v')

$$e = e_{ref} - C_c \cdot \log\left(\frac{\sigma_p'}{\sigma_{v,ref}'}\right) + C_r \cdot \log\left(\frac{\sigma_p'}{\sigma_v'}\right) \leq 13$$

Equation 3 – γ_{sat} = f (γ_w, G_s, e)

$$\gamma_{sat} = \gamma_w \frac{G_s + e}{1 + e}$$

Equation 4 – V_s = f (V_{s1}, σ_v', p_A, n)

$$V_s = V_{s1}\left(\frac{\sigma_v'}{p_a}\right)^n$$

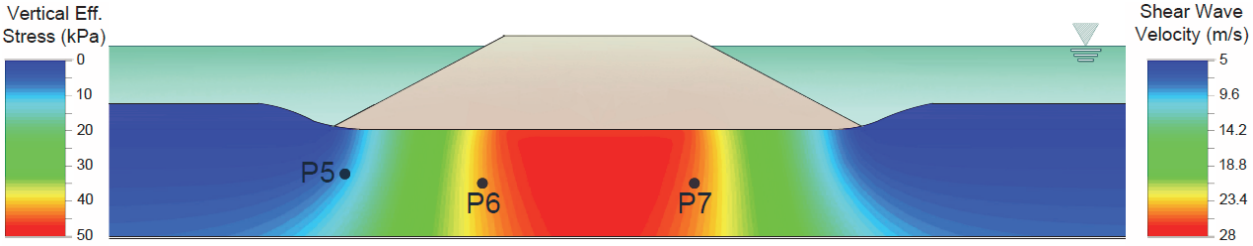

Figure 34 – Vertical effective stress and shear wave velocities profile of the peat stratum at 57g

6.3 Experimental Results & Data Analysis

Figure 35 shows samples of fast data recorded during Experiment 14 for Trial 4 (Strong Kobe). Acceleration records show that base input waves (Figure 35c) propagating through the model are amplified and de-amplified differently in the FF (Figure 35b) and CL arrays (Figure 35a). Accelerations time history at levee crest (A54, Figure 35a) indicates a tendency of response towards longer periods, with many cycles about the sustained acceleration (~0.2g) and peak amplitudes smoothly decreasing up until 38 seconds, almost beyond the input wave has ceased. Record of A24 at FF top (Figure 35b) shows a de-amplification of amplitudes in the soil column

free to vibrate, but suggests that a large portion of energy can still propagate through the soft material. Similar observation could be postulated on the work of Arulnathan et al. (2001) and Egawa et al. (2004) in centrifuge experiments, and of Tokimatsu and Sekiguchi (2006) on analyses of field records.

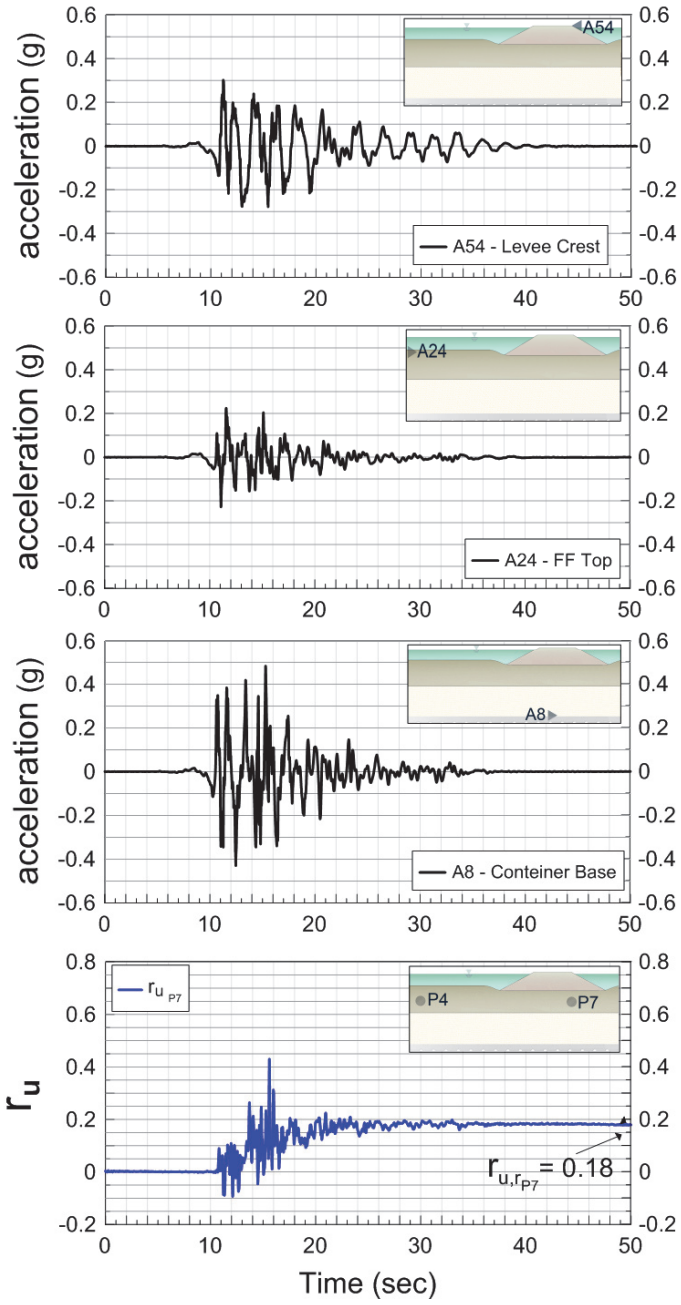

Figure 35 – Fast data time histories of accelerations at (a) levee crest, (b) free field peat top and (c) base of the container, and (d) excess pore pressures ratios at peat mid-elevation in the CL array during Trial 4 (Strong Kobe) of RCK02

Figure 35d also shows that excess pore pressure ratios increase in the CL (P7) array up until about 20 seconds, after which the input wave does not exceed 0.2g anymore. Residual excess pore pressure ratios were defined as the maximum steady average values reached during loading (~0.18 for Trial 4, Strong Kobe, Figure 35d).

6.3.1 Computed Shear Strains

Development of excess pore pressure is fundamentally related to cyclic shear strain (Vucetic, 1994). Plane-strain components of the Cauchy strain tensor (i.e., ε_{xx}, ε_{zz}, and γ_{xz}) mobilized during the centrifuge experiments were computed from recorded horizontal and vertical accelerometers embedded in the peat using bilinear quadrilateral interpolation as illustrated in Figure 36. The acceleration records were filtered and double-integrated in time to obtain displacement records (u_{ix}, u_{iz}). Strains were then computed from the displacements by treating the region between four sensor positions as a bilinear quadrilateral finite element. The solution for the strain components is derived using an isoparametric transformation (e.g., Zienkiewicz, 2000), and result in Eqs. 5-13. Components of the Cauchy strain tensor were computed at the corners, midpoints, and in the middle of the element as indicated by the filled circles on the isoparametric element inset in Figure 36. These calculations were repeated at every time step to obtain time histories for ε_{xx}, ε_{zz}, and γ_{xz}, and the calculations were performed for three different "elements" beneath the levee.

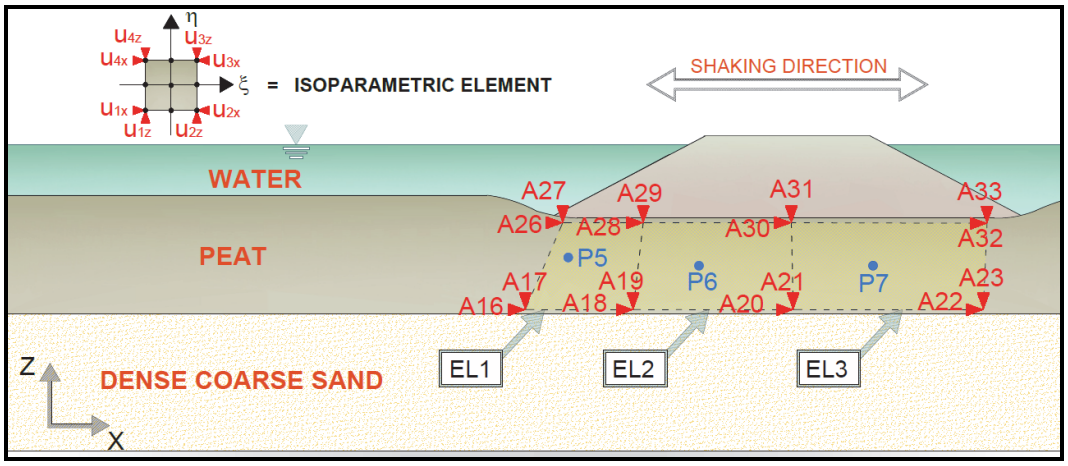

Figure 36 – Section of RCK02 model at 57g showing the quadrilateral elements and the isoparametric element

Equation 5 – {ε}

$$\{\varepsilon\} = \begin{Bmatrix} \varepsilon_x \\ \varepsilon_z \\ \gamma_{xz} \end{Bmatrix} = \begin{Bmatrix} u_{x,x} \\ u_{z,z} \\ u_{x,z} + u_{z,x} \end{Bmatrix} = [B]\{u\}$$

Equation 6 – {u}

$$\{u\} = \begin{bmatrix} u_{1x} & u_{1z} & u_{2x} & u_{2z} & u_{3x} & u_{3z} & u_{4x} & u_{4z} \end{bmatrix}^T$$

Equation 7 – [B]

$$[B] = \frac{1}{J}\begin{bmatrix} J_{22}N_{1,\xi} - J_{12}N_{1,\eta} & 0 & J_{22}N_{2,\xi} - J_{12}N_{1,\eta} & 0 & \dots \\ 0 & -J_{21}N_{1,\xi} + J_{11}N_{1,\eta} & 0 & J_{21}N_{2,\xi} - J_{11}N_{2,\eta} & \dots \\ -J_{21}N_{1,\xi} + J_{11}N_{1,\eta} & J_{22}N_{1,\xi} - J_{12}N_{1,\eta} & J_{21}N_{2,\xi} - J_{11}N_{2,\eta} & J_{22}N_{2,\xi} - J_{12}N_{2,\eta} & \dots \end{bmatrix}$$

$$\begin{bmatrix} \dots & J_{22}N_{3,\xi} - J_{12}N_{3,\eta} & 0 & J_{22}N_{4,\xi} - J_{12}N_{4,\eta} & 0 \\ \dots & 0 & -J_{21}N_{3,\xi} + J_{11}N_{3,\eta} & 0 & -J_{21}N_{4,\xi} + J_{11}N_{4,\eta} \\ \dots & -J_{21}N_{3,\xi} + J_{11}N_{3,\eta} & J_{22}N_{3,\xi} - J_{12}N_{3,\eta} & -J_{21}N_{4,\xi} + J_{11}N_{4,\eta} & J_{22}N_{4,\xi} - J_{12}N_{4,\eta} \end{bmatrix}$$

Equation 8 – (J11)

$$J_{11} = \frac{1}{4}\left(-x_1(1-\eta) + x_2(1-\eta) + x_3(1+\eta) - x_4(1+\eta)\right)$$

Equation 9 – (J12)

$$J_{12} = \frac{1}{4}\left(-z_1(1-\eta) + z_2(1-\eta) + z_3(1+\eta) - z_4(1+\eta)\right)$$

Equation 10 – (J21)

$$J_{21} = \frac{1}{4}\left(-x_1(1-\xi) - x_2(1+\xi) + x_3(1+\xi) + x_4(1-\xi)\right)$$

Equation 11 – (J22)

$$J_{22} = \frac{1}{4}\left(-z_1(1-\xi) - z_2(1+\xi) + z_3(1+\xi) + z_4(1-\xi)\right)$$

Equation 12 – {N1,ξ}

$$N_{i,\xi} = \left[-\frac{1}{4}(1-\eta) \quad \frac{1}{4}(1-\eta) \quad \frac{1}{4}(1+\eta) \quad -\frac{1}{4}(1+\eta)\right]^T$$

Equation 13 – {N1,η}

$$N_{i,\eta} = \left[-\frac{1}{4}(1-\xi) \quad -\frac{1}{4}(1+\xi) \quad \frac{1}{4}(1+\xi) \quad \frac{1}{4}(1-\xi)\right]^T$$

Figure 37 shows the ε_{xx}, ε_{zz}, and γ_{xz} histories for three points (A, B, C) along the mid-elevation of EL3. Values of γ_{xz} exceeding 6% were mobilized in the peat during this motion, with PBA of 0.52g. Such large shear strains are rarely encountered in geotechnical earthquake engineering problems that do not involve liquefaction or other forms of ground failure, but could be

mobilized in the centrifuge experiment because the peat layer is extremely soft. Similar amplitudes are expected in field conditions. The values of ε_{xz} are essentially identical at all three positions because the levee is much stiffer than the peat, and therefore exerted an essentially constant displacement boundary condition at the levee-peat interface. Values of ε_{zz} reach approximately 1.6 % beneath the center of the levee (point A), approximately 3 % at point B and a 4.3% in the toe region (Point C). The increase in amplitude moving from beneath the crest to beneath the toe is due to levee rocking during cyclic loading. Cappa et al. (2014) confirmed the rocking mechanism via dynamic analyses of this experiment and recognized rocking as an additional source of seismic demands on the foundation soils. Values of ε_{xx} are small (< 0.2%) at all three positions. The resulting mechanism involves vertical deformations caused by rocking and horizontal deformations caused by vertically propagating shear waves. For problems involving vertically propagating shear waves, the deviatoric strain is often assumed equal to γ_{xz}. However, the rocking deformation mode causes the amplitude and direction of the principle strain components to differ from those for vertically propagating shear waves, which necessitates a more thorough analysis of strain.

Rocking modes can impose extra demands on both embankments and underlying substrata by altering the state of stress. Rotated principal stresses in the levee section can result in reduced horizontal effective stresses in portions of the fill and foundation and lead to decreased soil liquefaction resistances. At the same time, other regions could suffer additional inertial loads, potentially leading to higher shear strain/excess pore pressure rates and augmenting the risk of vertical strains following reconsolidation.

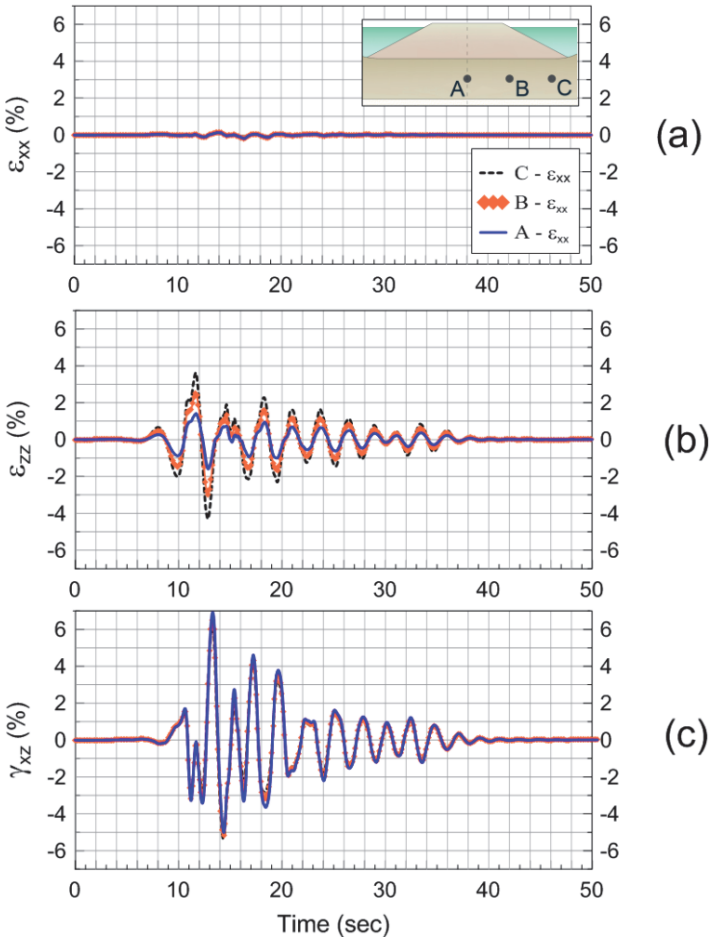

Figure 37 – Horizontal (a), vertical (b) and shear (c) strains at various mid-elevation locations beneath the levee during Strong Kobe motion, RCK02

6.3.2 Direct-Simple-Shear-Equivalent Deviatoric Strain Invariant

A deviatoric strain invariant that permits direct comparison between the centrifuge test data and the results of a constant-volume direct simple shear testing program conducted by Shafiee (2016) on Sherman Island peat is introduced. A common deviatoric strain invariant is the octahedral shear strain, γ_{OCT}, defined by Equation 14 for plane strain conditions in the x-z plane

(ε_{yy}=γ_{xy}=γ_{zy}=0). Note that γ_{OCT} is always positive, whereas the strain components ε_{xx}, ε_{zz}, and γ_{xz} may be positive or negative.

Equation 14 – γ_{OCT} = f (ε_{xx}, ε_{zz}, γ_{xz})

$$\gamma_{OCT} = \left(\frac{2}{3}\right) \cdot \sqrt{\left(\varepsilon_{xx}\right)^2 + \left(-\varepsilon_{zz}\right)^2 + \left(\varepsilon_{zz} - \varepsilon_{xx}\right)^2 + 6 \cdot \left(\frac{\gamma_{xz}}{2}\right)^2}$$

However, a problem is that γ_{OCT} is not equal to γ_{xz} for a constant-volume simple shear stress path (ε_{zz}=ε_{xx}=0). To facilitate a direct comparison with Shafiee's simple shear test results, we define a new direct-simple-shear-equivalent deviatoric strain invariant, $\gamma_{DSS,eq}$, by scaling the octahedral strain such that $\gamma_{DSS,eq}$ = γ_{xz} for an undrained simple shear stress path (Equation 15).

Equation 15 – $\gamma_{DSS,eq}$ = f (γ_{OCT})

$$\gamma_{DSS,eq} = \sqrt{\frac{3}{2}} \cdot \gamma_{OCT}$$

Figure 38 compares the amplitude of strain components ε_{xx}, ε_{zz}, γ_{xz} with $\gamma_{DSS,eq.}$ at the mid-height of the peat layer underneath the levee crest and toe. Beneath the levee crest, γ_{xz} is essentially identical to $\gamma_{DSS,eq}$, reaching a peak value of 6.2%. The two lines are very close to each other, deviating only slightly at times when ε_{zz} reaches a local peak. This is because the stress path beneath the levee crest is well-approximated by a direct simple shear stress path. By contrast,

beneath the levee toe $\gamma_{DSS,eq}$ is larger in magnitude than γ_{xz} during many of the cycles. Furthermore, the peak strain is slightly larger beneath the toe than beneath the crest, reaching a peak of 7.0%. The vertical strain ε_{zz} generated beneath the levee toe is more than double that beneath the levee crest (4.3% compared to 1.6%). This effect is due to levee rocking, and results in $\gamma_{DSS,eq}$ being larger than γ_{xz}. Hence, the soil in this region is exposed to a stress path that is more complicated than a simple shear stress path. Although ε_{zz} influences $\gamma_{DSS,eq}$ beneath the toe, γ_{xz} is the more influential component.

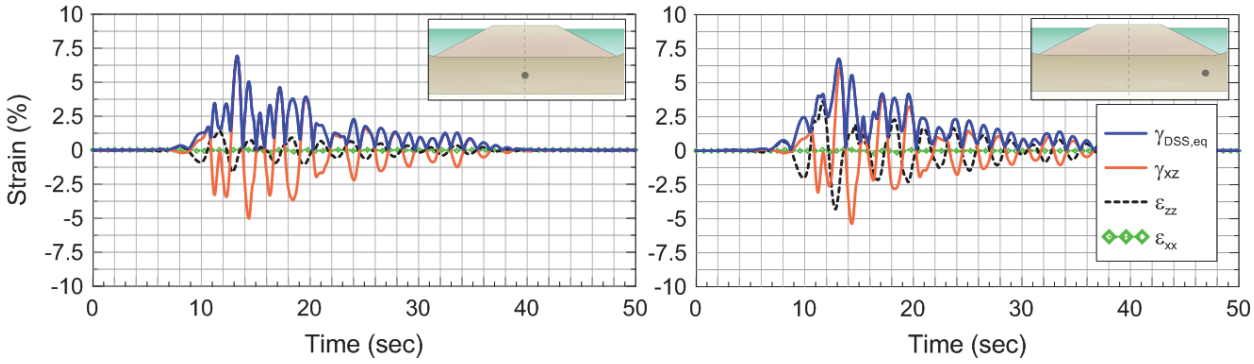

Figure 38 – Strain components during Strong Kobe motion (Trial 4) at mid-height of peat layer beneath (a) the levee crest and (b) the levee toe

6.3.3 Relationship between Excess Pore Pressure Generation and Shear Strain Amplitudes

Figure 39 shows records of $\gamma_{DSS,eq}$ and r_u for the strong Kobe motion. Pore pressure begins to exhibit a permanent increase when $\gamma_{DSS,eq}$ exceeds about 1%, and continues to accumulate until about *Time* = 20s, at which point r_u = 0.18. Small cycles of pore pressure response are observed, but a permanent increase does not continue beyond this point. Pore pressures remain high after

shaking ceases, indicating that the response of the peat at the position of P7 was essentially undrained during the time frame of strong shaking.

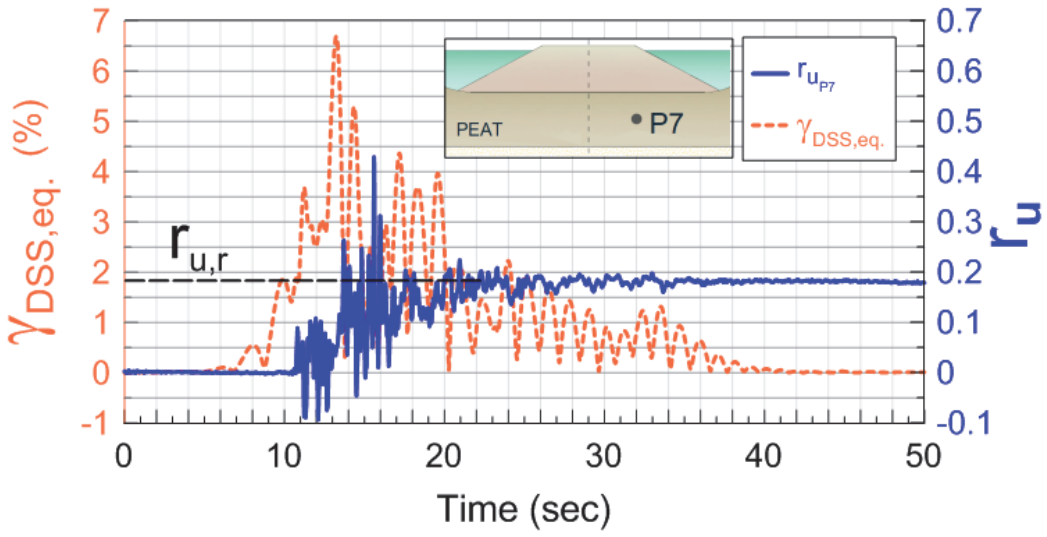

Figure 39 – Equivalent shear strain vs excess pore pressure ratio histories at P7 elevation during the Strong Kobe motion (Trial 4) for RCK02

Values of $r_{u,r}$ were computed for all of the ground motions imposed on the model, and are plotted versus *PBA* and the peak value of $\gamma_{DSS,eq}$ in Figure 40. These data are plotted for all three elements, for which pore pressure sensors P5, P6, and P7 lie near the center. The values of $\gamma_{DSS,eq}$ at the center of each element are plotted in Figure 40 because they lie closest to the pore pressure sensors. As anticipated, $r_{u,r}$ increase with increasing PBA and $\gamma_{DSS,eq}$. A maximum excess pore pressure ratio of 0.2 was reached at shear strain amplitudes around 7% (Figure 40). Values of $r_{u,r}$ remain very low for motions that do not exceed PBA = 0.1g, or $\gamma_{DSS,eq}$ = 1%. Vucetic (1994) postulated threshold shear strains for pore pressure generation in sands and clays, and found that the threshold strains were about an order of magnitude higher for clay ($\gamma_{tp} \approx 0.1\%$) than for sand

($\gamma_{tp} \approx 0.01\%$). The observed threshold strain for peat is about an order of magnitude higher than that for clay.

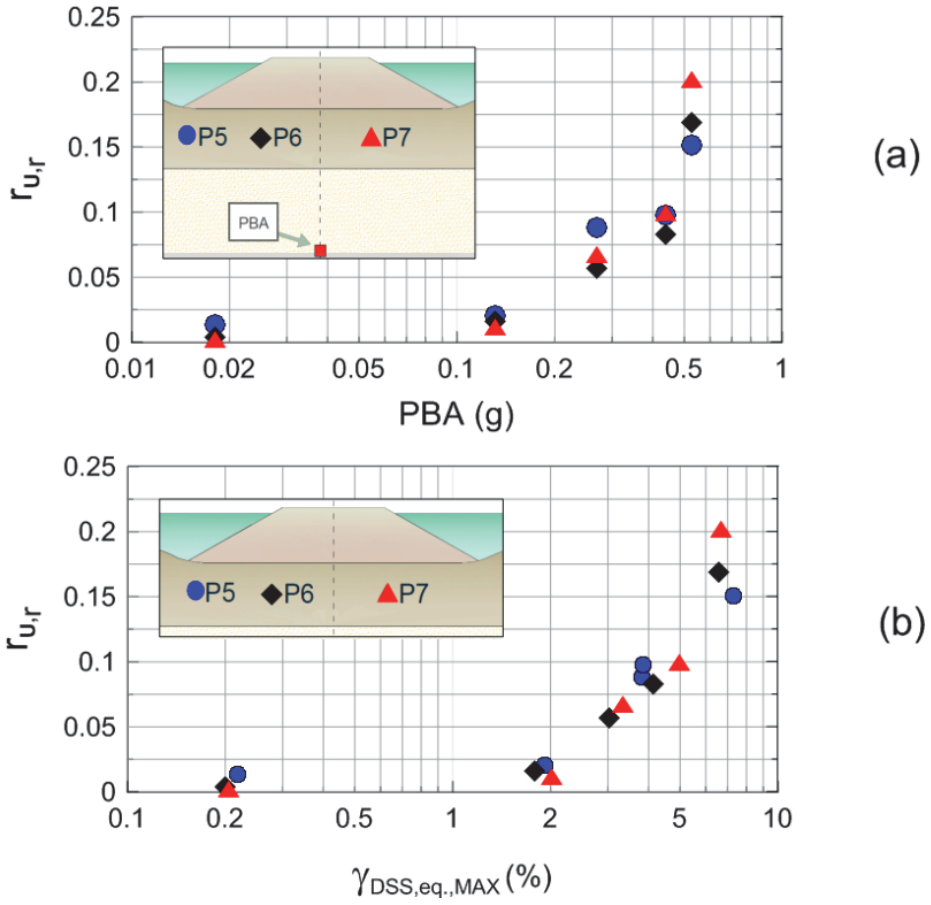

Figure 40 – Residual excess pore pressure $r_{u,r}$ vs (a) PBA and (b) $\gamma_{DSS,eq}$

Shafiee (2016) developed a regression equation (Equation 16) from their uniform cycles tests to estimate residual excess pore pressure ratio as a function of *OCR*, *OC*, *N*, γ_c and γ_{tp}; where *OCR* is overconsolidation ratio, *OC* is organic content, *N* is number of loading cycles, γ_c is the cyclic shear strain amplitude, and γ_{tp} is the threshold shear strain below which no excess pore pressure is generated. The value of γ_{tp} is a function of *OC* and was found to be $\gamma_{tp} = 0.7$ for *OC* values of $35\% < OC < 70\%$, such as for our peat ($OC = 69\%$).

Equation 16 – r_{ur} = f (γ_c, γ_{tp}, *N, OCR, OC*)

$$r_{u,r} = 0.316 \cdot \left(\gamma_c - \gamma_{tp}\right)^{0.619} \cdot N^{0.187} \cdot OCR^{-0.477} \cdot OC^{-0.499}$$

To facilitate a comparison with Shafiee's regression equation, we must first compute an equivalent number of uniform cycles from the broadband strain records. For purposes of comparison, we select 15 cycles because most of the direct simple shear tests were conducted for this number of cycles. Following a procedure described by Idriss and Boulanger (2008) for computing equivalent number of cycles for liquefaction triggering evaluation, consider two cases, *A* and *B*, that produce equal values of $r_{u,r}$, but correspond to different numbers of cycles, N_A and N_B, and different cyclic shear strain amplitudes, γ_{cA} and γ_{cB}. Plugging relevant quantities into Equation 16, the relationship between N_A, N_B, γ_{cA}, and γ_{cB} for a constant $r_{u,r}$ is given by Equation 17.

Equation 17 – Equivalent Number of Cycles

$$\frac{N_B}{N_A} = \left(\frac{\gamma_{cA} - \gamma_{tp}}{\gamma_{cB} - \gamma_{tp}}\right)^{3.31}$$

Consider a broadband record with N_{cyc} number of half-cycles exhibiting $|\gamma_c| > \gamma_{tp}$ for which we seek to compute a number of cycles, N_{ref}, corresponding to a reference strain amplitude, $\gamma_{c,ref}$. For the ith half-cycle (N_i = ½), Equation 16 is used to compute an equivalent number of cycles at $\gamma_{c,ref}$. These equivalent numbers of cycles are then summed to obtain N_{ref} using Equation 18.

Equation 18 – $N_{ref} = f(\gamma_c, \gamma_{c,ref}, \gamma_{tp})$

$$N_{ref} = \sum_{i=1}^{N_{cyc}} \frac{1}{2} \cdot \left(\frac{\gamma_{c,i} - \gamma_{tp}}{\gamma_{c,ref} - \gamma_{tp}} \right)^{3.31}$$

This procedure allows us to compute a number of equivalent uniform cycles for a particular reference shear strain, but for comparison with Shafiee's laboratory data, we seek instead the reference shear strain value, $(\gamma_{c,ref})_{N=15}$ associated with 15 uniform cycles. This is achieved by iterating on the procedure using Equation 18 until $N_{ref} = 15$.

Figure 41 shows an example of the aforementioned procedure, where $(\gamma_{c,ref})_{N=15}$ was derived from the $\gamma_{DSS,eq}$ time history calculated at P7 during Trial 4 (Strong Kobe). The circles in Figure 41 correspond to peaks exceeding the γ_{tp} threshold. Peaks below γ_{tp} were not accounted for in the calculation of $(\gamma_{c,ref})_{N=15}$, which in this case resulted to be about 3.4%. Figure 41 suggests that $\gamma_{tp} < (\gamma_{c,ref})_{N=15} < \gamma_{DSS,eq,Max}$ for time histories exceeding the γ_{tp} threshold.

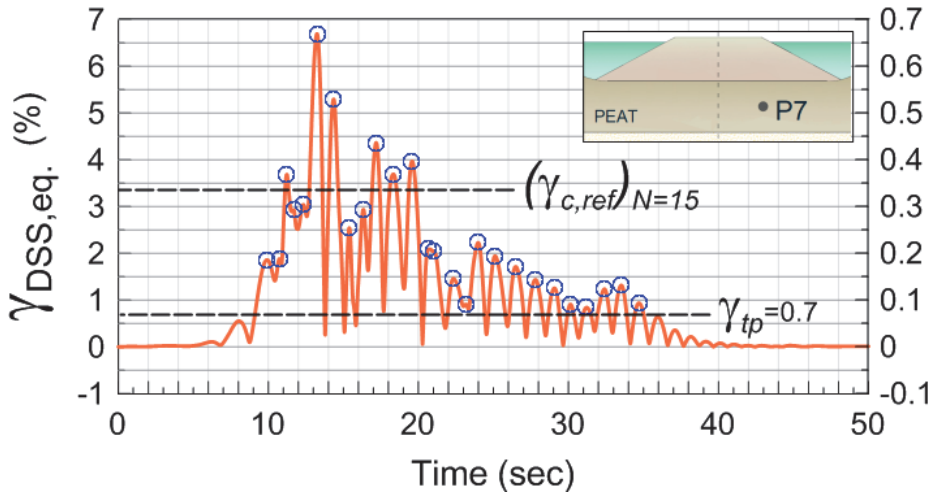

Figure 41 – Example of conversion from $\gamma_{DSS,eq}$ to $(\gamma_{c,ref})_{N=15}$ for strain time history at P7 for Strong Kobe (Trial 4) during Experiment 14, RCK02

Corresponding values of $(\gamma_{c,ref})_{N=15}$ were derived for all the $\gamma_{DSS,eq,Max}$ amplitudes shown in Figure 40, and data were then plotted in Figure 42 against the related recorded residual excess pore pressure ratios. Figure 42 also shows a continuous dashed line corresponding to the $r_{u,r}$ vs γ_c relation calculated for our centrifuge test according to Equation 16. The curve was estimated setting N=15 and selecting the input parameters to match the peat properties in the centrifuge: OCR = 1.3 and OC = 69%. OCR was assumed constant in order to generate the regression, although it was actually increasing during spinning. Despite the peat was remolded and the maximum past pressure (σ_p') could be assumed as the current effective pressure (σ_v'), the material underwent an important secondary compression stage, and OCR was calculated according to Eqs. 19-20 for the time span between end of primary consolidation after reaching 57g and the application of the Strong Kobe motion (Trial 4), which was the first to generate excess pore pressure (Figure 34).

Equation 19 – Δe = f (C_c, C_r, OCR)

$$\Delta e = (C_c - C_r) \cdot \log\left(\frac{\sigma_p'}{\sigma_v'}\right)^{OCR} = (C_c - C_r) \cdot \log(1)^{OCR}$$

Equation 20 – OCR = f (Δe, C_c, C_r)

$$OCR = 10^{\left(\frac{\Delta e}{C_c - C_r}\right)} = 10^{\left(\frac{\Delta e}{3.4}\right)}$$

Centrifuge data agree well with the regression equation, though the mobilized $r_{u,r}$ values are slightly higher for strains exceeding 3%. It is unclear whether this slight bias is caused by the response of the peat, or by the pore pressure transducers moving down slightly due to co-seismic settlement. In any case, the agreement is reasonable.

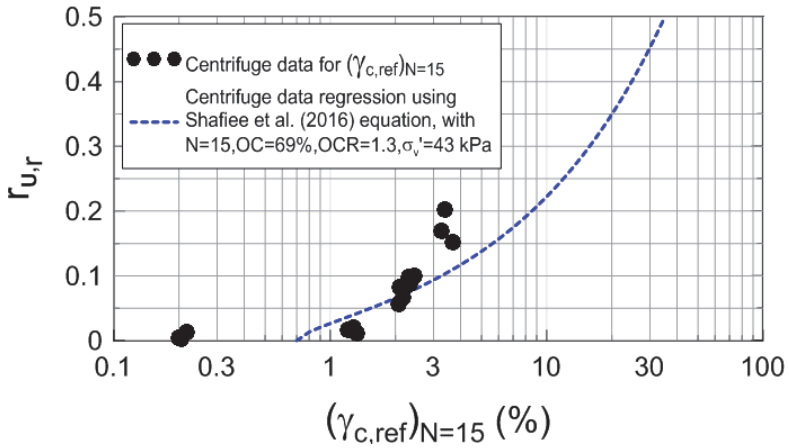

Figure 42 – Comparison of $(\gamma_{c,ref})_{N=15}$ for centrifuge data and regression line according to Shafiee (2016)

6.4 Chapter Summary and Conclusions

Strain and pore pressure measurements recorded during a large centrifuge experiment of a stiff levee structure resting on soft peat were used to evaluate the strain threshold for excess pore pressure generation of peat. The model was subjected to a series of scaled ground motions. Via simple FEM modeling, horizontal, vertical and shear strain components were calculated along different locations beneath the embankment and compared. Vertical strains indicated a rocking

mechanism of the levee, which can impose substantial extra-demands on the levee system and it is usually neglected in traditional seismic analysis. Shear strains of 7% were generated in the organic foundation material for a peak base acceleration of 0.52g, suggesting the potential for critical deformations.

Octahedral strain was selected as target deviatoric invariant to compare centrifuge results to DSS at constant volume lab test by Shafiee (2016). To facilitate the comparison, we derived an equation to estimate DSS equivalent cyclic strain amplitude from octahedral strain. An exponential relation of residual excess pore pressure ratios vs log of maximum DSS equivalent strain was observed, with a proposed threshold of about 1%. This threshold for peat is about 10 folds higher than for clay, and 100 folds than sand (Vucetic, 1994).

DSS equivalent strain histories were converted into uniform strain histories with reference strain amplitudes calculated to produce 15 uniform cycles. Reference strain amplitudes were then plotted with related residual excess pore pressure ratios and compared with predictions following a regression proposed by Shafiee (2016). Centrifuge data and regression predictions again suggest a threshold of about 1%, with the latter plotting slightly lower after 3% reference strain amplitudes. The cyclic threshold shear strain here described for generation of excess pore pressure in peats has, for many reasons, an inherently important significance in dynamic analyses. First, energy-based methods for estimating liquefaction potential have been shown to be more accurate than stress-based approaches, and can greatly benefit from such finding. Secondly, while in the past direct parameters of earthquake records (such as PGA) were used to describe the potential for pore pressure generation and liquefaction, it is nowadays clear that those are usually poor estimators of structure damage, especially for medium to long fundamental period structures such levees. For long distance and near fault ground motions, the

velocity time history has been indicated as a better descriptor of the earthquake potential on cyclic crest settlement. However, both PGV and PGA cannot be reliably used for excess pore pressure generation prediction because of the usual poorer fit if compared to cyclic shear strain amplitudes, as depicted in Figure 9. On the contrary, acceleration quantities are often used in simplified methods (Swaisgood, 2003) and semi-empirical Newmark-type analyses (Makdisi and Seed, 1978, Yegian et al. 1991, Watson-Lamprey and Abrahamson 2006, Bray and Travasarou, 2007, Rathje and Antonakos, 2011, Millet et al., 2014) to predict freeboard loss, furthermore excluding the contribution of the seismic SSI.

In turn, analysis and design of earth embankments on soft foundation should consider a coupled dynamic response, accounting for excess pore pressure generation and migration, rotation of stresses and SSI, site response, cyclic degradation and nonlinearities. 3D non-linear deformations analyses in software like Flac, PLAXIS or Opensees, are emerging as the computational demand decreases and more accurate constitutive model techniques have been proposed, such as single yield surface elastoplatic framework (Gens and Nova 1993; Liu and Carter 2001; Asaoka et al. 2000, Kavvadas and Amorosi, 2000), or kinematic hardening and bounding surface plasticity approaches (Rouainia and Muir Wood 2000; Kavvadas and Amorosi 2000; Baudet and Stallebrass 2004), although such methods were not developed for soft organic soils. A specific constitutive model for the cyclic response of peat has not been proposed yet. This novel cyclic threshold shear strain for peat represents an important finding that could be implemented in future constitutive models capable of capturing a fully-coupled soft foundation-stiffer embankment dynamic response during cyclic loading, correctly accounting for the increased demands. Future work will expand the findings presented in this chapter, and will focus on the SSI and site response aspects.

7. POST-SEISMIC SETTLEMENTS

Augmented rates of settlement in peat following cyclic loading were recently observed in lab tests and can result in dangerous additional free board loss. This chapter presents data from 9m radius and 1m radius tests that documented the same mechanism experimentally for the first time.

7.1 Introduction

Peat is known to be subjected to significant secondary compression deformations (Mesri et al., 1997, Mesri and Ajlouni, 2007, Fox et al, 1992, Dhowian and Edil, 1980), which often time control long-term settlements. The remarkable creep rate of peats is the result of (1) the unusually high void ratio and water contents in in-situ conditions, (2) the low strength (Hobbs 1986, Mesri and Ajlouni, 2007), and (3) the mechanism of stress redistribution from pore fluid to peat particles after fibers re-arrangement following loading (Taylor, 2012). Stress redistribution in organic soils depends on the peculiar micro vs macro-pore structures (Adams, 1963, Barry and Poskitt, 1972, Kogure and Ohira, 1979, Edil and Mochtar, 1984, Kogure 1993) and is still poorly understood, rendering estimation of post-cyclic settlements very difficult.

To the best of our knowledge, the only work in literature that has investigated the volumetric change response of peat to cyclic shear loading is by Shafiee et al. (2015). Their recent paper presented a break-through discovery by which peat undergoes a “clock-reset” following cyclic

loading over a ~1% cyclic shear strain threshold. This behavior was documented in the paper for an undisturbed sample of Delta peat during a multistage testing in the DSS at constant volume device they developed (Shafieel, 2016). The peat sample had an OCR = 4.9, C_c = 2.1, C_r = 0.14, effective stress of 12 kPa and OC = 55%. Each stage consisted of 15 strain-controlled cycles, where the strain amplitudes were increased from ~0.01% to ~10% and the specimen was let consolidating for approximately 20 mins in between each stage. Such novel mechanism observed in the lab has not been documented in experimental testing or numerical simulations, and it is critical for embankments atop peat foundations because the resulting augmented demands are not currently taken into account is seismic risk assessments. Our project investigated the cyclic and post-cyclic volume change of peat and proved experimentally the potential for a settlement rate increase.

7.2 Results of the 9m Radius Centrifuge Test

Increased settlement rates were first observed in the 9m radius tests. Figure 43 shows the g-field, pore pressures and settlements measured during spin-up, application of ground motions and spin-down of Experiment 14, for both FF and CL arrays. The green area represents the time span between $t_{0,consolidation}$ when target 57g acceleration field was reached and the application of the second strong shake (Trial 5, Large Loma Prieta, see Table 6). Figure 44 plots the portion of slow data highlighted by the shaded green area in Figure 43. The log-scale time axis in Figure 44 is reset to zero at $t_{0,consolidation}$. Both, free field and center levee arrays showed an increase of settlement rates during secondary compression (i.e. $\Delta\dot{u}_f > \Delta\dot{u}_0$) after the Strong Kobe motion

(Trial 4). Rates were determined by selecting settlement data corresponding to the time frame after pore pressures dissipated to pre-loading levels (i.e., primary consolidation has ceased, and secondary compression was entered). In the center levee array the preloading secondary compression rate (in log scale) was measured $\dot{u}_{0,\ L11\ (CL)}$ = 7.95 (model scale, Figure 44). The settlement rate during secondary compression after load application was $\dot{u}_{f,\ L11\ (CL)}$ = 9.45. This indicates a rate increase of 18%. In the free field, the pre-load settlement rate during secondary compression was approximately $\dot{u}_{0,\ L2\ (FF)}$ = 2.96. The post-load secondary compression settlement rate measured $\dot{u}_{f,\ L2\ (FF)}$ of 4.5. This represents a rate increase of 52%. This trend suggests the potential for an additional settlement of the foundation soil when cyclically loaded, which should be taken into account during analysis as a rate adjustment / reset.

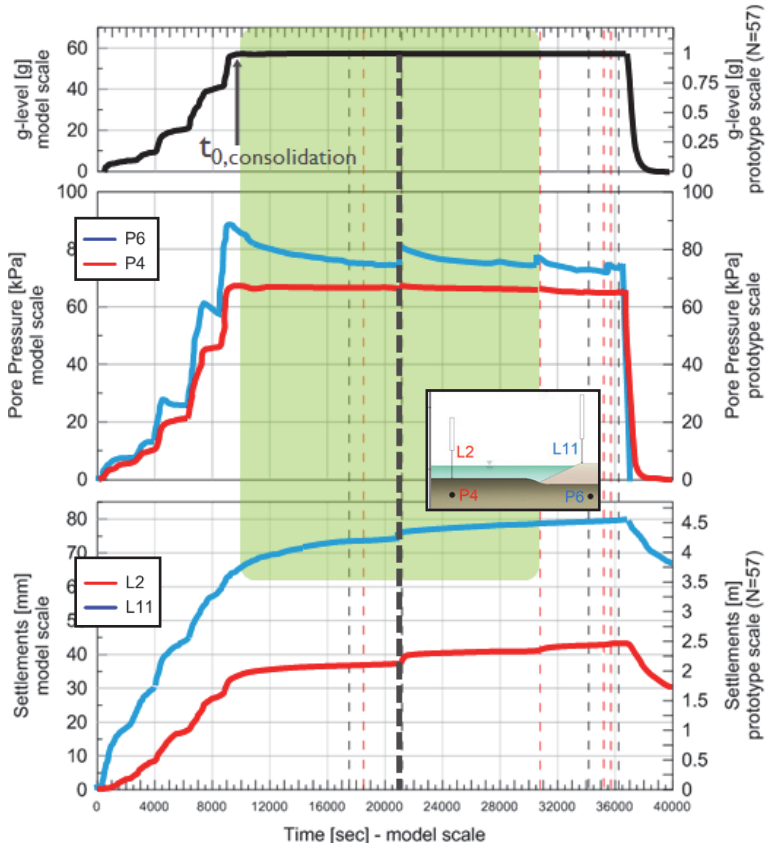

Figure 43 – Slow data records of (a) acceleration, (b) pore pressures and (c) vertical settlements during Experiment 14, RCK02

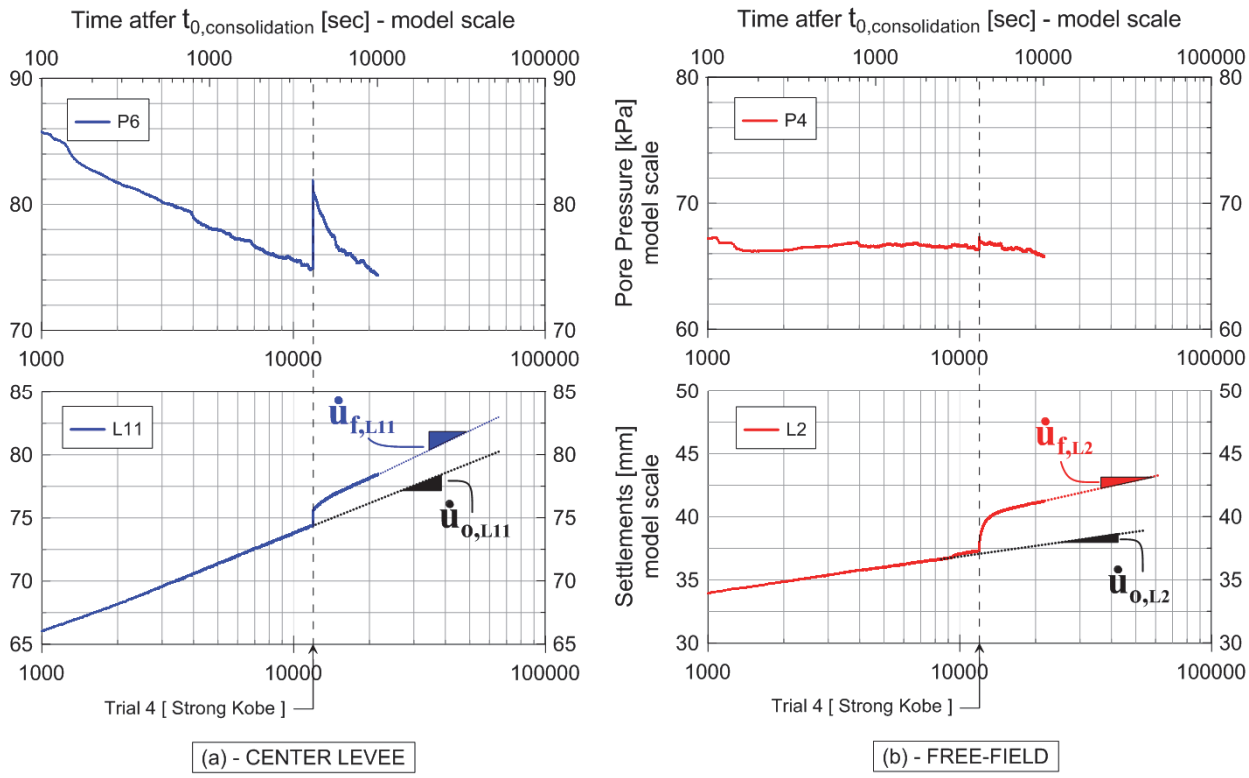

Figure 44 – Illustration of secondary compression rates after cyclic loading

Although Figure 44 certainly shows an increase in rate of settlement following the Strong Kobe motion, the rate before applying the motion was still too high to easily define the change after the shake. In theory, the model should have been spun for days up until showing a relatively small and constant creep rate before applying the ground motion, but this was not feasible for the 9m radius centrifuge experiments. In order to better capture such rate change mechanism an additional small centrifuge test was conducted. The small 1m radius Schaevitz test overcame limitations in time by initially over-consolidating the organic material through an increased gravitational field to accelerate the consolidation phase. Setup and results are discussed in the following sections.

7.3 Results of the 1m Radius Centrifuge Test

Experiment 16, conducted on the 1m radius Schaevitz centrifuge, focused on investigating the post-cyclic volume change behavior of peat. Setup and testing procedures were selected to highlight the secondary compression response.

Setup of Experiment 16 was similar to the last test conducted on the small centrifuge in August 2013 (Experiment 11), where a clayey levee was placed atop a peat layer after a preliminary consolidation at 1g of the organic material, and the system was then spun up to 50g and subjected to target ground motions. Contrary to Experiment 11 however; Experiment 16 forced the peat to over-consolidate at higher gravitational fields in order to decrease the rate of settlement during secondary compression before applying the ground motion series.

Experiment 16 was tested over two consecutive days because during the first one the recording system experienced technical issues. Figure 45 shows a side view of the model at 1g before start the first spinning day. A clayey levee of the same non-liquefiable material used for Experiments 12 and 14 was shaped to have dimensions (model scale) of 4 cm in height, 20 cm width at base and 10 cm at crest, with 5:4 slopes. The levee was underlain by a layer of peat, which was placed atop a coarse sand layer. Soil strata followed an "arch shape" because of the anticipated curvature effects created in the centrifuge during spinning. Dimensions reported hereafter correspond to thicknesses of the center levee arrays and in model scale, unless stated otherwise. Peat and coarse sand layers were prepared according to same procedures used for Experiments 12 and 14. The coarse sand layer was 2 cm thick. The peat slurry had an initial thickness of 10.5 cm and was consolidated for 19 hours under 3.5/4 cm of Nevada sand, after which it had settled

about 2.7 cm. After removing the Nevada sand layer and placing the clayey levee the peat continued to settle, reaching 7 cm of thickness before start spinning the first day (Figure 45). The model was instrumented with 4 PPTs, 2 LPs and 8 accelerometers, which recorded the static (slow) and dynamic (fast) response during testing. Calibration and exact sensor location data can be found at the NEES project warehouse.

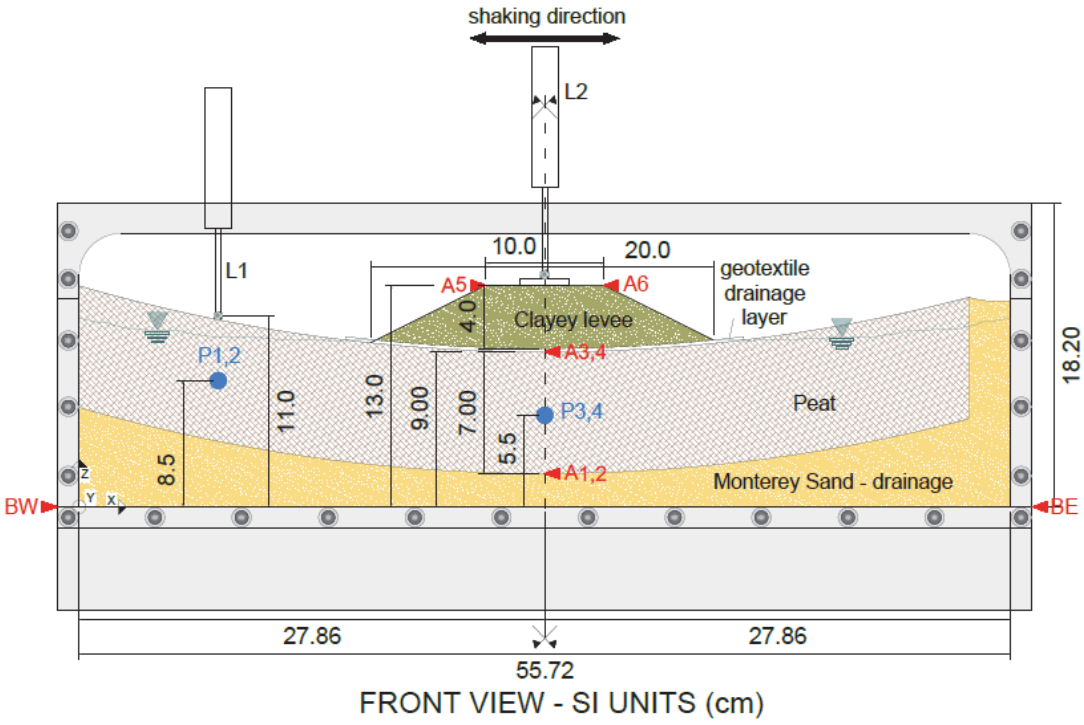

Figure 45 – Side view of Experiment 16 at 1g before start the first day of spinning

No ground motion wave was applied during the first spinning day, which therefore only served to consolidate the model. At the end of the first spinning day the peat in the center levee array had a permanent settlement of 1 cm. Before starting the second spinning day the peat was in fact 6 cm thick (Figure 46), and it was almost submerged because of the water expelled during

consolidation. We decided to not discharge the extra volume of water in order to prevent desiccation of the peat fibers.

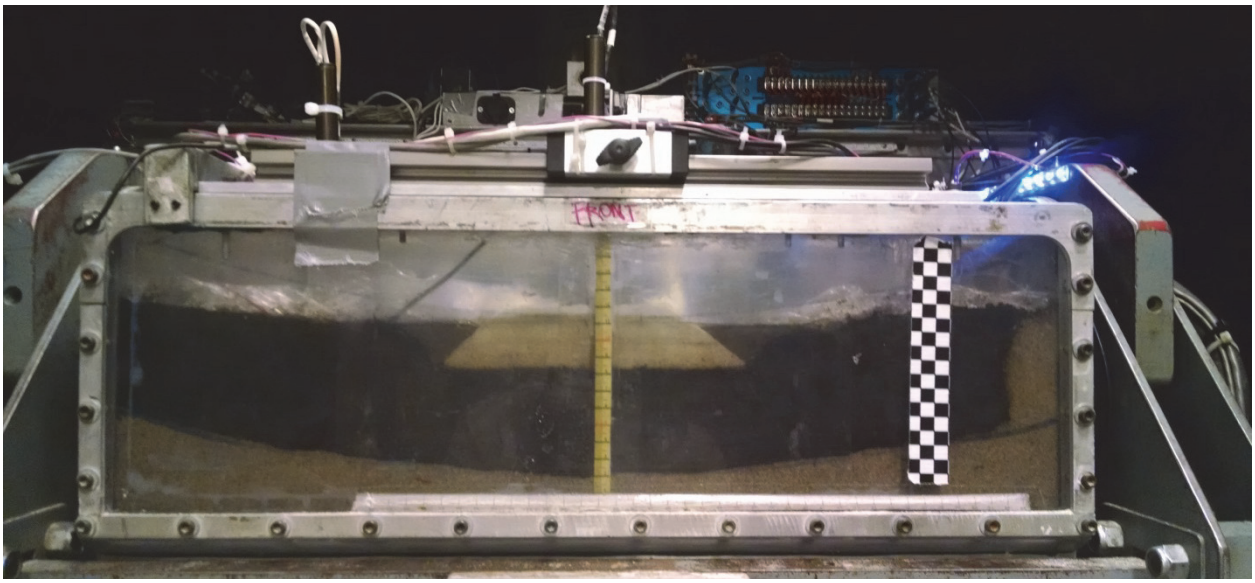

Figure 46 – Model before start second spinning day of Experiment 16

Figure 47 shows the slow data records of the second spinning day. The model was incrementally spun to initial target 55g in steps. When the target g-field was reached (approximately around 7300 s) the DAQ system timed out (for about 700 s), therefore we were forced to spin the model down and fix the problem in order to prevent loss of good quality data following shaking. The model was span back up to 55g continuously recording. Figure 47a indicates two particular times for starting the consolidation clock: $t_{0,consolidation}$ was set when we reached 55g again, while $t_{1,consolidation}$ when we reached our final target acceleration field of 50g before applying the ground motions.

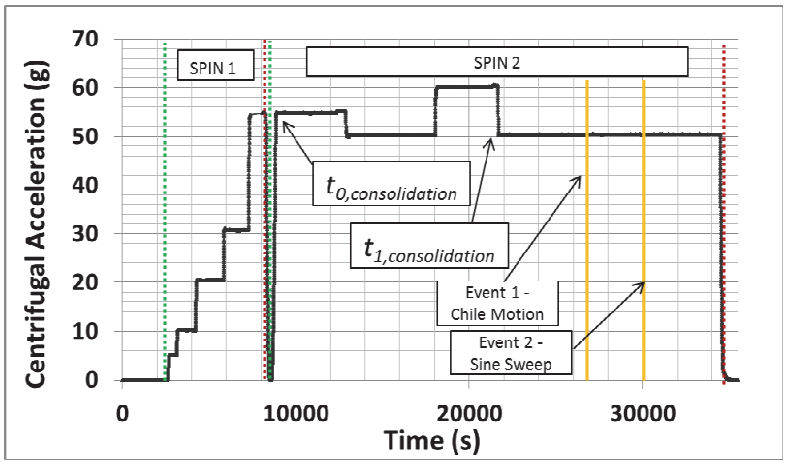

(a)

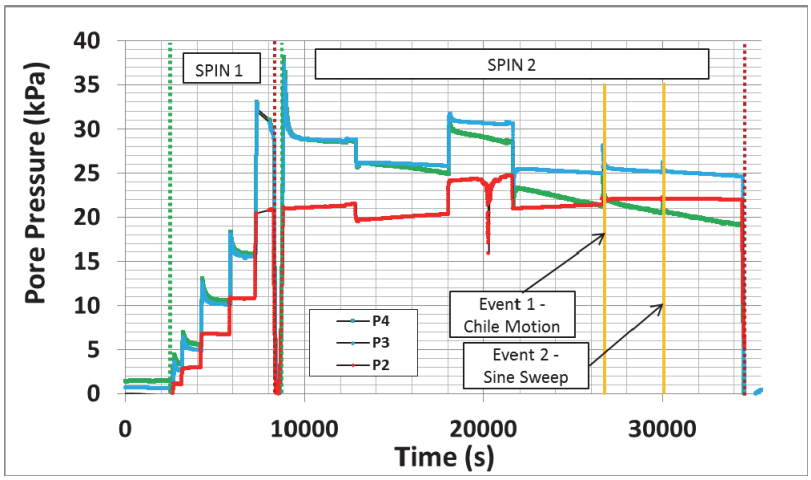

(b)

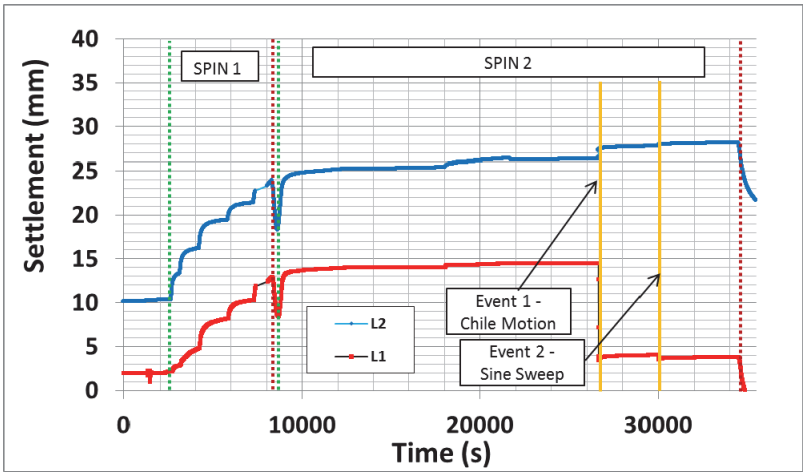

(c)

Figure 47 – Slow data of second spinning day of Experiment 16 showing (a) centrifugal accelerations, (b) pore pressure, and (c) settlements in model scale

Figure 48 plots center levee records of Figure 47 with the time clock reset to $t_{0,consolidation}$ and shows that the settlement rate for each stage of acceleration was varying. When 55g level was reached, the model was let consolidating for approximately 1 hour before decreasing the acceleration to target 50g to check stability and magnitude of the rate of settlement. The settlement rate at this stage was found to be $\dot{u}_{0,\,L2}$ = 74.2 cm/day in prototype scale (0.6183 mm/s in model scale). Comparison of rates at different g-levels should be made at prototype scale to have consistent units. When lowering the g-field from 55g to 50g the peat showed some relaxation (heave and pore pressure increase), after which the rate of settlement stabilized after 20 minutes to $\dot{u}_{1,\,L2}$ = 19.26 cm/day in proto-scale (0.1605 mm/s in model scale). The model was spun at 50g for an additional 65 minutes (2.5 days in proto-scale), and the rate of settlement towards the end of the stage stayed pretty stable (19.51 cm/day). We judged this rate was acceptable for capturing the secondary compression index increase, but we were aiming at achieving a lower magnitude of pre-loading rate of settlement to better appreciate the variation, therefore we increased the g-field to 60g for an additional hour. Settlement rate at 60g before spinning back to 50g was $\dot{u}_{2,\,L2}$ = 95.68 cm/day (0.6644 mm/s in model scale), almost 5 times higher than the previous 50g stage. The model was spun for approximately 60 minutes more at 50g before applying two grand motion waves (Strong Chile and Sine Sweep), indicated in Figure 48c. The rate of settlement before applying Event 1 (Strong Chile) was $\dot{u}_{3,\,L2}$ = 16.62 cm/day in proto-scale (0.1385 mm/s in model scale), which was about 15% less than of $\dot{u}_{1,\,L2}$ = 19.51 cm/day, but still a non-zero value. In theory, we would have kept following such consolidation procedure up until reaching a super small settlement rate, but due to spinning time constrains we decided it was time to move on to the second phase of the test and start applying the ground motion waves.

The first shake (Event 1, Strong Chile) was applied at about 18,000 seconds from $t_{0,consolidation}$, after almost 5 hours of consolidation at g-levels of 50g or higher, which roughly translate in 11 day in proto-scale. The model layout right before applying the first ground motion is shown in Figure 49. The peat layer beneath the levee had a thickness of about 4.4 cm. Effective stress at peat-mid elevation in the CL array was about 17.5 kPa. The Chile motion was scaled to have a PBA of about 0.95g, and generated 3.2 kPa of excess pore pressure beneath the levee, with a residual excess pore pressure ratio of about 0.19. The levee settled 1 mm in model scale, which translates to 5 cm in prototype. The 4.4 cm peat thickness at 50g correspond to a 220 cm, therefore the co-seismic settlement was about 5/220 = 2.3%. The rate of settlement (Figure 48c) after Event 1 was found to be $\dot{u}_{4,L2}$ = 21.46 cm/day in proto-scale (0.1788 mm/s in model scale), which is a 30% increase with respect to $\dot{u}_{3,L2}$ = 16.62 cm/day before the shake.

The model was spun for about an hour total after Event 1 before applying Event 2 (Sine Sweep), scaled to a PBA of 0.85g. The levee settled about 0.1 mm during Event 2, which translate to 0.5 cm in prototype. Excess pore pressure ratios of 0.07-0.09 were recorded in P3 and P4 beneath the levee. The rate of settlement (Figure 48c) after Event 2 and prior to spin the model down was found to be $\dot{u}_{5,L2}$ = 21.80 cm/day in proto-scale (0.1817 mm/s in model scale), which is similar to the rate before the shake. The model was let spinning for about 4500 seconds after applying Event 2 before stopping the test. Right before spinning down, L2 in the CL array recorded 28.2 mm of total settlement (Figure 48c), which corresponds to 40% vertical strain from initial 70 mm peat thickness.

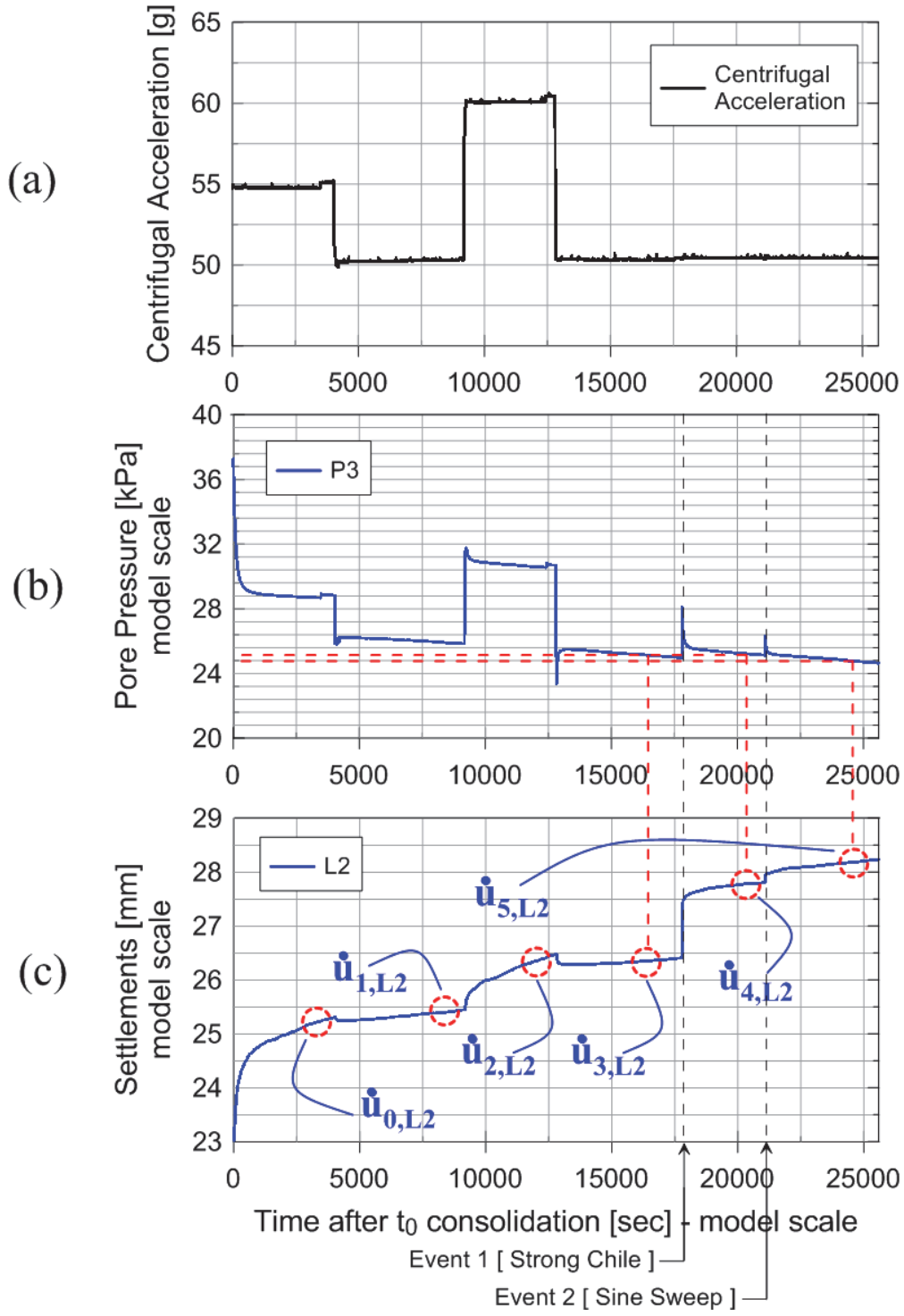

Figure 48 – Slow data of CL array in log scale of time after $t_{0,consolidation}$ showing (a) accelerations, (b) pore pressure and (c) settlements in model scale

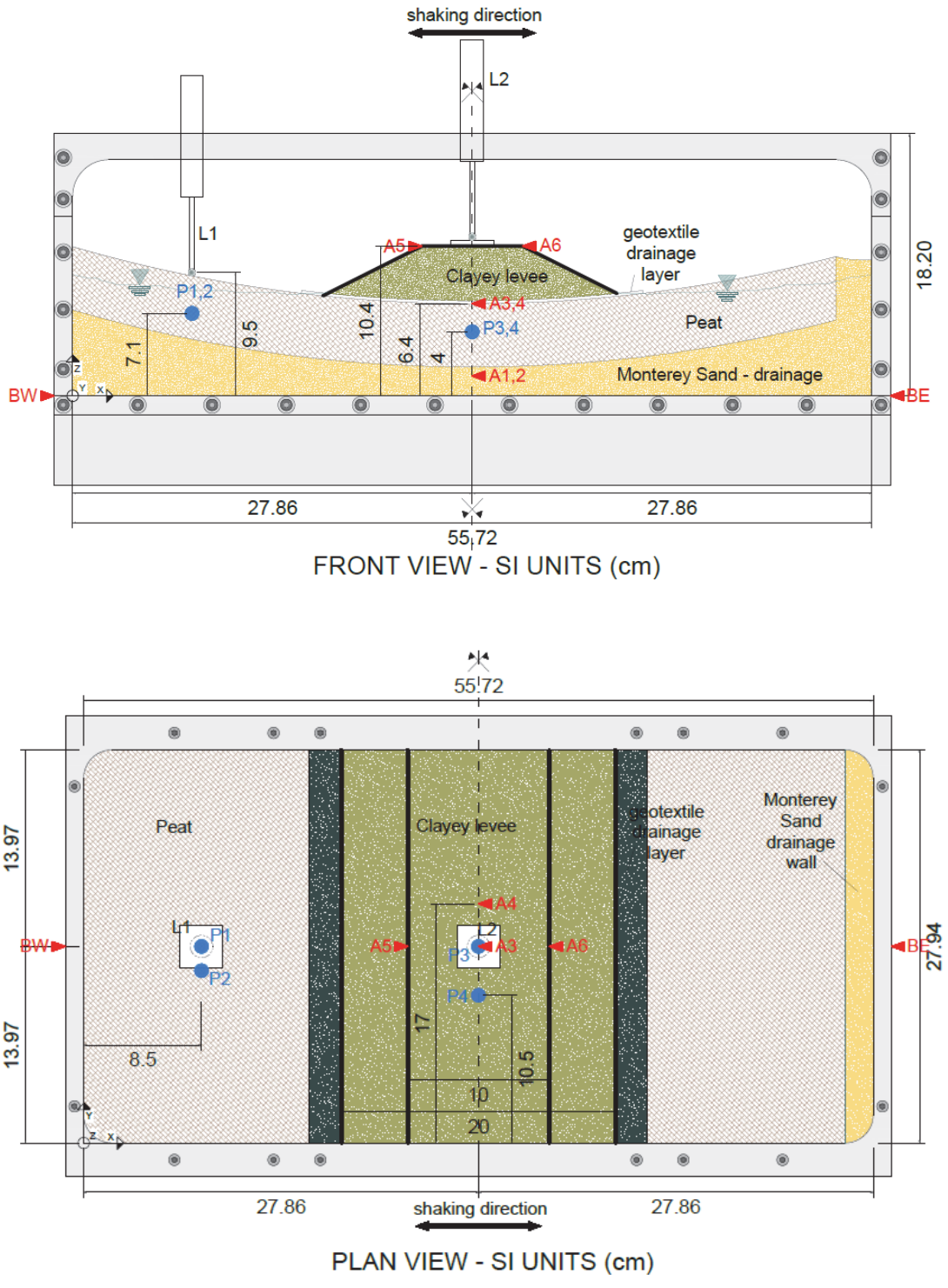

Figure 49 – Side view and plan of Experiment 16 at 1g before starting the spin on the second day

Table 9 contains the settlement rates at each stage for different quantities (in model and prototype scales). These values are independent of the selection of the consolidation clock reset ($t_{0,consolidation}$ or $t_{1,consolidation}$).

Table 9 – Settlement rates calculated for various stages of Experiment 16

Quant.	Unit	Scale	55g	50g	60g	50g	Event 1	Event 2
t_1	sec	model	10688	15573	19478	24533	27765	32167
s_1	mm	model	24.944	25.325	26.087	26.326	27.7	28.122
t_2	sec	model	12621	17610	21461	26561	29798	34208
s_2	mm	model	25.276	25.417	26.453	26.404	27.801	28.225
Δ Settl.	mm	model	0.332	0.092	0.366	0.078	0.101	0.103
Δ Time	sec	model	1933	2037	1983	2028	2033	2041
$Rate_1$	mm/sec	model	0.000172	0.000045	0.000185	0.000038	0.000050	0.000050
$Rate_2$	**mm/h**	**model**	**0.618**	**0.163**	**0.664**	**0.138**	**0.179**	**0.182**
$Rate_3$	cm/h	model	0.06	0.02	0.07	0.01	0.02	0.02
$Rate_4$	cm/h	proto	3.09	0.81	3.99	0.69	0.89	0.91
$Rate_5$	**cm/day**	**proto**	**74.2**	**19.5**	**95.7**	**16.6**	**21.5**	**21.8**
$Rate_6$	cm/week	proto	519.4	136.6	669.8	116.3	150.2	152.6
$Rate_7$	m/week	proto	5.1938	1.3658	6.6976	1.1631	1.5023	1.5261
			$u_{0,L2}$	**$u_{1,L2}$**	**$u_{2,L2}$**	**$u_{3,L2}$**	**$u_{4,L2}$**	**$u_{5,L2}$**

7.4 Chapter Summary and Conclusions

Slow data of Experiment 14 showed an increase in rate of secondary compression settlement of peat after the first strong ground motion (Strong Kobe, Trial 4), but the pre-quake rate was still too high and rendered estimation of the rate change difficult. An additional test (Experiment 16) was conducted on the 1m radius Schaevitz centrifuge to investigate this rate increase mechanism

following cyclic straining. Analyses of Experiment 16 data clearly show an increase in settlement rate following the two strong ground motions applied, confirming what observed in the lab by Shafiee (2016). Shafiee et al. (2015) showed a 1% cyclic shear strain threshold for such phenomenon to occur in the test they presented. More experiments are needed to investigate such threshold.

Augmented rates of secondary compression in peat following cyclic straining suggest the potential for an additional settlement of the foundation soil when cyclically loaded, which should be taken into account during analysis as a rate adjustment / reset. This novel mechanism has not been incorporated in any settlement prediction model in literature, and it can control the magnitude of deformations following an earthquake.

8. INERTIAL ASPECTS OF THE SSI

Inertial effects can result in augmented demands on both levee and foundation soil, and they have not been previously documented experimentally. Interaction features were identified and discussed in Chapter 6 while investigating strain components generated during Trial 4 (Strong Kobe) for Experiment 14. This chapter expands the SSI analysis by investigating the seismic response of the nonliquefiable clay levees of Experiment 12 and 14 during application of a sine sweep base excitation.

8.1 Seismic Response of Embankments on Peaty Soils

Regardless of the ground failure mechanism, its potential occurrence can only be reliably evaluated with a reasonably accurate characterization of seismic demand. Those demands can be associated with traditional wave propagation/site response effects, but also levee-foundation interaction mechanisms of the type investigated here. The interaction mechanism is analogous to a soil-structure interaction (SSI) problem, but unlike in a traditional SSI problem the emphasis here is on the effect of the interaction on the foundation soil, not the effect of the SSI on the response of the structure itself.

Most existing methods for demand characterization ignore the interaction mechanism as a source of demand. For example, the use of traditional r_d factors (Seed and Idriss, 1971) for the analysis of cyclic stress ratio (CSR) is based on 1-D wave propagation. Kishida et al. (2009b) formulated

2-D amplification factors to account for the increase in ground motion at the levee crest caused by topographic amplification through the levee cross-section. They did not, however, evaluate the influence of topographic amplification on stresses within and beneath the levee fills. Athanasopoulos-Zekkos and Seed (2013) considered 2-D wave propagation of levee-foundation systems using equivalent linear methods and evaluated CSR in the levee and foundation materials; those analyses suggest that high CSRs might be expected in the regions beneath the levee toe, but not beneath the levee crest. Those results are generally consistent with the interaction mechanism being investigated here.

Site response studies show that peat deposits amplify low-intensity ground motions, and de-amplify high-intensity ground motions, which is similar to the behavior of soft clays (e.g., Kramer 1996, Arulnathan 2000, Kishida et al. 2009a). Tokimatsu and Sekiguchi (2007) presented ground motion records for three sites very close to each other during the 2004 Mid Niigata earthquake, and reported that the strongest shaking (with a peak horizontal acceleration over 1g) occurred at a site underlain by a peat deposit, whereas shaking at a rock site and an inorganic soil site were lower. Therefore, the empirical evidence is that peat can transmit large-amplitude ground motions, and understanding the interaction between levees and underlying peat is therefore important.

8.2 Centrifuge Experiments

Setup, instrumentation, materials and construction procedures of Experiment 12 and 14 are discussed in Cappa et al. (2014 a,b) and in Chapter 5 of this manuscript. Figure 50 shows the

accelerometer layout for Experiment 14, identifies the free-field (FF) and center levee (CL) arrays, and points out the sensors whose record will be used in the analyses hereafter. Same notation was used for Experiment 12. Figure 51 shows vertical effective stress and V_s profiles for free field (FF) and center of levee (CL) conditions for both RCK01 and RCK02. The unit weight of the peat depends on vertical effective stress (Figure 52), i.e. the acceleration field while spinning.

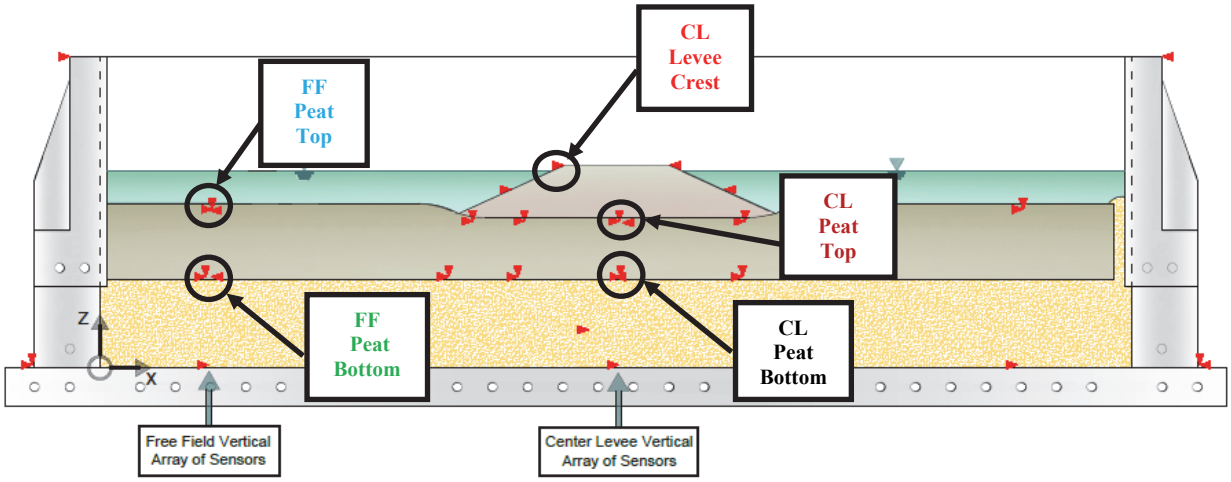

Figure 50 – FF and CL arrays for Experiment 14, and notation of important ICPs used in the analyses hereafter

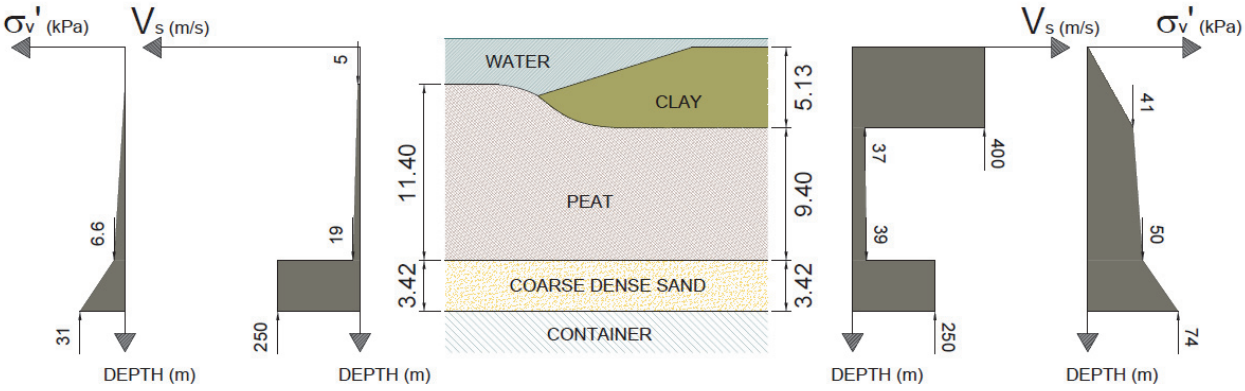

(a)

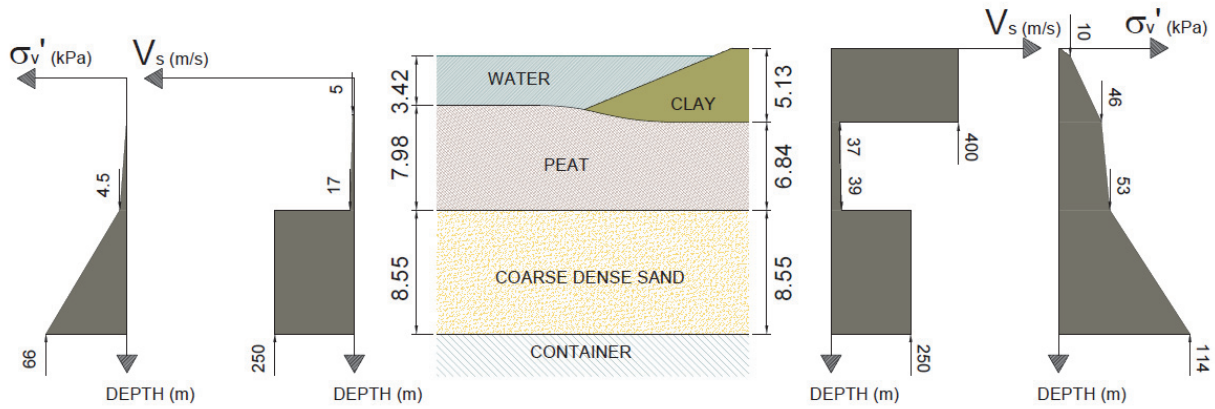

(b)

Figure 51 – FF and CL prototype soil profiles for RCK01 (a) and RCK02 (b)

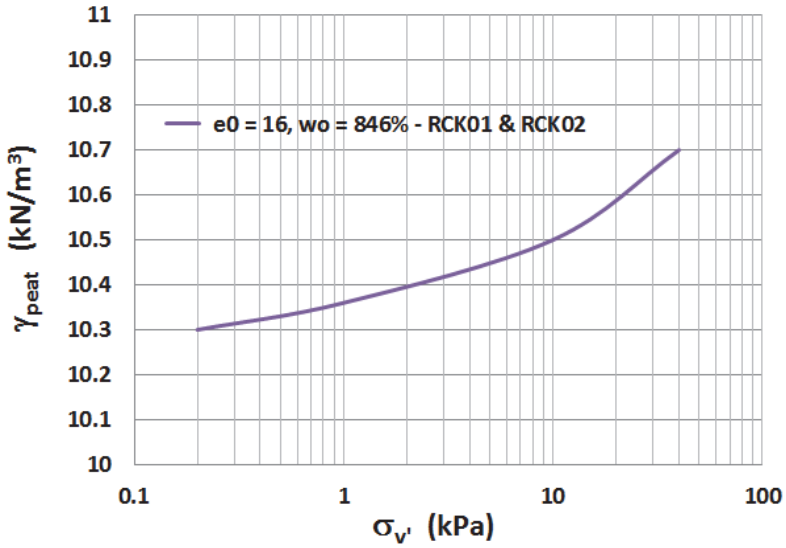

Figure 52 – Variation of peat unit weight with effective stress

8.3 Sine Sweep Characterization

The fundamental frequency of a structure is commonly estimated by applying a sweep function and finding the frequency producing the peak response. We applied a prototype-scale sine sweep

over a frequency range of 0.12 to 5.84 Hz. We sought a constant amplitude in velocity (to maintain similar strain levels), which produces variable acceleration and displacement amplitudes. The target peak acceleration amplitude was set at 0.02g at the centrifuge base. The sine sweep produced max strains in the FF and CL arrays of about 0.05 to 0.1% for both RCK01 and RCK02, which resides essentially within the linear elastic range of peat behavior (e.g., Kishida et al. 2009).

Figure 53 shows an example of the acceleration histories recorded for RCK01 and RCK02 at the peat base, free field peat ground surface and levee crest. The sensor positions are shown in Figure 50.

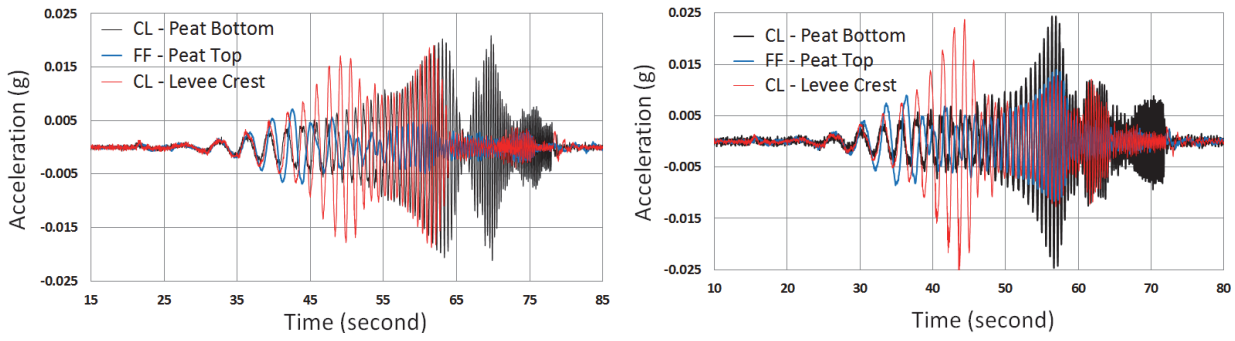

(a) – RCK01 (b) – RCK02

Figure 53 – Accelerations at peat bottom, free field peat top and levee crest for RCK01 (a) and RCK02 (b) during application of the Sine Sweep

Figure 54 shows horizontal acceleration histories for arrays in the FF (left) and CL (right) during application of the sine sweep in test RCK02. The results indicate that low frequencies at the top of the FF array are amplified and shifted in time relative to the base; whereas higher frequencies are de-amplified. In the CL array, the level of amplification is larger and occurs at a higher

frequency than in the FF. Amplification is also observed at different frequencies in the free-field compared with the levee center line due to differences in layer thicknesses and seismic velocities.

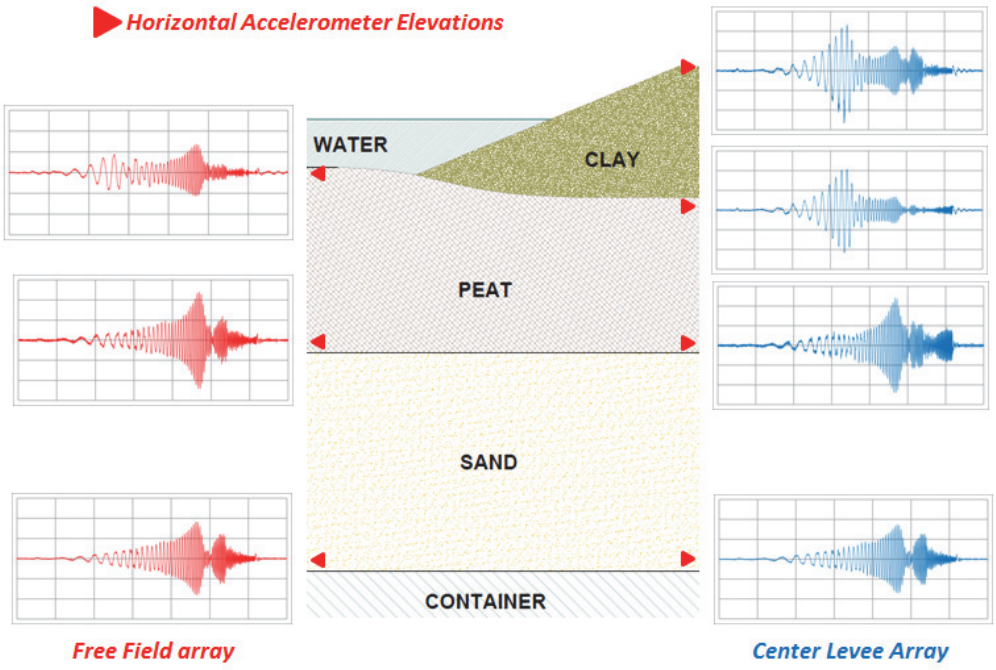

Figure 54 – Records of horizontal accelerometers for RCK02 for FF and CL arrays

8.4 Frequency Analysis and Transfer Functions

Data were recorded at a sampling frequency of 4167 Hz during application of the sine sweeps. Figure 55 shows Fourier amplitude spectra for both experiments for the CL array (multiple depths) and for the FF ground surface. The Fourier amplitude spectra of the acceleration time series show that the FF peat peaks at around 0.36 Hz, whereas the CL sensors have Fourier

amplitudes that peak near 0.63 Hz. The increased resonant-frequency for the CL condition results from the peat layer being thinner and stiffer than in the free-field due to consolidation beneath the levee.

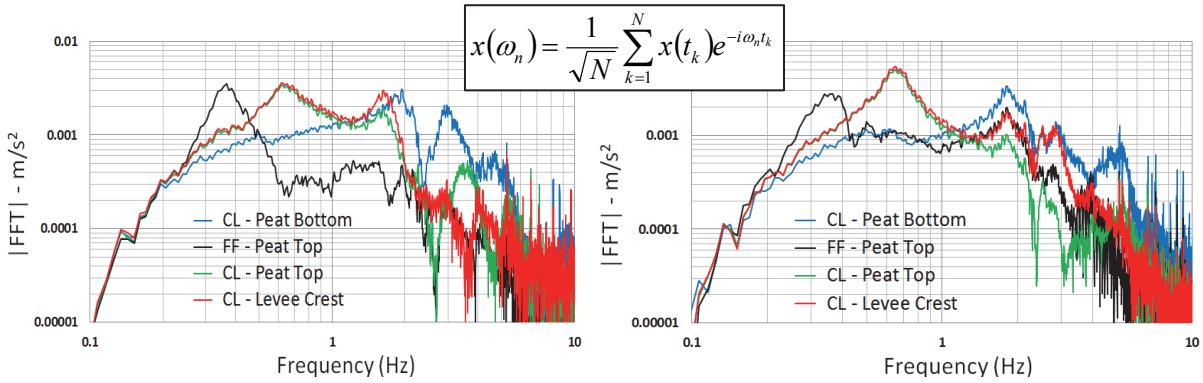

(a) – RCK01 (b) – RCK02

Figure 55 – Fourier amplitude spectra for (a) RCK01 and (b) RCK02. FFT algorithm is indicated as inset

To further interpret the recorded responses, we compute transfer functions from the data by taking ratios of the Fourier amplitude spectra (solid lines in Figure 55). Observed transfer functions are compared in Figure 55 to predictions from 1-D ground response analyses (using material properties Figure 51). The 1-D ground response analyses were performed with the intent of identifying features in the data that differ from the 1-D model predictions. Such differences may be interpreted in part as being associated with 2-D responses not captured by the analysis.

Input of the 1-D analyses are the profiles shown in Figure 58 and Figure 59, plus damping. Damping values were not measured directly. Initially, the recommendations of Kishida et al. (2009a) were utilized, but predicted significantly higher amplification than was measured. A damping ratio of 20% was found to produce reasonable agreement with the measured free-field amplification functions for both RCK01 and RCK02. Damping curves in centrifuge experiments have been found higher than in literature (Conti and Viggiani 2012; Elgamal et al. 2005).

According to Brennan et al. (2005) this is due to the increased loading frequencies in centrifuge testing, and for normally consolidated clay they observed an increase by 50 % in the dynamic damping when frequency is scaled from 1 to 50 Hz.

Figure 56 shows the transfer functions from data and 1-D ground response predictions for FF and CL profiles for RCK01. As with the Fourier amplitude in Figure 55, the transfer function in Figure 56a show a FF first mode at 0.36 Hz (2.77 sec). This peak is well captured by the 1-D ground response analysis. The transfer function ordinate at resonance is approximately 5. No clear second mode of vibration can be identified in the FF data, but is predicted by ground response analyses to be 0.87 Hz. The lack of a measured peak may be caused by higher damping at higher frequency, sensor resolution, or other unknown factors.

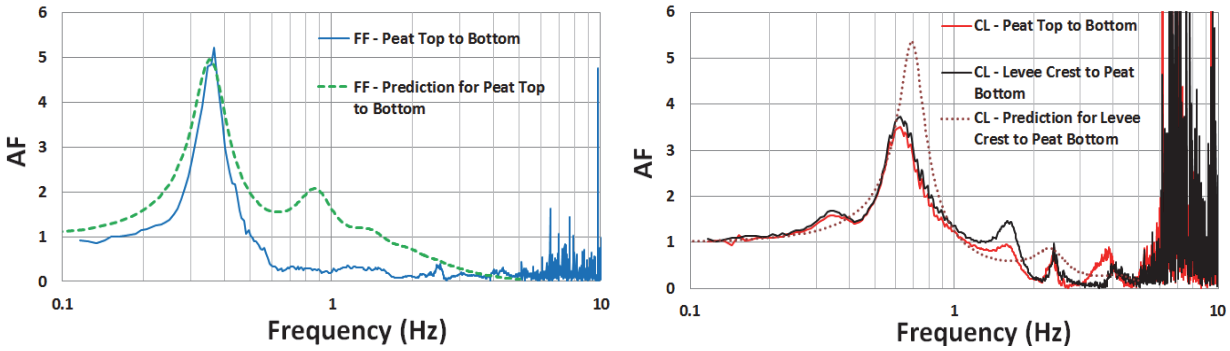

(a) – RCK01 (b) – RCK01

Figure 56 – Amplification factors for the FF (a) and CL (b) profiles for RCK01

For the CL array (Figure 56b) the maximum transfer function ordinate is 3.7 at a frequency of 0.63 Hz (1.59 sec). There are three additional local peaks at 1.65 Hz, 2.41 Hz and 3.83 Hz. The 1-D ground response analysis slightly overestimates the first mode frequency (0.68 Hz) and over predicts the peak amplification by about 50%. These features could be attributed to 2-D effects

not captured by the 1-D analysis. A second mode is predicted in the 1-D analysis for the CL array at 2.31 Hz, which is lower than the observed second mode of 1.65 Hz.

We hypothesize that the local peak near 1.65 Hz in the data is associated with a rocking mode, which naturally is not present in the 1-D analysis results. This hypothesis is tested by computing levee rotation using (1) a pair of vertical acceleration histories (divided by their horizontal separation distance to produce angular acceleration) from accelerometers at the peat-levee interface beneath the two edges of the embankment and (2) a pair of horizontal acceleration histories (divided by their vertical separation distance) from accelerometers at the levee base and crest in the CL array. Figure 57a shows the Fourier spectra of the levee rotational accelerations, which peak at 1.65 Hz, confirming that this mode from the transfer function in Figure 56b is from rotation. Figure 57b shows the transfer function of horizontal acceleration at the levee crest to that at the base, and again a peak occurs around 1.68 Hz, reinforcing the existence of a rocking mode.

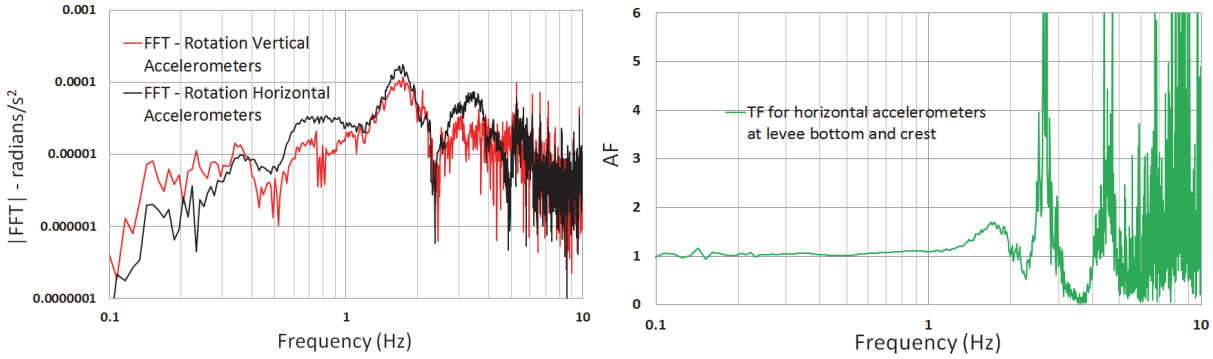

(a) – RCK01 (b) – RCK01

Figure 57 – Fourier spectra for vertical and horizontal pairs of accelerometers (a) and transfer function for the horizontal pair of accelerometers (b) for RCK01

Figure 58 shows a similar comparison between 1-D ground response analysis results and recorded data for RCK02. The recorded FF transfer function has a peak ordinate of 3.6 at 0.37 Hz (2.7 sec), which is well captured by 1-D analysis. The CL array transfer function has a peak ordinate of 5.4 (levee crest/peat bottom) at 0.69 Hz (1.45 sec). Two additional local peaks occur at 2.66 Hz and 3.91 Hz, which are comparable to the 3rd and 4th peaks observed in the recorded data for the same array in RCK01. The 1-D simulation overestimates the resonant frequency (0.88 Hz) but slightly under predicts amplification at resonance. The 1-D analysis also predicts a second mode peak near the 3.14 Hz that is again lower than the observed second mode of 2.68 Hz. Similar analyses of levee rocking are shown in Figure 59 and confirm that this peak in the transfer function is due to rotation.

We attribute the variable fundamental mode resonant frequencies from RCK01 and RCK02 of 0.63 and 0.69 Hz for the CL array to the varying peat thicknesses. However, proximity to the rigid wall of the container may also have played a role in the observed response. Further analysis of the data will be required to characterize these effects.

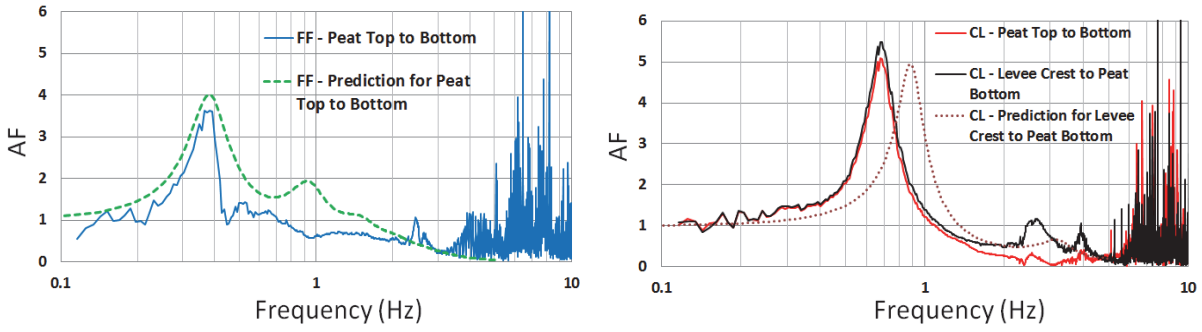

(a) – RCK02 (b) – RCK02

Figure 58 – Amplification factors for the FF (a) and CL (b) profiles for RCK02

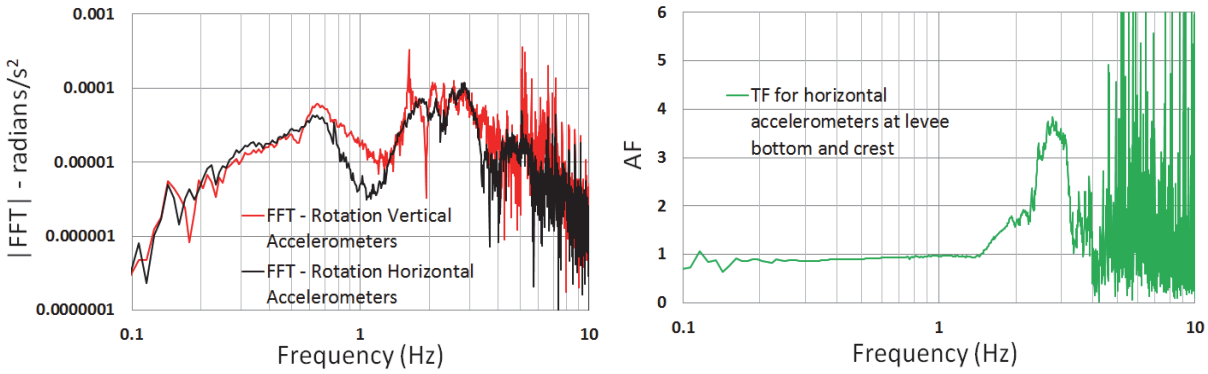

(a) – RCK02 (b) – RCK02

Figure 59 – Fourier spectra for vertical and horizontal pairs of accelerometers (a) and transfer function for the horizontal pair of accelerometer (b) for RCK02

8.5 Chapter Summary and Conclusions

We presented some preliminary results from centrifuge modeling of nonliquefiable embankments overlying peat of varying thickness during application of sine sweep waves. Some of the results reinforce expectations of levee response over soft soil: there is a strong resonant response driven by the soft foundation soil conditions and the large impedance contrast with underlying soils. However, other results are relatively new, especially the development of a substantial rocking response in the embankment that would appear to have the potential to significantly contribute to seismic demands in embankment and foundation soils near the embankment edges. These effects have been observed previously in analytical studies (Athanasopoulos-Zekkos and Seed, 2013), but to our knowledge have not be documented previously in experiments. Long-term implication and work underway include development of methods of analysis that can predict seismic demands on foundation soils and levee fill materials (particularly liquefiable levee fills) from embankment-foundation soil interaction

9. SANDY LEVEE PERFORMANCE

9.1 Introduction

The Delta earthquake scenario is one of the most important hazards facing the United States because the consequences of such an event would be unimaginably catastrophic considering that Delta water is the sole source for many agricultural communities and constitutes a significant fraction of urban water supply. Consensus among the scientific community is that the Delta earthquake scenario is a significant threat, but many Delta landowners and local engineers perceive the earthquake threat as a scare tactic created by special interests to justify construction of an alternative water conveyance system that bypasses the Delta. Much of their mistrust of the scientific community stems from a lack of understanding of liquefaction hazard, and there is an acute need to effectively and clearly communicate risk to lawmakers. To fill this gap, our 9m radius centrifuge experiments the modeled sandy levees (Experiment 13 and 15) were set up to visually capture and record the actual seismic performance of the systems to a target ground motion representative of the 500 year return period scenario estimated for the region (CDWR, 2009-6). For this purpose, the experiments were constructed in the rigid container with transparent side walls, which allowed for videotaping in flight. Videos and pictures of these experiments are available ate the project warehouse (http://nees.org/warehouse/project/1161). The primary educational objective of the entire project was indeed to help advise the important decisions that are currently being made regarding California's water distribution system. Videos

of these two experiments provide an excellent educational tool to demonstrate the effects of earthquakes on liquefiable levee fills.

9.2 Centrifuge Experiments

In both experiments, the sandy levee showed substantial vertical deformation. For Experiment 13 a premature failure of the pumping system and an excessively rigid spillway prevented the correct containment of the slough, therefore resulting in a hydrostatic water table when the levee was shook. Although this setup imposed decreased demands on the embankments, video tapes and sensor records showed liquefaction features and remarkable deformations. Experiment 15 was instead successful in diverting the water volume up until the target ground motion was applied. Figure 60 shows slow data quantities including centrifuge g-level, pore pressure, and settlement for Experiment 15 for a time span that encompasses spin-up, application of a step wave and three ground motions, and spin-down. The model was spun up in increments until the target acceleration of 57g was reached, with each increment approximately doubling the g-level. The incremental spin-up permitted pore pressures in the peat to decrease, and undrained shear strength to increase, so that the peat could support the load imposed by the levee. This process took approximately 3 hours. After reaching the target g-level, the model was permitted to consolidate for about 45 minutes. As pore pressures decreased, settlement continued to increase due to primary consolidation and secondary compression in the peat, and the levee showed signs of distress as a result of this settlement. The ground motions were imposed before the levee accumulated too much distress, and P6 was still decreasing slightly at this time. The total

consolidation settlement measured at the levee crest prior to the application of the first ground motion was 55 mm (L14), while 35 mm of settlement occurred in the free-field (L7). This consolidation settlement translates to prototype settlements of 3.13 m and 2.0 m for levee crest and free field, respectively.

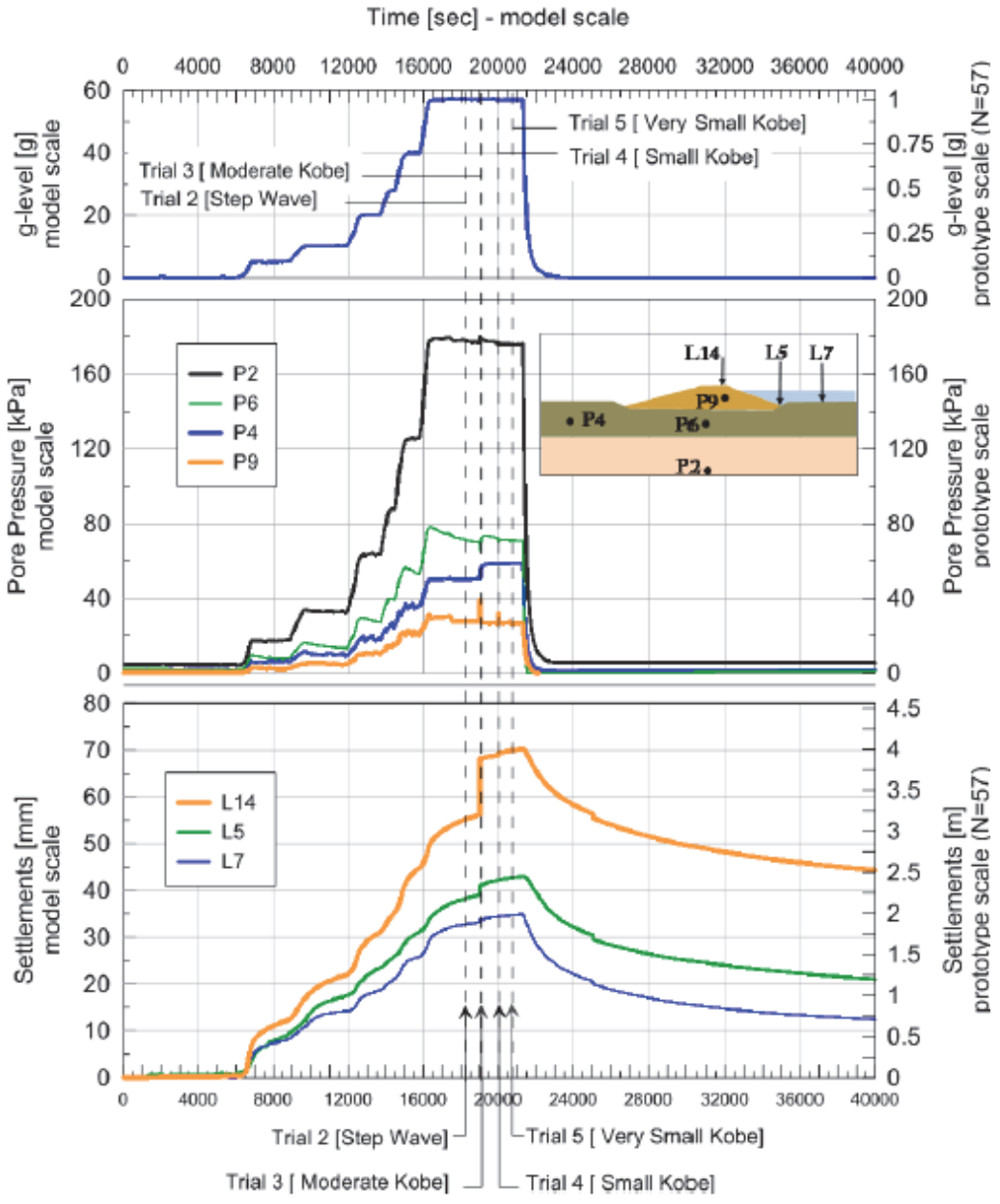

Figure 60 – Slow data Experiment 15

The moderate Kobe motion (Trial 3) had a peak base acceleration of 0.355g, and the levee fill liquefied and slumped, resulting in a breach with water from the channel pouring over the levee and eroding it away until the water elevation equalized on both sides of the levee (Figure 61). Settlements at the levee crest measured 13 mm to 16 mm in model scale, which translates to 0.71 m – 0.91 m in prototype. Videos capturing the liquefaction process and sandy levee failure are available on the NEES project warehouse. The excess pore pressure within the levee fill recorded by P9 abruptly rises during application of the Kobe motion and quickly dissipates due to the high permeability of the sand, whereas the excess pore pressure in the peat beneath the levee decreases slowly after the ground motion. Pore pressure in the free-field on the landward-side of the levee abruptly increases and remains elevated. This is due to the water in the channel being released, 15 thereby permanently elevating the groundwater table on the landward free-field side of the levee.

Two more ground motions with smaller amplitudes (Trial 4 and Trial 5, Table 6) were applied after the moderate Kobe motion to observe the threshold for liquefaction triggering in the levee fill and to simulate aftershocks. These motions induced a measurable pore pressure and settlement response. Fast data recorded during the moderate Kobe motion are shown in Figure 62, including acceleration, pore pressure, and settlement, all in prototype units. The peak base acceleration was 0.355g and the peak acceleration of the levee crest was 0.28g, indicating that the soil profile de-amplified the input motion. The pore pressure in the center of the sandy levee increased by approximately 30 kPa, which is equal to the initial vertical effective stress at the levee center, indicating the levee fill liquefied. Pore pressures in the sand remained elevated for the duration of shaking, then dissipated quickly after shaking ceased.

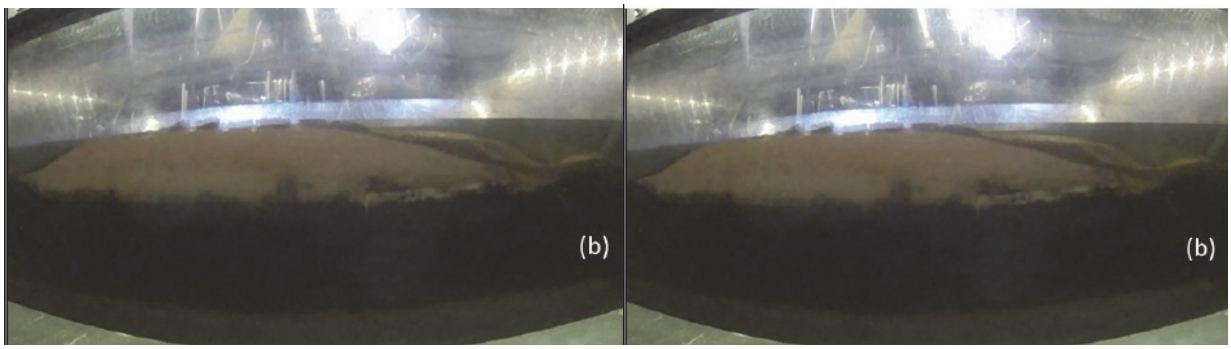

Figure 61 – Side view of Experiment 15 (a) before start spinning and (b) after application of the target Kobe motion (Trial 3)

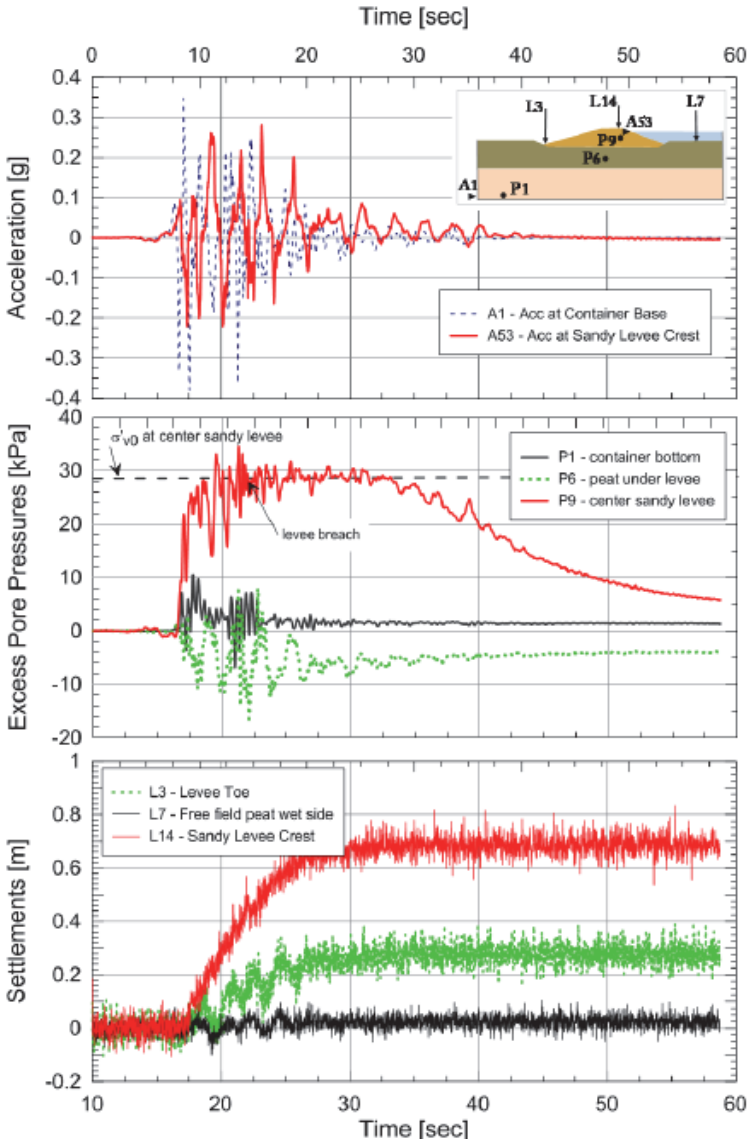

Figure 62 – Fast data for Experiment 15 during target Kobe motion (Trial 3)

Figure 62 also shows the excess pore pressure in the peat beneath the levee (P6) exhibited a dynamic response during shaking and a net reduction from the beginning to the end of shaking. This pore pressure response is caused by a combination of shearing and changes in total stress as the levee breached and water flowed over the top. Settlement records exhibit significant high frequency noise, but a dynamic response is evident superposed on the noise, and the permanent component is clear. The levee crest settled 0.7 m at the position of L14, which is near the center of the levee. The breach occurred where settlement was highest, between the center of the levee and the container wall.

9.3 Chapter Summary and Conclusions

Experiment 13 and 15 tested sandy levees atop peat characteristic of typical Delta levee systems. The models were consolidated and then subjected to target ground motions representative of the 500 year return period earthquake scenario with PBA of 0.35-0.4g. Failure and liquefaction of the model levees was clearly observed visually and demonstrated by recorded slow and fast data. These concrete data and tapes will provide legislators with a clear understanding of the problem and risk, and ultimately help make better informed decisions. Future work will use such data in order to develop a better integrated framework to reliably characterize the seismic response of sandy levee fill atop soft organic foundations.

10. THESIS SUMMARY, CONCLUSIONS AND FUTURE WORK

10.1 Thesis Summary

Four large scale 9m radius and twelve 1m radius centrifuge tests were performed at the NEES@UCDavis equipment site to study the seismic and post-seismic behavior of levee structures resting atop soft organic peat. The model configurations using a non-liquefiable levee focused on the seismic deformation potential of peat during primary consolidation and secondary compression. The tests performed with a sandy levee studied the liquefaction potential of saturated loose sand fill overlying soft peat as well as the levee-peat-interaction under different loading conditions. The models were subjected to scaled ground motions representative of the Sacramento – San Joaquin Delta. System instrumentation consisted of linear potentiometers, pore pressure sensors and accelerometers. Slow data recorded at 1Hz documented the settlements during spin up, application of ground motions, and spin down. Fast data sampled at 4167Hz measured the dynamic response of the system, the excess pore pressure increase and immediate settlements. Bender elements, miniature CPT and high definition/speed cameras helped collection of important data during testing.

Measured excess pore pressure and strains generated in the peat layer in the 9m radius tests were analyzed and compared with simple FEM analyses using bilinear quadrilateral elements. Shear strain amplitudes in the peat across the levee cross-section were found to be of similar magnitude, while vertical strains in the levee toe region were 2.5 times larger than strains beneath the levee center, experimentally documenting for the first time levee rocking under

seismic loading. Inertial rocking features were confirmed with analyses of transfer functions and Fourier spectra of rotational time histories, and can result in augmented demands, especially at levee toes. Centrifuge strain components were combined and compared with strain measurements from direct simple shear at constant volume tests on the same peat by studying the octahedral shear strain as deviatoric invariant, and were found in reasonable agreement. Excess pore pressure generation was mobilized at a proposed shear strain threshold of 1% and increased exponentially with strain amplitude thereafter. This novel 1% threshold proposed for peats is about 10 times higher than the threshold for clays suggested in literature and 100 times than sands (Vucetic, 1994). Residual excess pore pressures up to 0.2 were observed in the centrifuge experiment, suggesting the potential for significant volumetric strains in the highly compressible peat that would augment the risk of free board loss. Octahedral strains of up to 1% and 6% were achieved in the peat layer with ground motions waves with peak base acceleration of 0.15g and 0.52g respectively, indicating that large deformations were generated for low levels of cyclic loading. In-situ levees atop soft foundation are expected to be subject to such large deformations during similar ground motions intensities in the Delta. Following observations from slow data collected during the 9m radius investigations, an additional 1m radius centrifuge test investigated the post-cyclic volume change of peat and experimentally documented an increase in rate of settlement following cyclic straining of up to 30%, which would result in even higher free board loss. The sandy levee experiments tested typical Delta levees subjected to a target ground motion with peak base accelerations of 0.35-0.4g, representative of the 500 years return period hazard risk estimated for the region (DWR, 2009-6). Liquefaction of the levee fill and critical deformations were documented by both sensor records and video tapes, providing effective data that demonstrate the potential for a massive levee system failure.

10.2 Thesis Conclusions and Future Work

Findings of this project represent a step towards characterization of deformation modes of earthen embankments atop soft organic foundations. Results presented could lead directly to obtain a more comprehensive understanding of the technical impact of seismic hazards posed to levees in the Delta and worldwide. The research findings will be disseminated to earthquake engineers, social scientists, water resources engineers, environmental engineers, levee inspectors, insurance companies, emergency planners, agrarian societies and legislators, with the expected impact of flourishing a multi-disciplinary collaborative effort towards a more accurate analysis of the seismic vulnerability of the levees in the Delta, and ultimately better informed mitigation decisions.

This project is part of a broader research effort to develop a simplified framework for estimating the response of levees founded on soft soils. Other 6 graduate students are working in parallel and tackling the problem from different perspectives, e.g. numerical simulations, lab testing, new constitutive models, field testing and fragility curves. The collaborative spirit among the research team permitted to build upon the work of each other, creating a unique work environment and opening the floor to endless possibilities to expand the findings of this project.

Immediate future work will first focus on the SSI component of the levee system response. Data collected in the centrifuge experiments will permit the evaluation of elastodynamic soil-structure interaction analyses of the levee-peat system, which propose interaction springs that quantify the flexibility and energy dissipation associated with levee-foundation interaction in shear and

rotational vibration modes. Analyses of levee response to different input motions will also result in a better evaluation of shear and moment demands on the interaction springs. Characterization of springs and demands will be combined with constitutive models to develop a novel analytical framework. Constitutive models will be built upon the proposed 1% cyclic strain threshold for pore pressure generation, and upon the documented secondary compression rate increase in peats following moderate cyclic loading. Outcomes of such improved analyses will allow the characterization of cyclic stress demands and seismic coefficients at various locations within the levee. These demands would be useful for analysis of levee fill liquefaction potential and deformations. Total seismic demands would consist of those associated with the site response and those associated with the levee-foundation interaction (dynamic stress solutions), and could be used for example in liquefaction triggering or cyclic softening procedures. This simplified approach could be efficiently implemented as a routine for levee stability evaluation and allow a more reliable risk assessment, which in turn will result in infrastructure retrofit and/or construction decisions that will be more likely to maintain functionality of the water system during and following extreme events.

REFERENCES

Abdoun, T., Gonzalez, M., Thevanayagam, S., Dobry, R., Elgamal, A., Zeghal, M., Mercado, V. and El Shamy, U. (2013) "Centrifuge and Large-Scale Modeling of Seismic Pore Pressures in Sands: Cyclic Strain Interpretation", *Journal Geotechnical and Geoenvironmental Engineering*, Vol. 139, No. 8, pp. 1215-1234

Adams, J.I. (1963) "A Comparison of Field and Laboratory Consolidation Measurements in Peat", *Proceedings of 9th Muskeg Research Conference*, NRCC, 117-135

Ahnberg, H. (2006) "Strength of Stabilized Soil – A Laboratory Study on Clays and Organic Soils Stabilized with Different Types of Binder", *Dissertation, Lund University Publications*, https://lup.lub.lu.se/search/publication/546661

Arulanandan, K. and Scott, R.F. (1993-1994) "Verification of Numerical Procedures for the Analysis of Soil Liquefaction Problems", *Proceedings of the International Conference on the Verification of Numerical Procedures for the Analysis of Soil Liquefaction Problems,* Balkema, Rotterdam, Vols. 1 and 2

Arulnathan, R., Boulanger, R.W. and Riemer, M.F. (1998) "Analysis of Bender Element Tests", Geotechnical Testing Journal, Vol. 21, No. 2, pp. 120-131

Arulnathan, R. (2000) "Dynamic Properties and Site Response of Organic Soils", *Ph.D. thesis, University of California, Davis*

Arulnathan, R., Boulanger, R.W. and Idriss, I.M. (2001) "Site Response of Organic Soils", *4th International Conference on Recent Advances in Geotechnical Earthquake Engineering and Soil Dynamics*, Paper No. 6

Asaoka, A., Nakano, M. and Noda, T. (2000) "Superloading Yield Surface Concept for Highly Structured Soil Behavior", *Soils and Foundations*, Vol. 40, No. 2, pp.99-110

Athanasopoulos-Zekkos, A. and Seed, R.B. (2013) "Simplified Methodology for Consideration of Two-Dimensional Dynamic Response of Levees in Liquefaction-Triggering Evaluation", *Journal of Geotechnical and Geoenvironmental Engineering*, Vol. 139, No. 11, pp. 1911-1922

Bain, C.G., Bonn, A., Stoneman, R., Chapman, S., Coupar, A., Evans, M., Gearey, B., Howat, M., Joosten, H., Keenleyside, C., Labadz, J., Lindsay, R., Littlewood, N., Lunt, P., Miller, C.J., Moxey, A., Orr, H., Reed, M., Smith, P., Swales, V., Thompson, D.B.A., Thompson, P.S., Van de Noort, R., Wilson, J.D. and Worrall, F. (2011) "IUCN UK Commission of Inquiry on Peatlands", *IUCN UK Peatland Programme*, Edinburgh

Berry, P.L. and Poskitt, T.J. (1972) "The Consolidation of Peat", *Geotechnique*, Vol. 22, No. 1, pp. 27-52

Berry, P.L. and Vickers, B. (1975) "Consolidation of Fibrous Peat", *Journal of Geotechnical Engineering*", ASCE, Vol. 101, pp. 741-753

Boulanger, R.W., Arulnathan, R., Harder, L.F.J., Torres, R.A. and Driller, M.W. (1998) "Dynamic Properties of Sherman Island Peat", *Journal of Geotechnical and Geoenvironmental Engineering*, Vol. 124, No. 1, pp. 12-20

Brandenberg, S.J., Kutter, B.L. and Wilson, D.W. (2008) "Fast Stacking and Phase Corrections of Shear Wave Signals in a Noisy Environment", *Journal of Geotechnical and Geoenvironmental Engineering*, ASCE, Vol. 134, pp. 1154-1165

Bray, J.D. and Travasarou, T. (2007) "Simplified Procedure for Estimating Earthquake-Induced Deviatoric Slope Displacements", *Journal of Geotechnical and Geoenvironmental* Engineering, ASCE, Vol. 133, No. 4, pp. 381-392

Brennan, A.J., Thusyanthan, N.I. and Madabhushi, S.P.G. (2005) "Evaluation of Shear Modulus and Damping in Dynamic Centrifuge Tests", *Journal of Geotechnical and Geoenvironmental Engineering*, Vol. 131, No. 12, pp. 1488-1497

Building Seismic Safety Council (1997) "FEMA 302: NEHRP Recommended Provisions for Seismic Regulations for New Buildings and Other Structures, Part I – Provisions", *Building Seismic Safety Council*, Washington, DC, pp. 337

Cappa, R., Yniesta, S., Brandenberg, S., Stewart, J.P. and Lemnitzer, A. (2014a) "NEESR: Levees and Earthquakes: Averting and Impending Disaster- Data Report for Centrifuge Experiments 12L and 13L", *NEESHub, Final Project Report*, https://nees.org/warehouse/project/1161

Cappa, R., Yniesta, S., Brandenberg, S., Stewart, J.P. and Lemnitzer, A. (2014b) "NEESR: Levees and Earthquakes: Averting and Impending Disaster- Data Report for Centrifuge Experiments 14L and 15L", *NEESHub*, *Final Project Report*, https://nees.org/warehouse/project/1161

Cappa, R., Yniesta, S., Brandenberg, S., Stewart, J.P. and Lemnitzer, A. (2014c) "Centrifuge Experiments to Evaluate the Seismic Performance of Levees on Peaty Soils in the Sacramento-San Joaquin Delta", *ASDSO Dam Safety National Conference*, San Diego, CA

Cappa, R., Yniesta, S., Lemnitzer, A., Brandenberg, S. and Shaifee, A. (201a5) "Settlement Estimations of Peat during Centrifuge Experiments", *Geocongress 2015,* San Antonio, Texas, pp. 152-160

Cappa, R., Yniesta, S., Brandenberg, S. and Lemnitzer, A. (2015b) "Settlements and excess pore pressure generation in peaty soils under embankments during cyclic loading", *Geocongress 2015,* San Antonio, Texas, pp. 152-160

Cappa, R., Yniesta, S., Brandenberg, S., Stewart, J.P. and Lemnitzer, A. (2016) "Seismic and Post-seismic Behavior of Embankments atop Peat", paper under review

CDWR (2009-6) "Delta Risk Management Strategy – Executive Summary", Final Phase 1 Report, Risk Report: Section 6, pp. 114-115

Chandler, C.J. and Chartres, F.R.D. (1988) "Settlement Measurement and Analysis of Three Trial Embankments on Soft Peat Ground", *Baltic Conference on Soil Mechanics and Foundation Engineering on Peats and Deformations of Structures on Highly Compressible Soils*, Vol. 1, pp. 268-272

Cola, S. and Cortellazzo, G. (2005) "The Shear Strength Behavior of Two Peaty Soils", *Geotechnical and Geological Engineering*, Vol. 23, pp. 679-695

Conti, R. and Viggiani, G.M.B. (2012) "Evaluation of Soil Properties in Centrifuge Tests", *Journal of Geotechnical and Geoenvironmental Engineering*, Vol. 138, No. 7, pp. 850-859

Crane, R.C (1995) "Geology of the Mt. Diablo Region and East Bay Hills - Sangines, E.M. et al., eds*", Recent geologic studies in the San Francisco Bay Area: Society of Economic Paleontologists and Mineralogists*, Pacific Section 76, pp. 87–114

Dashti, S. (2009) "Toward Developing an Engineering Procedure for Evaluating Building Performance on Softened Ground", *Ph.D. Thesis, University of California, Berkeley, CA*

Den Haan, E.J. (1996) "A Compression Model for Non-Brittle Soft Clays and Peat", *Geotechnique,* Vol. 46, Issue 1, pp. 1-16

Deverel, S.J. and Leighton, D.A. (2010) "Historic, Recent, and Future Subsidence, Sacramento-San Joaquin Delta, California, USA", *San Francisco Estuary and Watershed Science*, Vol. 8, Issue 2

Dhowian, A.W. and Edil, T.B. (1980) "Consolidation Behavior of Peats", *Geotechnical Testing Journal*, Vol. 3, No. 3, pp. 105-114

Dobry, R., Ladd, R.S., Yokel, F.Y., Chung, R.M. and Power, D. (1982) *"*Prediction of Pore Water Pressure Buildup and Liquefaction of Sand during Earthquakes by the Cyclic Strain Method*"*, *National Bureau of Standards Building Science Series 138*, Washington, DC, 1982, pp.154

DWR (1995) "Sacramento-San Joaquin Delta Atlas", *California Department of Water Resources*

DWR (2007) "Delta Emergency Operations Plan – Concept Paper", *California Department of Water Resources*

Edil, T.B. and Mochtar, N.E. (1984) "Prediction of Peat Settlement", *Proceedings of Symposium on Sedimentation and Consolidation Models*, ASCE, San Francisco, pp. 411-424

Edil, T.B., Fox, P.J. and Lan, L.T. (1994) "Stress-Induced One-Dimensional Creep of Peat", *Advances in Understanding and Modelling the Mechanical Behavior of Peat*, Balkema, Rotterdam, pp. 3-18

Edil, T.B. and Wang, X. (2000) "Shear Strength and K_o of Peats and Organic Soils," Geotechnics of High Water Content Materials, *ASTM STP 1374*, ASTM International, West Conshohocken, PA, pp. 209-225

Egawa, T., Nishimoto, S. and Tomisawa, K. (2004) "An Experimental Study on the Seismic Behavior of Embankments on Peaty Soft Ground through Centrifuge Model Tests", *13th World Conference on Earthquake Engineering*, Paper No. 36

Elgamal, A., Yang, Z., Lai, T., Kutter, B.L. and Wilson, D.W. (2005) "Dynamic Response of Saturated Dense Sand in Laminated Centrifuge Container", *Journal of Geotechnical and Geoenvironmental Engineering*, Vol. 131, No. 5, pp. 598-609

Finch, M. (1985) "Earthquake Damage in the Sacramento-San Joaquin Delta", *California Geology*, pp. 39-44

Fox, P.J., Edil, T.B. and Lan, L.T. (1992) "C_α/C_c Concept Applied to Compression of Peats", *Journal of Geotechnical Engineering*, ASCE, Vol. 118, Issue 8, pp. 1256-1263

Fox, P.J. and Edil, T.B. (1994) "Micromechanics Model for Peat Compression", *Advances in Understanding and Modelling the Mechanical Behaviour of Peat*, Balkema, Rotterdam, pp. 159-166

Fugro (2009) "Characterization of Potential Seismic Sources in the Sacramento-San Joaquin Delta, California", *Final Technical report for USGS under Award Number 08HGGR0056*

Fuis, G.S. and Mooney, W.D. (1990) "Lithospheric Structure and Tectonics from Seismic-Refraction and other Data", *The San Andreas Fault System*, USGS, Paper No. 1515, pp. 207-238

Gens, A. and Nova, R. (1993) "Conceptual Bases for a Constitutive Model for Bonded Soils and Weak Rocks", *Symposium on Geotechnical Engineering of Hard Soils – Soft Rocks*, Athens, Vol. 1, pp. 485-494

Greensfelder, R.W. (1974) "Maximum Credible Rock Acceleration from Earthquakes in California", *California Division of Mines and Geology,* Map Sheet MS-23

Grimstad, G. and Degago, S. (2010) "A Non-Associated Creep Model for Structured Anisotropic Clay (n-sac)", *Numerical Methods in Geotechnical Engineering*, Taylor & Francis Group

Hanrahan E.T. (1954) "An Investigation of Some Physical Properties of Peat", *Géotechnique*, London, England, Vol. 4, No. 2, pp. 108-123

Hanrahan, E.T., Dunne, J.M. and Sodha, V.G. (1967) "Shear Strength of Peat", *Proceedings of the Geotechnical Conference*, Norwegian Geotechnical Institute, Oslo, Norway, Vol. 1, pp. 193-198

Hendry, M.T., Sharma, J.S., Martin, C.D. and Barbour, S.L. (2012) "Effect of Fiber Content and Structure on Anisotropic Elastic Stiffness and Shear Strength of Peat", *Canadian Geotechnical Journal*, Vol. 49, pp. 403-415

Hendry, T.M., Martin, C.D. and Barbour, S.L. (2013) "Measurement of Cyclic Response of Railway Embankments and Underpaying Soft Peat Foundations to Heavy Axle Loads", *Canedian Geotechnical Journal*, Vol. 50, pp. 467-480

Holtz, R.D., Kovacs, D.W. and Sheahan T.C. (2011) "An Introduction to Geotechnical Engineering (2nd Edition)", *Prentice-Hall*

Hsu, C.C. and Vucetic, M. (2006) "Threshold Shear Strain for Cyclic Pore-Water Pressure in Cohesive Soils", *Journal of Geotechnical and Geoenvironmental Engineering*. Vol. 132, No. 10

Huat, B.B.K., Kazemian, S., Prasad, A., and Barghchi, M. (2011) "State of an Art Review of Peat: General Perspective", *International Journal of the Physical Sciences*, Vol. 6, Issue 8, pp. 1988-1996

Idriss, I.M. and Boulanger, R.W. (2008) "Monograph MNO-12: Soil Liquefaction during Earthquakes", *EERI*, Oakland, CA

Ingebritsen, S.E., Ikehara, M.E., Galloway, D.L. and Jones, D.R. (2000) "Delta Subsidence in California; the Sinking Heart of the State", *U.S. Geological Survey*, Fact Sheet FS-005-00

Jain, S.K. and Nanda, A. (2010) "On the Nature of Secondary Compression in Soils", *Indian Geotechnical Conference*, Vol. 2, pp. 1121-1124

Joosten, A. (2010) "The Global Peatland $C0_2$ Picture", *Wetlands International*

Kaat A. and Joosten, H. (2008) "Fact Book for UNFCCC Policies on Peat Carbon Emissions", *Wetlands International*, Ede, pp. 26

Karol, R.H. (2003) "Chemical Grouting and Soil Stabilization (3rd Edition)", *Dekker*, New York

Kavvadas, M. and Amorosi, A. (2000) "A Constitutive Model for Structured Soils", *Geotechnique*, Vol. 50, No. 3, pp. 263-273

Kazemian, S., Huat, B.B.K., Prasad, A. and Barghchi, M. (2011) "A State of Art Review of Peat: Geotechnical Engineering Perspective", *International Journal of the Physical Science*, Vol. 6, No. 8, pp. 1974-1981

Kazemian, S. and Moayedi, H. (2014) "Improvement of Settlement Problems of Fibrous Peat", *Application of Nanotechnology in Pavements, Geological Disasters, and Foundation Settlement Control Technology*, ASCE GSP (Geotechnical Special Publications Book Series) No. 244

Kishida, T., Boulanger, R.W., Abrahamson, N.A., Wehling T.M. and Driller, M.W. (2009a) "Regression Models for Dynamic Properties of Highly Organic Soils", *Journal of Geotechnical and Geoenvironmental Engineering*, ASCE, Vol. 135, pp. 533-543

Kishida, T., Boulanger, R.W., Abrahamson, N.A., Driller, M.W. and Wehling T.M. (2009b) "Site Effects for the Sacramento-San Joaquin Delta", *Earthquake Spectra*, EERI, Vol. 25, No. 2, pp. 301-322

Kogure, K. and Ohira, Y. (1979) “A Structure Model of Highly Organic Soils”, *Proceedings of the Symposium on Organic Soils*, *JSSMFE* (Japanese Society for Soil Mechanics and Foundation Engineering), pp-11-16 (in Japanese)

Kogure, K. (1993) “An Analytical Prediction of Consolidation Settlement of Fibrous Peat Under Loading”, *Proceeding of the Third International Conference on Case Histories in Geotechnical Engineering*, St. Louis, Missouri, Paper No. 13.06

Kramer, S.L. (1996) “Dynamic Response of Peats”, *Final Research Report WA-RD 412.1*, Washington State Transportation Center, University of Washington, Seattle, Washington

Kramer, S.L. (2000) “Dynamic Response of Mercer Slough Peat”, *Journal of Geotechnical and Geoenvironmental Engineering*, Vol. 126, No. 6, pp. 504-510

Krug, E.H., Cherven, V.B., Hatten, C.W. and Roth, J.C. (1992) “Subsurface Structure in the Montezuma Hills, Southwestern Sacramento Basin”, Cherven, V.B. and Edmondson W.F. Eds., *Structural Geology of the Sacramento Basin, Annual Meeting, Pacific Section, Society of Economic Paleontologists and Mineralogists*, Vol. MP-41, pp. 41-60

Kutter, B.L. (1992) "Dynamic Centrifuge Modeling of Geotechnical Structures", *Transportation Research Record,* TRB, National Research Council*,* Vol. 1336, pp. 24-30

Kutter, B.L., Manzari, M.T., Zeghal, M., Zhou, Y.G. and Armstrong, R.J. (2014) "Proposed Outline for LEAP Verification and Validation Processes", *the Fourth International Conference on Geotechnical Engineering for Disaster Mitigation and Rehabilitation* (4th GEDMAR), September 16th-18th, Kyoto, Japan

Ladd, C.C, Foott, R., Ishihara, K., Schlosser, F., and Poulos, H.G. (1977) “Stress-Deformation and Strength Characteristics”, *Proceedings of the 9th International Conference on Soil Mechanics and Foundation Engineering*, Tokyo, Vol. 1, pp. 421-494

Ladd, C.C. (1991) “Stability Evaluation during Staged Construction”, *Journal of Geotechnical Engineering Division*, ASCE, Vol. 117, No. 4, pp. 540-615

Lan, L.T. (1992) “A Model for One-Dimensional Compression of Peat”, *Ph.D. Thesis*, University of Wisconsin-Madison, Department of Civil and Environmental Engineering, Madison, Wisconsin

Landva, A.O. and La Rochelle, P. (1983) “Compressibility and Shear Characteristics of Radforth Peats”, *Testing of peat and organic soils*, STP 820, ASTM, West Conshohocken, Pennsylvania, pp. 157–191

Lee, J.S. and Santamarina, J.C. (2005) “Bender Elements: Performance and Signal Interpretation”, *Journal of Geotechnical and Geoenvironmental Engineering*, Vol. 131, No. 9, pp. 1036-1070

Lemnitzer, A., Cappa, R., Yniesta, S. and Brandenberg, S.J. (2015) “Centrifuge Testing of Model Levees atop Peaty Soil: Experimental Data”, *Earthquake Spectra Journal*, EERI, Manuscript ID #032715EQS048

Leoni, M., Karstunen, M. and Vermeer, P.A. (2008) “Anisotropic creep model for soft soils”, *Géotechnique,* Vol. 58, No. 3, pp. 215-226

Liu, M.D. and Carter, J.P. (2001) “A Conceptual Framework for Modelling the Mechanical Behavior of Structured Soils”, *Computer Methods and Advances in Geomechanics*, Vol. 1, pp. 347-354

Lobbestael, A. and Athanasopoulos-Zekkos, A. (2013) “The Effect of Input Frequency on Dynamic Soil-Structure Interaction of Levees with Cutoff Walls”, Geo-congress 2013, pp. 1260-1269

Long, M. (2005) "Review of Peat Strength, Peat Characterization and Constitutive Modelling of Peat With Reference to Landslides", *Studia Geotechnica et Mechanica*, Vol. 27, No. 3, pp. 67-90

MacFarlane, I.C. (1969) "Engineering Characteristics of Peat", *Muskeg engineering handbook*, University of Toronto Press, Canada, pp. 78–126

Makdisi, F. and Seed, H. (1978) "Simplified Procedure for Estimating Dam and Embankment Earthquake-Induced Deformations", *Journal of Geotechnical Engineering*, Vol. 104, No. 7, pp. 849-867

Marachi, N.D., Dayton, D.J. and Dare, C.T. (1983) "Geotechnical Properties of Peat in San Joaquin Delta", *Testing of Peats and Organic Soils*, ASTM STP 820, ASTM International, West Conshohocken, PA, pp. 207-217

Mesri, G. and Ajlouni, M.A. (2007) "Engineering Properties of Fibrous Peat", *Journal of Geotechnical and Geoenvironmental Engineering*, Vol. 133, No. 7, pp. 850-866

Mesri, G. and Castro, A. (1987) "The C_α/C_c Concept and K_o during Secondary Compression" Journal of Geotechnical Engineering, Vol. 113, No. 3, pp. 230-247

Mesri, G. and Godleski, P.M. (1977) "Time- and Stress-Compressibility Interrelationship", *Journal of Geotechnical Engineering*, ASCE, Vol. 103, No. 5, pp. 417-430

Mesri, G., Stark, T.D., Ajlouni, M.A. and Chen, C.S. (1997) "Secondary Compression of Peat with or without Surcharging", *Journal of Geotechnical and Geoenvironmental Engineering*, Vol. 123, No. 5, pp. 411-421

Meyer, Z. (1997) "Consolidation Model for Organic Soils", *Proceedings of the Institution of Civil Engineers - Ground Improvement*, Vol. 1, Issue 4, pp. 239-248

Meyer, Z., Coufal, R., Kowalów, M. and Szczygielski, T. (2012) "Peat Consolidation - New Approach", *Archives of Civil Engineering*, Volume 57, Issue 2, pp. 173–186

Millet, R., Chowdhury, K., Julian, E., Seed, R., Balakrishnan, A. and Perlea, V. (2014) "Seismic Vulnerability Evaluation of Levees in California's Central Valley", *ASDSO Dam Safety Conference*, San Diego, CA

Moreno, C.A. and Rodriguez, E.E. (2004) "Dynamic Behavior of Bogota's Subsoil Peat and It's Effect in Seismic Wave Propagation", *13th World Conference on Earthquake Engineering, Vancouver*, Canada, Paper 2632

Mortezaie, A.R. (2012) "Cyclic Threshold Strains in Clay versus Sands and the Change of Secant Shear Modulus and Pore Water Pressure at Small Cyclic Strains", *PhD Thesis*, UCLA

Moss, R. and Hollenback, J. (2011) "Seismic Response of Peaty Organic Soils as a Levee Foundation Material", *Geo-Frontiers 2011*, pp. 3097-3106

Mount, J.F. and Twiss, R. (2005) "Subsidence, Sea Level Rise, Seismicity in the Sacramento-San Joaquin Delta", *San Francisco Estuary and Watershed Science*, Vol. 3, Issue 5

Mualchin, L. and Jones, A.L. (1992) "Peak Acceleration from Maximum Credible Earthquakes in California", *California Department of Conservation, Division of Mines and Geology*, Open-File Report 92-01

ATC 83 / NIST GCR 12-917-21 (2012) "Soil-Structure Interaction for Building Structures", *National Institute of Standards and Technology*, U.S. Department of Commerce

Oikawa, H. and Miyakawa, I. (1980) "Undrained Shear Characteristics of Peat", *Soils and Foundations*, Vol. 20, No. 3, pp. 91-100

O'Kelly, B.C. and Zhang, L. (2013) "Consolidated-Drained Triaxial Compression Testing of Peat", *Geotechnical Testing Journal*, Vol. 36, No.3, pp. 1-12

Okamura, M. and Tamamura, S. (2011) "Seismic Stability of Embankment on Soft Soil Deposit", *International Journal of Physical Modelling in Geotechnics*, Vol. 11, Issue 2, pp. 50-57

Pichan, S. and O'Kelly, B.C. (2012) "Effect of Decomposition on the Compressibility of Fibrous Peat", *GeoCongress 2012*, pp. 4329-4338

Prevost, J.H. (1977) "Mathematical Modelling of Monotonic and Cyclic Undrained Clay Behavior", *International Journal for Numerical and Analytical Methods in Geomechanics*, Vol. 1, pp. 195-216

Rathje, E.M. and Antonakos, G. (2011) "A Unified Model for Predicting Earthquake-Induced Sliding Displacements of Rigid and Flexible Slopes", *Engineering Geology*, Vol. 122, pp. 51-60

Reinert, E.T., Stewart, J.P., Moss, R.E.S. and Brandenberg, S.J. (2014) "Dynamic Response of a Model Levee on Sherman Island Peat: A Curated Data Set", *Earthquake Spectra*, May 2014, Vol. 30, No. 2, pp. 639-656

Rio, J., Greening, P. and Medina, L. (2003) "Influence of Sample Geometry on Shear Wave Propagation using Bender Elements", *3rd International Symposium on Deformation Characteristics of Geomaterials – Lyon 2003*, Balkema, Rotterdam, pp. 963-967

Rogers, J.D., and Storesund, R. (2011) "Geologic Setting of the Sacramento-San Joaquin Delta", NSF RESIN Project Meeting at UC Berkley, Invited Lecture

Sasaki, Y. (2009) "River Dike Failures during the 1993 Kushiro-Oki Earthquake and the 2003 Tokachi-Oki Earthquake", *Earthquake Geotechnical Case Histories for Performance-Based Design*, ISSMGE TC4 2005-2009 Term Volume, pp.131-157

Seed, H.B. and Idriss, I. M. (1971) "Simplified Procedure for Evaluating Soil Liquefaction Potential", *Journal of Geotechnical Engineering Division*, ASCE, Vol. 97, No. 9, pp. 1249-1273

Shafiee, A., Brandenberg, S.J. and Stewart J.P. (2013) "Laboratory Investigation of the Pre- and Post-cyclic Volume Change Properties of Sherman Island Peat", *Geocongress 2013*, San Diego, CA, pp. 139-148

Shafiee, A., Stewart, J.P. and Brandenberg, S.J. (2015) "Reset of Secondary Compression Clock for Peat by Cyclic Straining", *Journal of Geotechnical and Geoenvironmental Engineering*, Vol. 141, No. 3

Shafiee, A. (2016) "Cyclic and Post-Cyclic Behavior of Sherman Island Peat", *PhD Thesis*, UCLA

Sivasithamparam, N., Karstunen, M. and Bonnier, P. (2015) "Modelling Creep Behavior of Anisotropic Soft Soils", *Computers and Geotechnics*, Vol. 69, pp. 46-57

SJC (2014) "County General Plan – Seismic and Geological Hazard", San Joaquin County, http://www.sjgov.org/commdev/cgi-bin/cdyn.exe/handouts-planning_GP-V3-III-A?grp=handouts-planning&obj=GP-V3-III-A

Stewart, D.P., Chen, Y.R. and Kutter, B.L. (1998) "Experience with the Use of Methylcellulose as Viscous Fluid in Centrifuge Models", *ASTM International*, Vol. 21, No. 4, pp. 365-369

Stokoe, K.H. II, Bay, J.A., Rosenbald, B.L., Hwang, S.K. and Twede, M.R. (1996) "In situ Seismic and Dynamic Laboratory Measurements of Geotechnical Materials at Queensboro Bridge and Roosevelt Island", *Geotechnical Engineering Report No. GR94-5*, Civil Engineering Department, University of Texas at Austin, Texas

Swaisgood, J.R. (2003) "Embankment Dam Deformations Caused by Earthquakes", *International Pacific Conference on Earthquake Engineering*, Paper No. 14

Thompson, J. (2006) "Early Reclamation and Abandonment of the Central Sacramento-San Joaquin Delta", *Sacramento History Journal*, Vol. VI, No. 1-4

Tokimatsu, K. and Sekiguchi, T. (2006) "Effects of Nonlinear Properties of Surface Soils on Strong Ground Motions Recorded in Ojiya During 2004 Mid Niigata Prefecture Earthquake", *Soils and Foundations*, *Japanese Geotechnical Society*, Vol. 46, No. 6, pp. 765-775

Tokimatsu, K. and Sekiguchi, T. (2007) "Effects of Dynamic Properties of Peat on Strong Ground Motions during 2004 Mid-Niigata Prefecture Earthquake", *4th International Conference on Earthquake Geotechnical Engineering*, Paper No. 1531

Torres, R.A., Abrahamson, N., Brovold, F., Cosio, G., Driller, M.W., Harder, L.F. Jr., Marachi, N.D., Neudek, C.H., O'Leary L.M., Ramsbotham, M. and Seed, R. (2000) "Seismic vulnerability of the Sacramento-San Joaquin Delta levees", *Report of Levees and Channels Technical Team, Seismic Vulnerability Sub-team to CALFED Bay-Delta Program*, 30 p.

Unruh, J.R., Dumitru, T.A. and Sawyer, T.L. (2007) "Coupling of Early Tertiary Extension in the Great Valley Forearc Basin with Blueschist Exhumation in the Underlying Franciscan Accretion Wedge at Mount Diablo, California", Geological Society of American Bulletin, Vol. 119, No. 11/12, pp. 1347-1367

USGS (2003) "Earthquake Probabilities in the San Francisco Bay Region, 2002-2031", *Working Group on California Earthquake Probabilities, U.S. Geological Survey*, Open-File Report 03-214

Vermeer, P.A. and Neher, H.P. (1999) "A Soft Soil Model that Accounts for Creep", *Beyond 2000 in Computational Geotechnics: 10 years of Plaxis International*, Balkema, Rotterdam, pp. 249-261

Vucetic, M.V. (1994) "Cyclic Threshold Shear Strains in Soils", *Journal of Geotechnical Engineering*, Vol. 120, No. 12, pp. 22008-2228

Walker, L.K. and Raymond, G.P. (1968) "The Prediction of Consolidation Rates in a Cemented Clay", *Canadian Geotechnical Journal*, Vol. 5, No. 4, pp. 192-216

Wang, Y.H., Lo, K.F., Yan, W.M. and Dong, X.B. (2007) "Measurement Biases in the Bender Element Test", *Journal of Geotechnical and Geoenvironmental Engineering*, Vol. 133, No. 5, pp. 564-574

Watson-Lamprey, J. and Abrahamson, N. (2006) "Selection of Ground Motion Time Series and Limits on Scaling", *Soil Dynamics and Earthquake Engineering*, Vol. 26, pp. 477-482

WEC (2013) "World Energy Resources: Peat", *World Energy Council 2013*

Wehling, T.M., Boulanger, R.W., Arulnathan, R., Harder, L.F. Jr. and Driller, M.W. (2003) "Nonlinear Dynamic Properties of a Fibrous Organic Soil", *Journal of Geotechnical and Geoenvironmental Engineering*, Vol. 129, No. 10, pp. 929-939

Wesnousky, S.G. (1986) "Earthquakes, Quaternary Faults, and Seismic Hazard in California", *Journal of Geophysical Research*, Vol. 91, No. B12, pp. 12,587-12,631

Whitman, R.V. and Lambe, P.C. (1986) "Effect of Boundary Conditions upon Centrifuge Experiments Using Ground Motion Simulation", *Geotechnical Testing Journal*, Vol. 9, No. 2, pp. 61-71

Wilson, D.W., Farrell, T.M., and Kutter, B.L. (1994) "An Overview and Relevance of Experimental Data From VELACS Project Model Nos. 7, 11, and 12", Proceedings, *Verification of Numerical Procedures for the Analysis of Soil Liquefaction Problems*, Balkema, Rotterdam, Vol. 2, pp. 1657-1680

Wong, R.C.K., Thomson, P.R. and Choi, E.S.C. (2006) "In Situ Pressure Responses of Native Peat and Soil under Train Load: A Case Study", *Journal of Geotechnical and Geoenvironmental Engineering*, Vol. 132, No. 10, pp. 1360-1369

Yamaguchi, H., Ohira, Y., Kogure, K. and Mori, S. (1985) "Undrained Shear Characteristics of Normally Consolidated Peat under Triaxial Compression and Extension Conditions", *Soils and Foundations, Japanese Society of Soil Mechanics and Foundation Engineering*, Vol. 25, No.3, pp.1-18

Yegian, M., Marciano, E. and Ghahraman, V. (1991) "Earthquake-Induced Permanent Deformations: Probabilistic Approach", *Journal of Geotechnical Engineering*, Vol. 117, No. 1, pp. 18-34

Yin, J.H., Zhu, J.G. and Graham, J. (2002) "A New Elastic Viscoplastic Model for Time-Dependent Behaviour of Normally and Overconsolidated Clays: Theory and Verification", *Canadian Geotechnical Journal*, Vol. 39, pp. 157-173

Yniesta, S., Lemnitzer, A., Cappa, R. and Brandenberg, S.J. (2015a) "Vacuum Pluviation Device for Achieving Saturated Sand", *Geotechnical Testing Journal*, Vol. 38, No.3

Yniesta, S., Cappa, R., Lemnitzer, A. and Brandenberg, S.J. (2015b) "Centrifuge Testing of Levees: Saturation Techniques during Model Construction", *IFCEE & Geo-Congress 2015*, San Antonio, USA, March 2015

Zhang, L. and O'Kelly, B.C. (2013) "Constitutive Models for Peat – A Review", *Proceedings of the 12th International Conference on Computational Plasticity – Fundamentals and Applications (COMPLAS XII)*, Barcelona, Spain, 3rd-5th September 2013, pp. 1294-1304

Zainorabidin, A. and Wijeyesekera, D.C. (2008) "Geotechnical Characteristics of Peat", *Proceedings of the AC&T*, pp. 71-78

Zeghal, M., Manzari, M.T., Kutter, B.L. and Abdoun, T. (2015) "LEAP: Selected Data for Class C Calibrations and Class A Validations", *Geotechnics for Catastrophic Flooding Events*, Taylor and Francis Group, London

Zienkiewicz, O. C. (2000) "The Finite Element Method Volume 1: The Basis", 5th Ed., *Butterworth-Heinemann*

APPENDIX A: DEVELOPMENT OF SATURATION PROCEDURES

A.1 Challenges in Saturation of Sands in Centrifuge Models with Organic Soils

Accurate saturation of the sandy levee was a crucial step in our centrifuge test. Correct reproduction of undrained shearing behavior, such as liquefaction, is directly related to the degree of saturation of granular materials. In nature, sands below water table are usually well saturated since trapped gasses dissolve and migrate with time. In laboratory test, several techniques are commonly employed to speed these processes up, but in some cases methods such backpressure or vacuum saturation cannot be used because they would result in altering the model. This was the case for our tests: peat is highly gassy material that continuously degrades when exposed to air; when remolded specimens are subject to vacuum techniques the large gas particles migrate and simply destroy the model. In addition, each large scale centrifuge investigations comprised two stages (clayey levee and sandy levee), and the container was not taken out of the arm in between, therefore extra challenges were posed by the limited work space (lid and sensors were not removed) and restricted access to other pluviation devices (dry pluviator).

An additional challenge was posed by the selection of viscous water as pore fluid in order to reduce the seeping rate through the sandy levee and therefore lowering the demand on the pump (see Section 2.4). Viscous water is notoriously difficult to use in saturation of sands, and it becomes virtually impossible for saturation purposes when the viscosity exceeds 30 centistokes.

A.2 A new pluviation technique

Various trials in the laboratory prior to model construction were utilized to arrive at the appropriate construction technique for our tests. We first tried simply pluviating dry sand into water, and found that the p-wave velocity measured using an ultrasound device was less than 800 m/s, which indicated that the sand was unsaturated. We postulated that gas bubbles adhered to the sand particles as the particles broke the surface tension of the fluid, and entrapped gases resulted from this pluviation technique. To pre-saturate the sand, we developed the pluviation device shown in Figure 63 (Yniesta et al. 2015). Dry sand is placed into the acrylic chamber, and a vacuum is applied to the top of the chamber to pull the air out. As the vacuum is released, CO_2 is slowly allowed to percolate from the bottom of the chamber. After flushing with CO_2, the container is again brought under vacuum and de-aired water is introduced from the bottom of the container. Once the sand is saturated, the nozzle is placed into the surface of the water in the container, and the valve at the bottom of the nozzle is opened. We found that sand would not flow through the nozzle unless we injected high pressure water through a coil at the bottom of the chamber to cause the sand to boil. Using this procedure, we were able to achieve p-wave velocities in the range from 1570 to 1640 m/s at atmospheric pressure (i.e., with zero back-pressure), which indicates that a high degree of saturation was obtained.

Although the device worked well in the lab, we found that the volume of sand required for use on the centrifuge rendered the device somewhat impractical in terms of time required to saturate and pluviate enough material inside the container. For this reason, an alternative procedure was developed in which Nevada sand was mixed with water under vacuum in a large mixing chamber (Figure 64), and subsequently siphoned and stored in a large bin under water. Measured p-wave

velocities were higher than 1500 m/s for sand prepared in this manner. The saturated sand was then siphoned again from the bin into the model container through a small tube. Relative density of the sand prepared in this manner was approximately 35%, which indicates that the depositional energy was small, but not zero as is commonly associated with water pluviation techniques. This is consistent with the observation that a high velocity jet of sand and water was injected into the centrifuge model container through the tube, so depositional energy was not zero. Shear wave velocity measurements inside the levee fill were recorded during testing of RCK02 at different g-fields and suggest the sandy fill to have shear wave velocity of V_s = 200 m/s at 57g and V_s = 60 m/s at 1g. Shear wave velocity parameters for RCK02 where found to be V_{s1} = 198 m/s and n = 0.26. Additional details of saturation procedures for RCK01 and RCK02 are included in Cappa et al. (2014 a,b).

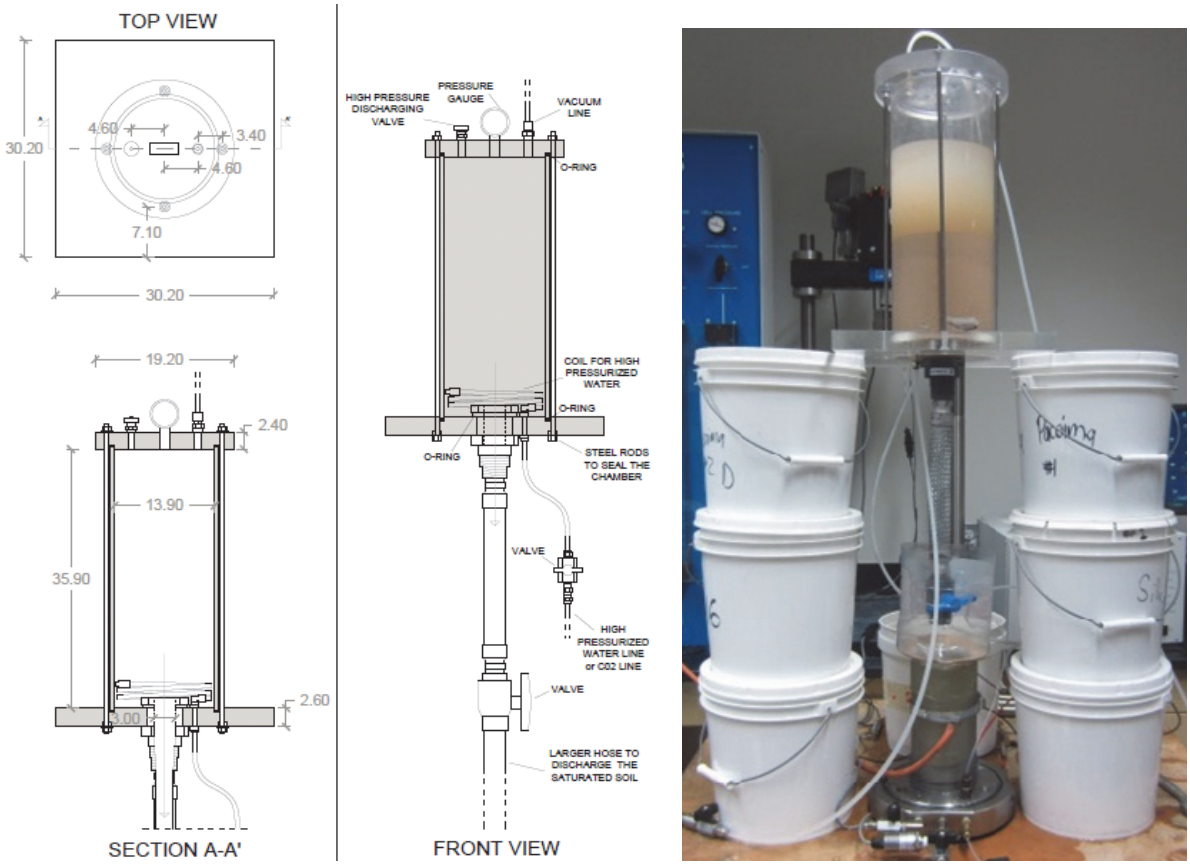

Figure 63 – Water pluviation saturation device (Yniesta et al., 2015a)

Figure 64 – Electric mixing chamber available at the facility